TRANSIENT PRESSURE WAVES IN HILLSLOPES

George W Waswa

Thesis

Submitted in fulfillment of the requirements for the degree of
Doctor of Philosophy (PhD)

School of Engineering
University of KwaZulu-Natal

May 2013

TRANSIENT PRESSURE WAVES IN HILLSLOPES

PhD thesis

Waswa GW

School of Engineering, University of KwaZulu-Natal, South Africa

SUPERVISORS

Prof Simon A Lorentz

Associate Professor: Process Hydrology

Centre for Water Resources Research

School of Agricultural, Earth and Environmental Sciences

University of KwaZulu-Natal

Private Bag X01, Scottsville 3209

South Africa

Prof Pieter AL le Roux

Associate Professor: Hydropedology

Department of Soil, Crop and Climate Sciences

University of the Free State

P.O. Box 339, Bloemfontein 9300

South Africa

TRANSIENT PRESSURE WAVES IN HILLSLOPES

PhD thesis

Waswa GW

School of Engineering, University of KwaZulu-Natal, South Africa

SUPERVISORS' CONSENT

As the candidate's Supervisor I agree/do not agree to the submission of this thesis.

Simon A Lorentz	Date

As the candidate's co-Supervisor I agree/do not agree to the submission of this thesis.

Pieter AL le Roux	Date

TRANSIENT PRESSURE WAVES IN HILLSLOPES

PhD thesis

Waswa GW

School of Engineering, University of KwaZulu-Natal, South Africa

DECLARATION

I, **George W Waswa**, declare that:

1. The research reported in this thesis, except where otherwise indicated, is my original work.

2. This thesis has not been submitted for any degree or examination at any other university.

3. This thesis does not contain other persons' data, pictures, graphs or other information, unless specifically acknowledged as being sourced from other persons.

4. This thesis does not contain other persons' writing, unless specifically acknowledged as being sourced from other researchers. Where other written sources have been quoted, then:

   a. their words have been re-written, but the general information attributed to them has been referenced;

   b. where their exact words have been used, their writing has been placed inside quotation marks, and referenced.

5. Where I have reproduced a publication of which I am an author, co-author or editor, I have indicated, in detail, which part of the publication was actually written by myself alone and have fully referenced such publications.

6. This thesis does not contain text, graphics or tables copied and pasted from the Internet, unless specifically acknowledged, and the source being detailed in the thesis and in the Reference section.

George W Waswa	Date

TRANSIENT PRESSURE WAVES IN HILLSLOPES

PhD thesis

Waswa GW

School of Engineering, University of KwaZulu-Natal, South Africa

DEDICATION

To

my mother,

my teachers

and

the tax payers of Germany, Kenya and South Africa

TRANSIENT PRESSURE WAVES IN HILLSLOPES

PhD thesis

Waswa GW

School of Engineering, University of KwaZulu-Natal, South Africa

ACKNOWLEDGEMENTS

I thank **God, the Almighty,** for granting me life (Psalm 150:6) and good health (Matthew 6:25) without which, absolutely nothing would have been accomplished. I thank Him for providing me with all the necessary resources during the entire study. He constantly expanded my imagination, replenished my energies (1 Kings 17:16), removed every barrier, opened every gate and turned opponents into allies (Isaiah 54).

I thank the following institutions and persons for their support during this study:

- The **German Academic Exchange Service** (**DAAD**), Germany, for granting me the Scholarship to pursue this study.
- The **Water Research Commission** (**WRC**), South Africa, for providing funds for research instruments, equipment, materials and field trips.
- The **Umgeni Water Chair for Water Resources**, University of KwaZulu-Natal, South Africa, for providing funds to attend to the examiners comments and write more papers from the thesis.
- The **Masinde Muliro University of Science and Technology** (**MMUST**), Kenya, for granting me study leave and for the payback scholarship, in form of a continued salary to my family.
- The **School of Engineering (SE),** University of KwaZulu-Natal (UKZN), for the JW Nelson Fund Award, which enabled me to attend some academic meetings, notably the 15th SANCIAHS (2011) and 16th SANCIAHS (2012) Symposiums, where presentations from the study were awarded Silver Prizes. This award also enabled me to attend the 13th WaterNet Symposium (2012).
- My supervisors, **Prof Simon A Lorentz** and **Dr Pieter AL le Roux**, for introducing to me this very interesting subject of transient pressure waves in hillslopes. Their encouragement, guidance and support, from the initial to the final level of this study, enabled me to develop an understanding of the subject.
- The **anonymous reviewers** (those who recommended rejection and those who recommended acceptance) of the manuscripts that have formed part of this thesis. Their

challenging comments enabled me to gain in-depth insight and understanding of the subject.

- The **anonymous examiners of this thesis,** for their positive and constructive comments.

- **Mr Cobus Pretorius**, the Chief Technician at the SE and CWRR, for his technical advice and assistance with, instrumentation.

- **Dr Sharon Rees**, for tirelessly identifying numerous language errors in my many draft documents.

- **Fiona Higginson,** postgraduate administrator at the School of Engineering, and **Kim Henry** the academic administrative officer – Higher degrees College of Agriculture, Engineering and Science, for coordinating the registration process.

- The academic staff at the School of Engineering and the Centre for Water Resources Research (CWRR): **Prof Cristina Trois** (Dean and Head of the School of Engineering), **Prof Jeff F Smithers**, **Prof Tilahun S Workneh**, **Mrs Tinisha Chetty**, **Prof Graham PW Jewitt**, **Prof Carel N Bezuidenhout**, **Dr Aidan Senzanje**, **Dr Gikuru Mwithiga**, **Prof Roland Schulze, Prof Vincent Chaplot** and **Mr Louis Lagrange** for being good role models.

- **David Clark** for troubleshooting many of my computer software problems.

- **Sean Thornton-Dibb** for giving me access to the field database and in building pdf files.

- **Mark Horan** for organizing office space, a desk and computer facilities.

- **Suzanne Kunz** for replenishing my printing credits.

- **Natasha Moneyvalu** for coordinating the provision of office stationery and communication.

- **Richard Kunz** for coordinating the orientation programme, through which I familiarize myself with EndNote software.

- **Alistair D Clulow**, **Carl Freese**, **Hurtley H Bulcock** and **Matthew Becker** for helping me with field work.

- The staff at the Library of Life Sciences and Cecil Renaud Library, UKZN (particularly, **Yakesh Jagesar**, **Nicky Pitout** and **John Timms**) for keeping up with my many interlibrary requests.

- My colleagues, **Benon Zaake**, **Julius Kollongei**, **Thawani Sanjika**, and **Phesheya Dlamini,** with whom I shared an office (Room 220B), for their blessings on many mornings.

- **Mama Zanele Nxele** for keeping our office and working environment clean.

- The **organizers and participants of road races in South Africa**, for making this sport truly enjoyable and relaxing.

- The pastors and the members of the **Burangasi Church of Christ (Bungoma),** the **Kakamega Redeemed Gospel Church (Kakamega)**, the **Scottsville Baptist Church (Scottsville)**, for their prayers.

- I am thankful to my brothers **Simiyu**, **Wafula**, **Nyongesa**[*], **Barasa**, **Wekesa** and my sisters **Kadogo** and **Fanis** and **their families,** for their prayers and support accorded to me and my family.

- I am grateful to my lovely wife, **Irene**, and our children, **Nasimiyu**, **Simiyu** and **Nabwile**, for their patience and tolerance. They can be rewarded in fullness only by God, the Almighty.

- I am forever grateful to my mother **Margaret**, the servant of God, the precious retired primary teacher and my long time true friend, for her discipline, encouragement, guidance and prayers. I thank her for the sacrifices she made for my education.

George W. Waswa 208529656@stu.ukzn.ac.za, waswageorge@gmail.com

---

[*] Our beloved brother Antony Nyongesa Waswa passed on, when I was just about to hand in this thesis for examination. We loved him. May God rest his soul in eternal peace.

… "No wise man, enchanter, magician, or diviner can explain … the mistery …, but there is God in heaven who reveals misteries. …"

Daniel 2: 27 – 28

TRANSIENT PRESSURE WAVES IN HILLSLOPES

PhD thesis

Waswa GW

School of Engineering, University of KwaZulu-Natal, South Africa

ABSTRACT

Previous studies found that during a rainfall event, pre-event water, which exists in the catchment before the event, may appear in significant amounts in the stream stormflow hydrograph. Pre-event water is predominantly groundwater. Among the mechanisms that have been proposed to explain the rapid mobilization of pre-event water from hillslopes are: (1) groundwater ridging (GWR) i.e. the rapid rise of a water table in environments, where the capillary fringe, or the zone of tension saturation, is very close to the ground surface and (2) the Lisse Effect (LE) i.e. the rapid response of a groundwater level to pressurized pore air in the unsaturated zone. Published literature explains that GWR is caused by the application of a small amount of water on the ground surface. On the LE, it is explained that pressurized pore air acts at the water table, resulting in a rapid rise of the water level in a well, screened below the water table. These explanations are insufficient on the physical processes involved in GWR and the LE. The objectives of this study were: (1) to use the commonly observed catchment hydrological processes i.e. tensiometric pore water pressure, shallow groundwater levels, rainfall data and the hydraulic properties of soils, to quantify and describe the physical processes involved in GWR and the LE mechanisms; (2) to perform laboratory experiments, in order to understand the physical processes involved in the LE; and (3) to develop a mathematical theory that can describe the physical processes in the LE. Results indicated that GWR and the LE are caused by the addition (elevation) of potential energy in water within the capillary fringe. In GWR, the additional energy is from the intense rainfall. In the LE, the additional energy is from compressed pore air in the unsaturated zone. In both mechanisms, the added energy diffuses through the capillary fringe, as a downward pressure wave, releasing the tension forces in water. As soon as the downward pressure wave-front arrives at the water table, the water table begins to ascend, as an upward pressure wave. The ascending water table steepens the hydraulic gradient, which results in the rapid groundwater fluxes, without the recharge of the water table by the infiltration profile.

Key words: *capillary fringe, compressed pore air, diffusion equation, groundwater fluxes, pressure potential energy, rapid water table response*

TRANSIENT PRESSURE WAVES IN HILLSLOPES

PhD thesis

Waswa GW

School of Engineering, University of KwaZulu-Natal, South Africa

PUBLICATIONS

1. Waswa GW, Clulow AD, Freese C, le Roux PAL and Lorentz SA (2013), Transient pressure waves in the vadose zone and the rapid water table response. Vadose Zone Journal. doi:10.2136/vzj2012.0054

Contributions (for details, see the Introduction, Section 1.7)

Waswa GW	Formulated and wrote the paper, analysed the data, discussed the results and corresponded with the journal editor.
Clulow AD	Assisted in programming the loggers, assisted with some instruments, made comments in the manuscript and provided moral support.
Freese C	Assisted in collecting field data and provided moral support.
le Pieter PAL	Made comments in the proposal and provided moral support.
Lorentz SA	Assisted in provision of materials and instruments, made comments in the manuscript and granted access to field database.

2. Waswa GW and Lorentz SA (under review), Theory of diffusion of energy through capillary fringe and a water table rise in the Lisse Effect phenomenon. Vadose Zone Journal

Contributions (for details, see the Introduction, Section 1.7)

Waswa GW	Formulated and wrote the paper; formulated and developed the theory, performed laboratory experiments, analysed the data, discussed the results and corresponding with the journal editor.
Lorentz SA	Assisted in provision of materials and instruments and made comments in the manuscript.

TRANSIENT PRESSURE WAVES IN HILLSLOPES

PhD thesis

Waswa GW

School of Engineering, University of KwaZulu-Natal, South Africa

TABLE OF CONTENTS

CHAPTER 1

INTRODUCTION

CHAPTER 2

TRANSIENT PRESSURE WAVES IN THE VADOSE ZONE AND THE RAPID
WATER TABLE RESPONSE

CHAPTER 3

THEORY OF DIFFUSION OF ENERGY THROUGH CAPILLARY FRINGE AND A WATER TABLE RISE IN THE LISSE EFFECT PHENOMENON

CHAPTER 4

SUMMARY AND CONCLUSIONS

TRANSIENT PRESSURE WAVES IN HILLSLOPES

PhD thesis

Waswa GW

School of Engineering, University of KwaZulu-Natal, South Africa

LIST OF FIGURES

TRANSIENT PRESSURE WAVES IN HILLSLOPES

PhD thesis

Waswa GW

School of Engineering, University of KwaZulu-Natal, South Africa

LIST OF TABLES

TRANSIENT PRESSURE WAVES IN HILLSLOPES

PhD thesis

Waswa GW

School of Engineering, University of KwaZulu-Natal, South Africa

NOTATION AND ABBREVIATIONS

C Specific water capacity [L^{-1}]

d_e Energy diffusivity (diffusion constant) in soil water [L^{2}T^{-1}]

$D(\theta)$ Hydraulic diffusivity (a function of soil water content) [L^{2}T^{-1}]

erfc   Complementary error function

E_r Time rate change in energy content in the capillary fringe [ML^{2}T^{-3}]

E_c Energy content in the capillary fringe [ML^{2}T^{-2}]

g Gravitational acceleration [LT^{-2}]

h_a Pore air pressure [L]

h_b Pore air entry pressure of the soil [L]

h_w Pore water pressure [L]

H_w Dimensionless pore water pressure

K_{sat} Saturated hydraulic conductivity [LT^{-1}]

$K(\theta)$ Unsaturated hydraulic conductivity (a function of soil water content) [LT^{-1}]

L The operator in the Laplace transform

L^{-1} The operator in the inverse Laplace transform

s The time parameter (complex number) in the Laplace transform

t Time coordinate [T]

T Dimensionless time coordinate

t_p Time to peak response of the potential pressure [T]

t_r Time lapse between the moment compressed pore air pressure is imposed on the upper boundary of the capillary fringe and the time that the water table begins to respond [T]

U Unit cross-sectional area (perpendicular to the vertical space coordinate) of the capillary fringe [L^2]

$u(t)$ Heaviside unit step function

y The vertical space coordinate [L]

Y Dimensionless space coordinate

y_{cf} Depth of the capillary fringe [L]

y_{uz}	Depth of unsaturated zone [L]
y_w	Depth of ponded water on the soil surface [L]
β_{tcf}	Boundary , top of the capillary fringe
β_{ss}	Boundary, soil surface
β_{wt}	Boundary, water table (bottom of the capillary fringe)
θ	Soil water content [$L^3 L^{-3}$]
θ_r	Residual soil water content [$L^3 L^{-3}$]
θ_s	Saturated soil water content [$L^3 L^{-3}$]
Θ	Relative saturation
κ	Energy conductivity of soil pore water [LT^{-1}]
λ	Pore size distribution index in Brooks-Corey equation
v	Wave celerity $= dK(\theta)/d\theta$
ρ_w	Density of water [ML^{-3}]
ρ_s	Bulk density of soil [ML^{-3}]
ϕ	Porosity of the porous medium [$L^3 L^{-3}$]
∞	Infinity
B-C	Brooks-Corey
CF	Capillary fringe
CS	Coarse sand (0.50 – 2.00 mm)
EW	Event water
FS	Fine sand (0.053 – 0.25 mm)
GW	Groundwater (in some cases referring to water below the water table and in some cases referring to all the water below the ground)
GWR	Groundwater ridging
H	Hydraulic head
HOF	Hortonian overland flow
Kg	Kilograms
LE	Lisse Effect
MS	Medium sized sand (0.25 – 0.50 mm)
N	Newton
OH	Groundwater observation hole
PP	Pressure potential
S&C	Silt and clay (<0.053 mm)
SOF	Saturated overland flow
SW	Soil water
Tens	Tensiometer

TDR Time domain reflectometry

UZ Unsaturated zone

V Volume

WT Water table

z Elevation head

TRANSIENT PRESSURE WAVES IN HILLSLOPES

PhD thesis

Waswa GW

School of Engineering, University of KwaZulu-Natal, South Africa

CHAPTER 1

INTRODUCTION

1.1   Background to the Study

1.1.1   General importance

Understanding the sources, pathways (flow routes) and residence times of stream water in a catchment is important for the management of water resources. These three variables can be derived from the analysis of water in the stream stormflow hydrograph.

1.1.2   Stormflow hydrograph

Initially, based on the concept of infiltration capacity (Horton, 1933), it was observed that a stream stormflow hydrograph is composed of direct surface runoff i.e. Hortonian overland flow (HOF), which is not absorbed by soils. Later, Hewlett and Hibbert (1967) refuted the process of HOF in forested catchments and proposed the concept of variable source area (VSA), in which the extent of area contributing to stormflow, changes temporarily during a storm event. This concept holds that the saturated area in a catchment interacts dynamically, with the intensity of rainfall, depending on its antecedent soil moisture (Betson and Marius, 1969; Dunne and Black, 1970b, 1970a; Dunne *et al.*, 1975). As a detailed process of VSA, Dunne and Black (1970a) suggested the process of saturation overland flow (SOF), in which stormflow is composed of (1) excess rainfall from the area saturated by subsurface water, and (2) return flow from under the ground surface, usually near stream channels. Subsurface processes, such as lateral macropore flows and perched groundwater above less conductive

layers, have also been observed to contribute to the stormflow hydrograph (Mosley, 1982; McDonnell, 1990; Turton *et al.*, 1992; Lorentz *et al.*, 2004; Wenninger *et al.*, 2008).

1.1.3   Pre-event water in the stormflow hydrograph

The processes of HOF and the SOF imply that much of the water in the stormflow should have a similar isotopic signature as that of the event water i.e. rainfall. However, with the advent of the use of hydrochemical and isotopic techniques (Craig, 1961), it has been found that pre-event water, which is resident in the catchment before the rainfall event, may appear in significant amounts (Table 1.1) in the stream stormflow hydrograph (Sklash and Farvolden, 1979). A review by Buttle (1994) indicates that pre-event water supplies at least 50% of streamflow at peak discharge in small- and medium-sized basins.

1.1.4   Proposed mechanisms for the rapid mobilization of pre-event water

Pre-event water can be surface water, e.g. streamwater and water held in small reservoirs/depressions. However, in most catchments, pre-event water is predominantly groundwater, held in the unsaturated zone and saturated zone (in the capillary fringe and below the phreatic surface), of which its motion is usually considered too slow to form a significant fraction of a stream stormflow hydrograph. In response to this paradox (Kirchner, 2003), researchers have proposed mechanisms that can account for the rapid mobilization of pre-event water (groundwater) from catchment soil and geological profiles. These mechanisms include macropore flows (McDonnell, 1990), transmissivity feedback (Kendall *et al.*, 1999), translatory flow (Hewlett and Hibbert, 1967; Bishop *et al.*, 1990), kinematic waves (Nolan and Hill, 1990), surface storage (Buttle and Sami, 1992 and Waddington *et al.*, 1993), pressure wave effects (Torres *et al.*, 1998), near-stream groundwater ridging (Sklash and Farvolden, 1979; Gillham, 1984), i.e. the rapid rise of a water table in environments, where the capillary fringe, or the zone of tension saturation, is very close to the ground surface and the Lisse Effect, i.e. groundwater level response to compressed pore air ahead of a wetting front (Torres *et al.*, 1998; Lorentz *et al.*, 2004). The role of the Lisse Effect in the rapid mobilization of pre-event water (groundwater) has only been speculated by Lorentz *et al.* (2004), who have stated that during a rainfall event, "the invading wetting front traps and pressurizes air in the pore structure between the front and

the groundwater, thus increasing the hydraulic gradient of the groundwater towards the stream."

Groundwater ridging and the Lisse Effect are referred to as transient pressure wave mechanisms, because the groundwater levels respond to pressure, and not to the recharge of the water table via the infiltration profile. Furthermore, the capillary fringe, or the zone of tension saturation, may play a significant role in these two mechanisms.

Table 1.1 Example of studies that have observed pre-event water in the stormflow hydrograph and their causal mechanisms. EW is event water, PW is pre-event water, SW is pre-event water in the vadose zone, and GW is pre-event water in the saturated zone below the water table.

Reference, study site	Water components in the stormflow hydrograph	Mechanisms
Bazemore *et al.* (1994), USA	10% EW, 25-36%SW & 54%GW in total storm runoff; and 15% EW, 50-65% SW & 20% GW in peak flow	Macropore flow
Bonell *et al.* (1990), New Zealand	38-64% PW of peak discharge	
Buttle (1994), Canada	60% PW of total stream flow during snowmelt	Surface storage
Dewalle *et al.* (1988), USA	1% EW, 24% SW, 75% GW	Piston flow & Macropores
Midgley and Scott (1994), South Africa	<5% EW, >95 GW	
Ogunkoya and Jenkins (1993), Scotland	26%EW,40%SW, 78%GW instantaneous contribution, 15%EW, 19%SW, 66%GW in total storm runoff	Groundwater ridging
Sklash and Farvolden (1979), New Zealand	<19%EW, >81%PW	Groundwater ridging
Sklash *et al.* (1986), New Zealand	<25%EW, >75%PW	Groundwater ridging
Turton *et al.* (1995), experimental	69%EW, 31%PW	Macropores
Waddington *et al.* (1993), Canada	30% EW, 70% PW	Surface storage & preferential flow
Wenninger *et al.* (2004), Germany	80% GW	
Wenninger *et al.* (2008), South Africa	16-26% PW of the event runoff	Macropores and pipes

The capillary fringe is a completely saturated zone, i.e. ($\theta = \theta_s$), just like the zone below the water table, as shown in Figure 1.1. However, the water in the capillary fringe is under tension force, i.e. ($\psi < 0$), just like the water found in the unsaturated zone (see Figure 1.1). Hence pressure is the only variable between the water in the capillary fringe and the water under the phreatic surface. Any phenomenon, therefore, that can rapidly vary the pressure in the capillary fringe may result in a rapid response of a water table, without the recharge of groundwater via the infiltration profile.
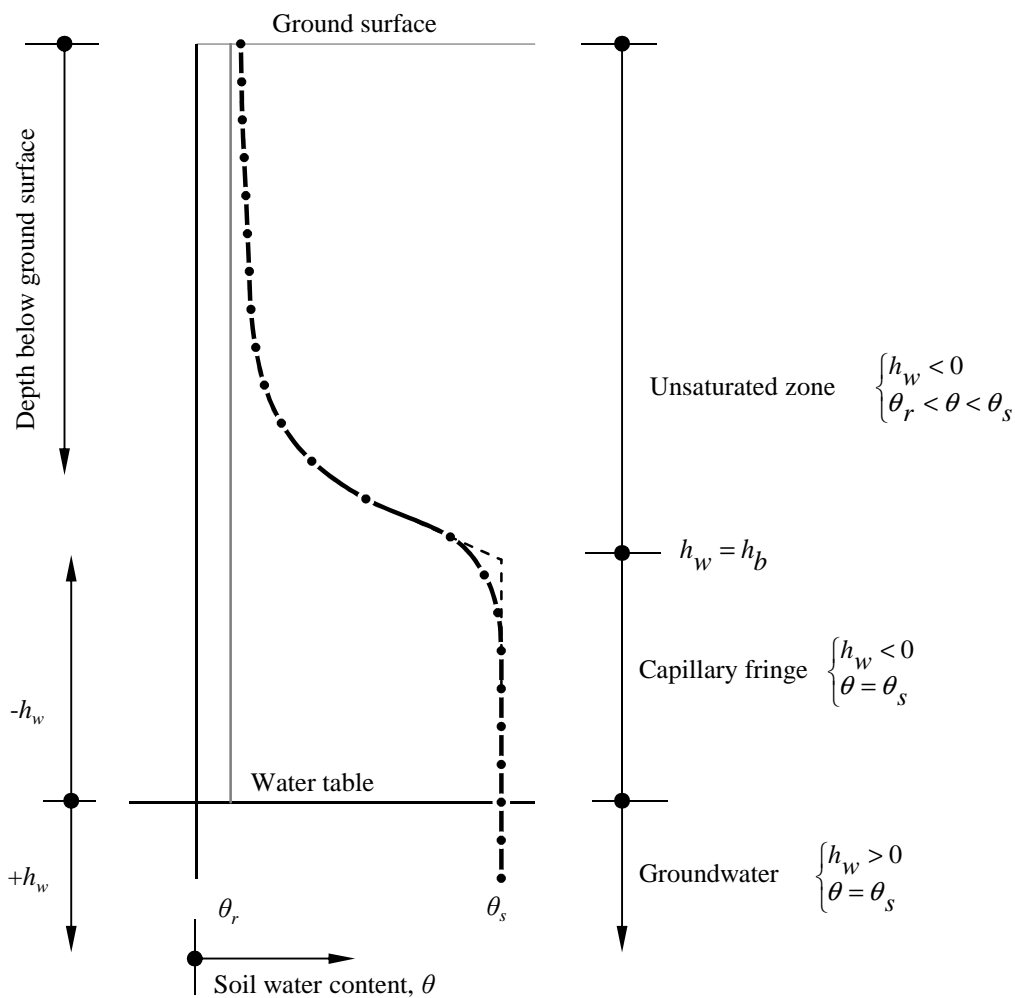
Figure 1.1 Properties and position of the capillary fringe in the structure of the groundwater. h_w is pore water pressure, h_b is pore air entry pressure, θ_r is residual soil water content, θ_s is saturated soil water content (modified from Gillham, 1984).

1.2   Transient Pressure Wave Mechanisms

In this study, a wave is considered, as "any recognizable signal that is transferred from one part of the medium to another, with a recognizable velocity of propagation. The signal may be any feature of the disturbance, such as a maximum, or an abrupt change in some quantity, provided that it can be clearly recognized and its location at any time can be determined. The signal may distort, change its magnitude, and change its velocity, provided it is still recognizable," (Whitham, 1974). Similarly, Wenninger *et al.* (2004) have defined a pressure wave effect, as the rapid reaction of groundwater levels induced by pressure, in which the pressure wave velocity is much faster than the water flow velocity.

1.2.1   Groundwater ridging

Groundwater ridging has been observed in environments, where the water table is shallow and the capillary fringe is close to, or intersects, the ground surface. These conditions are common in wetland zones. Findings from field experiments (Gillham, 1984; Novakowski and Gillham, 1988; Abdul and Gillham, 1989), laboratory experiments (Abdul and Gillham, 1984) and theoretical studies (Jayatilaka and Gillham, 1996; Jayatilaka *et al.*, 1996; Khaled *et al.*, 2011) have indicated that, in such environments, a very small amount of water introduced at the ground surface, results in a disproportionately large and instantaneous rise of a water table, compared with the expected rise from the specific yield concept. Many investigators and authors e.g. Heliotis and DeWitt (1987) and Weeks (2002) have adopted this explanation and hypothesized that in groundwater ridging, a small amount of water is required to fill the capillary menisci and bring the water table close to the ground surface. The rapid rise of the water table makes the hydraulic gradient steep and seepage area wide to the stream channel. As a result, significant amounts of pre-event water in the vadose zone and groundwater (under the phreatic surface) is induced into the stream channel, forming a significant portion of the stream stormflow. Nevertheless, on testing this hypothesis during snowmelt in a wetland zone, Buttle and Sami (1992) failed to observe a rapid water table response and groundwater fluxes to a nearby stream.

The role of groundwater ridging in the rapid mobilization of pre-event water was first proposed by Sklash and Farvolden (1979). However, a detailed experimental investigation of groundwater ridging was first performed by Gillham (1984).

Gillham's (1984) experiment

Gillham (1984) set up a field experiment (see Figure 1.2a), in which two tensiometers were installed at different depths in a soil profile. The shallower tensiometer (A) was within the capillary fringe and 3 cm below the ground surface. The deeper tensiometer (B) was positioned at the water table, 40 cm vertically below the shallower one. The capillary fringe, which was about 43 cm high, extended to the ground surface. 0.3 cm of water was rapidly applied on the ground surface and the reactions of the tensiometers were monitored.
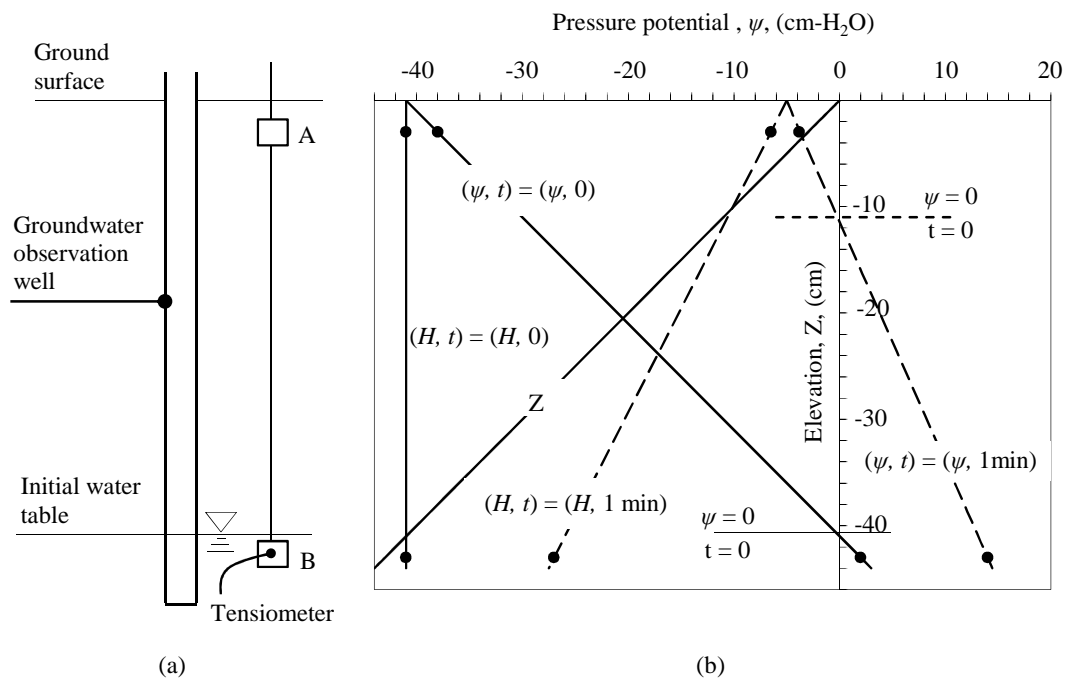
Figure 1.2 (a) Experimental set-up and instrumentation at Borden, Ontario, Canada and (b) vertical head distribution to the application of water and 1 minute after the application (H = hydraulic head, ψ = pressure potential). (a) and (b) are modified from Gillham (1984). Tensiometer A and B were installed at 3 cm and 43 cm, respectively, below the ground surface.

Some of the results reported by Gillham (1984), shown in Figure 1.2b and Figure 1.3, indicate that, one minute into the experiment, the shallower tensiometer recorded a greater change in fluid pressure (of about 32 cm-H_2O) than the change recorded by the deeper tensiometer (of about 13 cm-H_2O). By linear interpolation, from the values of the tensiometers, Gillham (1984) indicated that the water table had risen to about 30 cm above

the deeper tensiometer (Figure 1.2b). This rise of 30 cm in the water table implies that the deeper tensiometer would have recorded a change in fluid pressure of a value close to 30 cm-H_2O, however, it recorded a much lower value (13 cm-H_2O). These contradicting results were not observed in a similar experiment carried out later by Novakowski and Gillham (1988).
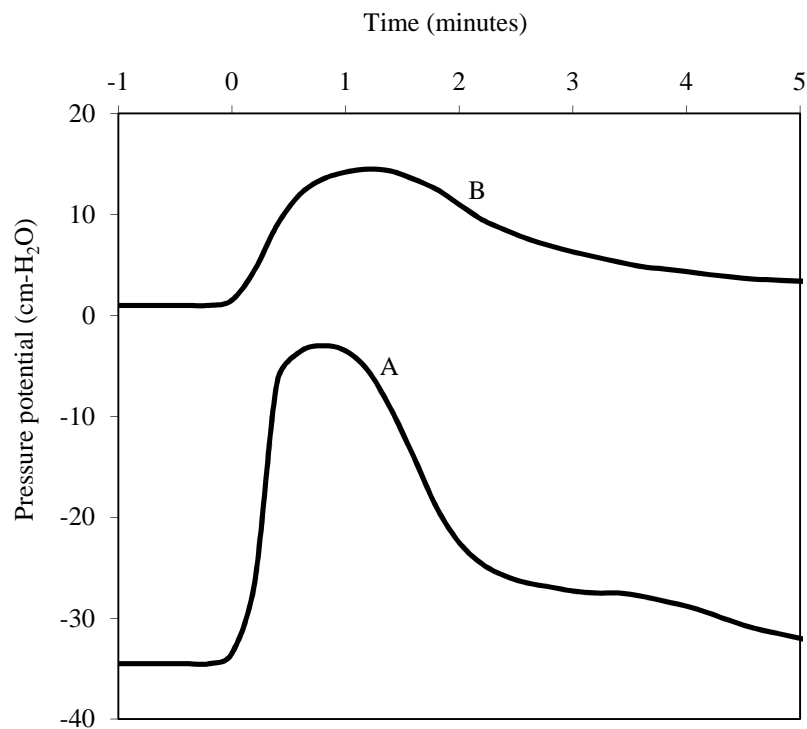
Figure 1.3 The responses of the shallow tensiomer, A, and the deep tensiometer, B, to the surface application of 3 mm of water (modified from Gillham, 1984).

Novakowski and Gillham's (1988) experiment

A significant difference, between the experiment of Novakowski and Gillham (1988) and that of Gillham (1984), is the number of tensiometers installed within the capillary fringe. By installing more tensiometers within the capillary fringe, Novakowski and Gillham (1988) observed the development of two distinct water tables (Figure 1.4). For instance, after 3 minutes into the experiment, water table conditions developed at about 7 cm and 18 cm below the ground surface (Figure 1.4). At 10 minutes into the experiment, there appeared to be three water tables: at about 9 cm, 11 cm and 15 cm, below the ground surface. On these

two occasions, the true water table was observed at the lowest depth. It is important to note that, if only two tensiometers, i.e. Tensiometers 1 and 5, were used (without Tensiometer 4 and 3), as in the case of the experiment of Gillham (1984), and by linear extrapolation from their readings, the water table would have erroneously been placed far above its true position. A scenario, similar to Gillham (1984), in which the water table rise is higher than the change in fluid pressure by the deeper tensiometer, would have occurred.

It is important to note that in the experiments of Gillham (1984) and Novakowski and Gillham (1988), the shallower tensiometers (e.g. Tensiometer A and Tensiometer 5, respectively) responded more rapidly, and to significantly higher maximum values, than the deeper tensiometers (e.g. Tensiometer B and Tensiometer 3, respectively) (Figure 1.3 and Figure 1.5).
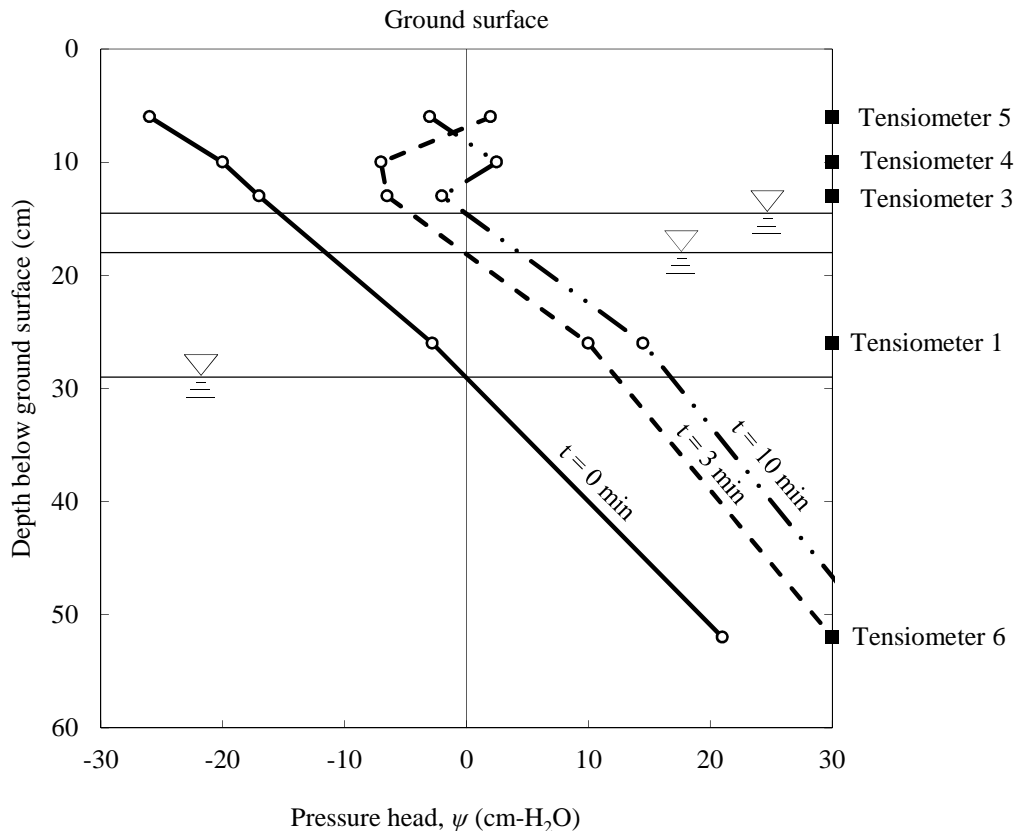
Figure 1.4 Pressure head verses depth profiles, showing the elevation of the water table in the trough area during experiment by Novakowski and Gillham (1988)

A review of these two experiments is concluded by stating that, the 'perched shallower water tables,' observed by Novakowski and Gillham (1988), may have been caused by the diffusion of energy (downward pressure wave) from the upper boundary of the capillary fringe (ground surface) towards the water table. The water, which was applied on the ground surface, injected a substantial amount of energy into the capillary fringe. This injected energy converted the tension pressure into positive pressure in water within the capillary fringe, as it propagated downwards, hence creating perched water table conditions. It is also possible that a similar process occurred in the experiment of Gillham (1984). However, the interpolation carried out by Gillham (1984), resulted in the placement of a water table at an erroneously higher position than the true position, as indicated by the deeper tensiometer (Figure 1.2). It should be noted that the energy injected into the capillary fringe, attenuates, as it propagates downwards. This explains the higher responses of the shallower tensiometers than the deeper tensiometers in Gillham's (1984) experiment (Figure 1.3), as well as in Novakowski and Gillham's (1988) experiment (Figure 1.5).
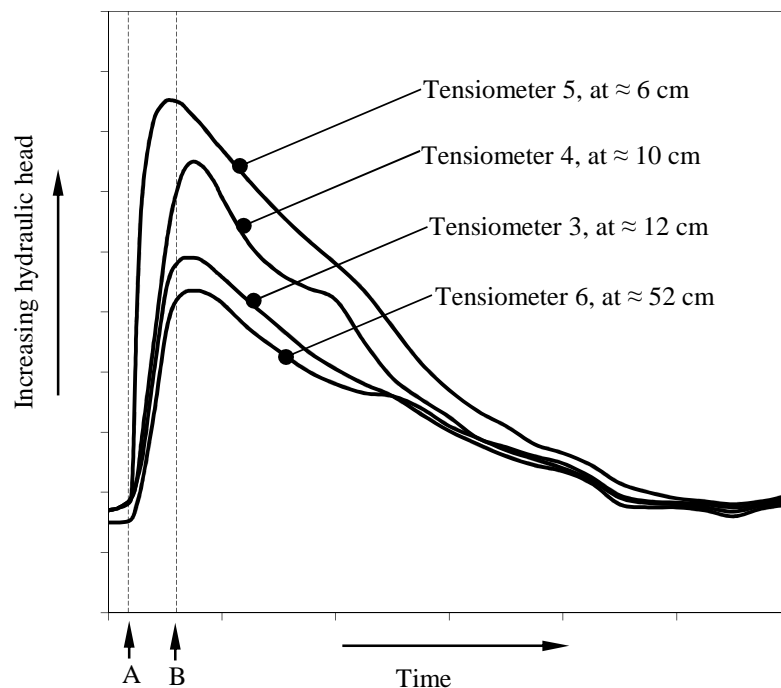
Figure 1.5 The trends of the hydraulic heads at different depths, below ground surface. A is the start-time and B is the stop-time, for the application of simulated rainfall to the ground surface (Modified from Novakowski and Gillham, 1988).

1.2.2   The Lisse Effect

The Lisse Effect is likely to occur where the water table is deep enough to allow a sufficient unsaturated zone, with a sufficient and continuous volume of pore air above the capillary fringe. During intense rainfall event, or a flooding event on the ground surface, a wetting front may cap the near surface. If the lateral escape routes of air are limited, due to the tortuosity of the pathways, and the vertical counterflow of air is impeded by the infiltration profile, further downward movement of the wetting front compresses and increases the pressure in the air ahead of the wetting front. The pressure in the air is transferred to the water table, resulting in a water level rise in a well screened below the water table (Weeks, 2002). This phenomenon was named the Lisse effect after the Lisse village in Holland, where the phenomenon was first observed and described by Hooghoudt (1947), cited in Heliotis and DeWitt (1987) and Weeks (2002).

With the continued downward movement of a wetting front, a state is reached whereby the pressure in the entrapped air exceeds the pressure head of the infiltration profile above. When this state is reached, some of the entrapped air counterflows upwards against the infiltration profile (Brustkern and Morel-Seytoux, 1970). Part of the counterflow air discharges into the atmosphere and part of it is encapsulated within the infiltration profile. The encapsulated air occupies space which would otherwise be occupied by water, hence reducing the saturated moisture content of the infiltration profile (Fayer and Hillel, 1986; Constantz *et al.*, 1988).

The effect of compressed pore air ahead of a wetting front on the rate of infiltration, and on total infiltration, has been intensively studied, using laboratory column experiments (Powers, 1934; Wilson and Luthin, 1963; Peck, 1965; Vachaud *et al.*, 1974; Touma *et al.*, 1984; Wang *et al.*, 1998), theoretical analysis (Brustkern and Morel-Seytoux, 1970; McWhorter, 1971; Wang *et al.*, 1997), as well as field observations (Horton, 1940; Dixon and Linden, 1972). All these studies demonstrate that the entrapped pore air ahead of the wetting front has an inhibiting effect on the liquid intake by a porous media.

It has also been reported that the elevated pressure in air contributes to the pressure potential term in the hydraulic head of the groundwater (Freeze and Cherry, 1979; Bond and Collis-George, 1981), which is reflected in the rapid rise of water levels in wells that are screened below the water table (Freeze and Cherry, 1979; Weeks, 2002). However, all these studies do not demonstrate clearly the physical processes involved in the Lisse Effect.

For instance, in explaining the Lisse Effect, Freeze and Cherry (1979) ignored the presence of a capillary fringe and indicated that compressed pore air pressure acts directly on the water table, resulting in an equivalent rise in the water level in a well, which is screened below the water table (i.e., $\gamma \Delta H = dP_a$ in Figure 1.6a). Weeks (2002) recognized the presence of the capillary fringe (Figure 1.6b). However, his qualitative and quantitative description of the Lisse Effect followed very closely that of Freeze and Cherry (1979) and did not consider the pressure changes in the capillary fringe. For instance, Weeks (2002) state that "the Lisse Effect results in a very rapid water level rise in the well, despite the fact that the water table is essentially unaffected, with a water-level recession lasting for several hours to a few days." This statement implies the absence of the capillary fringe and that the compressed pore air exerts pressure directly on the water table, displacing, or pushing, some of the groundwater into the observation well, in a process that does not affect the water table, which purportedly remains in its original position. Furthermore, Weeks (2002) proposed that the water level rise, ΔH, in a well (Figure 1.6b) can be estimated by the equation:-

$$\Delta H = P_A \left(\frac{m}{h - m} \right), \qquad\qquad [1.1]$$

where, m is the depth of wetting front penetration, P_A is atmospheric pressure expressed in terms of water column height, and h is the distance from the top of the capillary fringe to land surface. Many researchers, e.g. Healy and Cook (2002) and Guo *et al.* (2008), have used Eq. [1.1] and argued that the water level, in a well that is screened below the water table, rises to equal the increase in air pressure in the unsaturated zone. While Eq. [1.1], which is derived from the Boyle's law of pressure-volume relationship, may be useful in estimating the change in compressed pore air pressure, it may overestimate the Lisse Effect water level rise. This is because it does not account for the losses in energy, or even the time delay, that may occur due to the presence of the capillary fringe, which lies between the unsaturated zone and the initial water level in a well, screened below the water table (see Figure 1.6b).
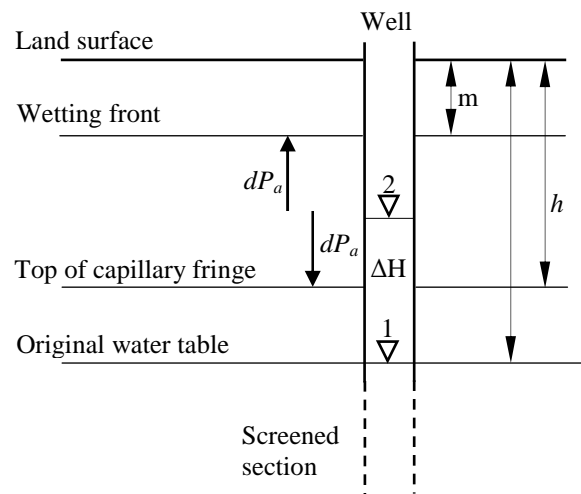
(b) Modified from Weeks (2002)
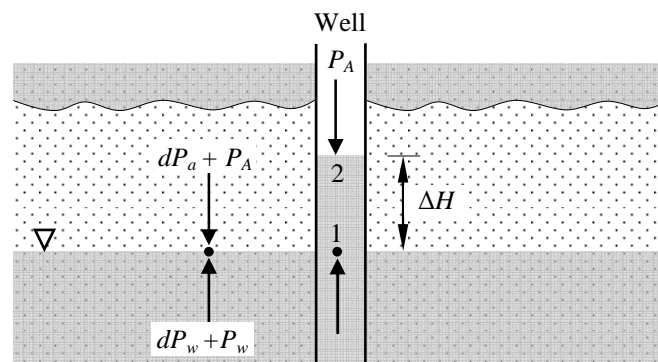
(a) Modified from Freeze and Cherry (1979)

Figure 1.6 The Lisse Effect, as explained by (a)Freeze and Cherry (1979), who expressed that $\gamma\Delta H = dP_a$ and (b) Weeks (2002), who expressed that $\Delta H = dP_a = P_A\left\{m/(h-m)\right\}$. ΔH is the rise in a water level in a well, dP_a is the change in pressure in pore air in the unsaturated zone, P_A is the atmospheric pressure, m is the depth of the infiltration profile, h is the depth from the ground surface to the top boundary of the capillary fringe, γ is the specific weight of water.

Earlier experimental studies on the Lisse Effect also ignored the role of the capillary fringe. Linden and Dixon (1975) observed a water table response to compressed pore air pressure ahead of a wetting front, in a border-irrigation field experiment, in which the role of the capillary fringe was not considered. Marui *et al.* (1993) studied the effect of compressed pore air on groundwater fluxes, using soil column apparatus, in which they monitored tensiometric pore water pressure, compressed pore air pressure and groundwater fluxes. Marui *et al.* (1993) observed that groundwater fluxes started and increased rapidly, as soon

as compressed pore air pressure in the unsaturated zone increased. However, these researchers did not monitor volumetric water content and the influence of the capillary fringe.

No scientific study, hitherto, has demonstrated the role of the capillary fringe in the rapid response of the groundwater level in the Lisse Effect.

1.3 Problem Statement

From the above review, it is concluded that the physical processes involved in the Lisse Effect water table response are not understood. In addition, the explanation of groundwater ridging mechanism, as it appears in the existing literature is insufficient, in regard to the physical mechanisms involved in the rapid rise of the water table.

1.4 Research Hypotheses

First, it is hypothesized that common physical processes, which involve the capillary fringe, occur in the groundwater ridging and the Lisse Effect mechanisms. In these mechanisms, the rapid water table response occurs due to the introduction of additional energy in the capillary fringe. In groundwater ridging, the additional energy is derived from the intensity of rainfall. In the Lisse Effect, the additional energy is derived from compressed pore air in the unsaturated zone, above the upper boundary of the capillary fringe.

The second hypothesis is that the injected energy propagates by diffusion process, from the upper boundary of the capillary fringe towards the water table, as a downward pressure wave. This downward pressure wave releases tension forces in water within the capillary fringe. As soon as the downward pressure wave front arrives on the water table, the water table starts to ascend, as an upward pressure wave. This hypothesis may explain the delay in the response (contrary to the expected instantaneous response) of the shallower tensiometer (after the application of water), which was observed and reported by Gillham (1984). It may also explain the lag in the response of the shallow groundwater levels behind the tensiometers, as observed and reported by Gillham (1984).

The third hypothesis is that, due to energy losses within the capillary fringe, the total rise of the water table would be less than the total amount of energy introduced in the capillary fringe. This hypothesis may explain the more rapid reaction and recovery rates, and the higher total responses, in the shallower tensiometers than in the deeper tensiometers, observed in the experiments of Gillham, 1984) and Novakowski and Gillham (1988).

The fourth hypothesis is based on the fact that pressure is the only variable between the water in the capillary fringe and the water under the water table. It is hypothesized, therefore, that any phenomena that can cause rapid perturbations in pressure within the capillary fringe may cause the water table to rapidly respond, without the recharge of groundwater by the infiltration profile. This implies that any amount of water, applied gently at the ground surface, cannot cause a rapid water table response in groundwater ridging. The magnitude of the water table response in groundwater ridging, therefore, may vary proportionally with the intensity of rainfall. This hypothesis may explain the failure of some researchers, e.g. Buttle and Sami (1992), to observe rapid water table response under snowmelt conditions. This is because the melting of snow (Gerdel, 1948) may not introduce additional energy in the capillary fringe, rapidly enough, to cause a rapid water table response.

1.5   Research Objectives

The objectives of this study are: (1) to use commonly observed catchment hydrological processes i.e. tensiometric pore water pressure, shallow groundwater levels, rainfall data and the hydraulic properties of soils, to quantify and describe the physical processes involved in the transient pressure wave mechanisms, namely, groundwater ridging and the Lisse Effect; (2) to perform laboratory experiments, in order to understand the physical processes involved in the Lisse Effect; and (3) to develop a mathematical theory that can describe the physical processes involved in the Lisse Effect and thus, the pneumatically pressurized groundwater fluxes.

1.6   Overview of the Methodologies

The methods used in this study are field observations, laboratory experiments and mathematical modeling. Field data of tensiometric pore water pressure, shallow groundwater levels, rainfall, the hydraulic and geometric properties of soils, and stream discharges were analyzed. From this analysis, the physical processes involved in groundwater ridging transient pressure wave mechanism, were identified and described. This analysis of the field data enabled also the identification of signals of the Lisse Effect rapid water table response and the pneumatically pressurized groundwater fluxes. Two sets of laboratory column experiments were then carried out. The first set of experiments was carried out, in order to gain an understanding of the physical processes involved in the Lisse Effect water table response and the pneumatically pressurized groundwater fluxes. Having understood the process involved in the rapid water table response in groundwater ridging and the Lisse Effect, a mathematical theory was developed, to specifically represent the physical processes involved in the latter mechanism. The mathematical theory was developed from first principles, the law of conservation of energy and the continuity equation. The second set of experiments was performed, therefore, in order to obtain the data for verification of the developed theory. The laboratory experiments consisted of a column of soil in a PVC pipe, which was instrumented with pore-air pressure probes, pore-water pressure probes, volumetric water content sensors, a groundwater outflow tube and a piezometer.

1.7   Significance of the Thesis

1.7.1   Contribution of the thesis to the scientific knowledge base

- This study explicitly expressed and recognized that pressure is the only primary variable between the water within the capillary fringe and the water below the water table.
- This study supports the argument by Gillham (1984) that the capillary fringe plays a significant role in groundwater ridging.
- This study, however, refutes Gillham's (1984) argument, that only a very small amount of water is required to cause the rapid water table response in groundwater ridging mechanism.

- Based on 1, above, this study extends the explanation of groundwater ridging by demonstrating that the magnitude of the rise of a water table is proportional to the amount of energy introduced into the capillary fringe. The amount of energy introduced varies directly with the intensity of rainfall, as these intensities are associated with different energy levels.

- This study demonstrated that the capillary fringe also plays a significant role in the rapid response of water levels in the Lisse Effect phenomenon. Here the additional energy introduced into the capillary fringe is derived from pressurized pore air in the unsaturated zone.

- In both groundwater ridging and the Lisse Effect, the additional energy injected into the capillary fringe is transmitted downwards by the diffusion/conduction process through the soil water, towards the water table.

- A one-dimensional diffusion equation, of the form $d_e \, \partial h_w^2 / \partial y^2 = \partial h_w^2 / \partial t^2$, for the propagation of energy through a capillary fringe, was developed and presented. d_e is the energy diffusivity coefficient. This equation, which was derived from the law of conservation of energy and continuity equation, when solved for appropriate boundary and initial conditions, can yield pore water pressure potential, h_w, at any depth, $y > 0$, below the upper boundary of the capillary fringe, $y = 0$, and at any time, t, when compressed pore air pressure, h_a, is rapidly imposed on the boundary $y = 0$. This equation can predict the water level rise in wells (change in pressure potential at the initial water table) in the Lisse Effect.

- The results from the developed equation and the laboratory experiments indicated that, due to energy losses in the capillary fringe, the water level in a well does not rise to equal the compressed pore air. This contradicts earlier theories by e.g. Freeze and Cherry (1979), Weeks (2002) and Guo *et al.* (2008), who proposed that the water level in a well rises, to equal the compressed pore air pressure.

- From the derived equation, this study proposes new material parameters, which are important in the analysis and understanding of diffusion of energy through soil water. The first is the energy diffusivity, d_e. This is analogous to thermal and hydraulic diffusivity, employed in understanding the flow of heat through solids and the flow of fluids through porous media, respectively. The second is the energy conductivity, κ, encapsulated in the energy diffusivity, $d_e = \kappa / \rho_w g$, in which ρ_w is the density of water and g is the gravitational constant. Parameter κ

is analogous to thermal and hydraulic conductivity, applied in the study of flow of heat through solids and flow of fluids through porous media, respectively.

- In this study, a probe for measurement of compressed pore air pressure was designed and fabricated. The probe, which was fabricated from a PVC cylindrical solid and a hydrophobic membrane, was successfully used in the laboratory experiment. This probe may also be effective under field conditions.

1.7.2 Personal contributions to the scientific knowledge base

The contribution of this thesis to scientific knowledge base is encapsulated in two manuscripts. The first manuscript, which forms Chapter 2 of the thesis, has been published in the Vadose Zone Journal. The second manuscript, which forms Chapter 3 of the thesis, was submitted to the Vadose Zone Journal and is still under review. The names appearing on the manuscripts are George W Waswa, Simon A Lorentz, Pieter AL le Roux, Alistair D Clulow and Carl Freese. Here is the account of the contribution of each individual.

This thesis was entirely composed and written by George W Waswa, who, in this section, is referred to as the author. The content and scientific arguments in the entire thesis are, the result of many hours spent by the author: (1) pondering over the primary data obtained from field observations and laboratory experiments; (2) analyzing and evaluating published data contained in journal articles; and (3) reading and evaluating theories published in journal articles and text books. As a result, the envisioned contribution of the thesis towards the scientific knowledge base, as stated in the previous section, is largely the author's. If any of the new theories proposed from this study appears illogical, incoherent or inconsistent, then that is to be accounted for solely by the author and not the other persons, whose names are appearing on the manuscripts.

However, the general subject presented in this thesis, and which forms the basis of the manuscripts, originated from the author's main supervisor, Prof. Simon A. Lorentz, who was also instrumental in fine tuning and focusing the study in its formative (proposal) stage. He occasionally made comments during the developmental stages of the subject and in the manuscripts. Prof. Lorentz was also the principal researcher in the project, from which field data were obtained. He also provided funding for the research instruments used in the study. For these reasons, the name of Prof. Lorentz appears on the first, as well as on the second, manuscript.

Prof Pieter AL le Roux is the author's second supervisor. Prof le Roux is one of the main researchers in the catchment, from where field data were obtained. Prof le Roux occasionally commented on the proposal of the study. Mr. Alistair Clulow helped with some of the instruments used in this study. He helped in programming the loggers and occasionally gave comments on the first manuscript. Carl Freese helped in the collection of field data. For these reasons, the names of Prof le Roux, Mr. Clulow and Mr. Freese, appear in the first manuscript.

1.8 Outline of the Thesis

This is a paper-based thesis and consists of four chapters. The study is introduced and concluded in Chapter 1 and Chapter 4, respectively. Chapter 2 and Chapter 3 are based on the manuscripts that had been submitted to a journal for review and publication. The literature cited in each chapter is contained in the list of Reference, at in the end of the respective chapters, but before the Appendices.

Chapter 1 introduces the study subject. It defines the background information for the problem to be studied. It also contains a literature review and an analysis of the published results, from which the problem to be studied is identified. The objectives of the study, and an overview of the methodologies used, are also included in Chapter 1. The details of the methods used to achieve the three objectives (see Section 1.5) are presented in Chapters 2 and 3.

Chapter 2 reports on the results of the analysis of field data, in which it was demonstrated that groundwater ridging is principally an energy-driven mechanism and dependant on the intensity of rainfall. Also reported in this Chapter are the signals of the Lisse Effect water table response, quantified from the analysis of the field data. Results of a laboratory experiment, which was carried out to verify the field Lisse Effect signals, are also reported. The role of the capillary fringe and the physical processes involved in the groundwater ridging and the Lisse Effect water table responses are evident in the results contained in this chapter. The results and discussion presented in Chapter 2 satisfy Objectives 1 and 2. The main recommendation from Chapter 2 is to develop a mathematical theory that can represent the physical processes involved in the Lisse Effect water table response. This recommendation forms the main problem to be investigated in Chapter 3.

A mathematical theory, of the diffusion of energy through the capillary fringe and the Lisse Effect water table response, is developed and presented in Chapter 3. By idealizing the forces acting on the capillary fringe, and the use of the law of conservation of energy and the continuity equation, a one-dimensional diffusion form of equation is derived. This equation is solved by the method of Laplace transform and for the appropriate initial and boundary conditions. The usefulness of the developed equation is evaluated by comparing the theoretical results and the results obtained from the laboratory experiments. The results and discussion presented in Chapter 3 satisfy Objective 3. A summary of the findings and recommendations for future research, arising from the present study, are presented in Chapter 4.

1.9 References

Abdul, AS, Gillham, RW. 1984. Laboratory studies of the effects of the capillary fringe on streamflow generation. Water Resour. Res. 20(6), 691-698.

Abdul, AS, Gillham, RW. 1989. Field studies of the effects of the capillary fringe on streamflow generation. J. Hydrol. 112(1-2), 1-18.

Bazemore, DE, Eshleman, KN, Hollenbeck, KJ. 1994. The role of soil water in stormflow generation in a forested headwater catchment: synthesis of natural tracer and hydrometric evidence. J. Hydrol. 162(1-2), 47-75.

Betson, RP, Marius, JB. 1969. Source areas of storm runoff. Water Resour. Res. 5(3), 574-582.

Bishop, KH, Grip, H, O'Neill, A. 1990. The origins of acid runoff in a hillslope during storm events. J. Hydrol. 116(1-4), 35-61.

Bond, WJ, Collis-George, N. 1981. Ponded infiltration into simple soil systems: 3. The behavior of infiltration rate with time. Soil Sci. 131(6), 327-333.

Bonell, M, Pearce, AJ, Stewart, MK. 1990. The identification of runoff production mechanisms using environmental isotopes in a tussock grassland catchment, eastern otago, New Zealand. Hydrol. Process. 4(1), 15-34.

Brustkern, RL, Morel-Seytoux, HJ. 1970. Analytical treatment of two-phase infiltration. J. Hydraul. Div. , Amer. Soc. Civ. Engrs. 96(HY12), 2535-2548.

Buttle, JM. 1994. Isotope hydrograph separations and rapid delivery of pre-event water from drainage basins. Prog. Phys. Geog. 18(1), 16-41.

Buttle, JM, Sami, K. 1992. Testing the groundwater ridging hypothesis of streamflow generation during snowmelt in a forested catchment. J. Hydrol. 135(1-4), 53-72.

Constantz, J, Herkelrath, WN, Murphy, F. 1988. Air encapsulation during infiltration. Soil Sci. Soc. Am. J. 52(1), 10-16.

Craig, H. 1961. Standard for Reporting Concentrations of Deuterium and Oxygen-18 in Natural Waters. Science (New York, NY) 133(3467), 1833.

Dewalle, DR, Swistock, BR, Sharpe, WE. 1988. Three-component tracer model for stormflow on a small Appalachian forested catchment. J. Hydrol. 104(1-4), 301-310.

Dixon, RM, Linden, DR. 1972. Soil air pressure and water infiltration under border irrigation. Soil Sci. Soc. Am. J. 36(6), 948.

Dunne, T, Black, RD. 1970a. An experimental investigation of runoff production in permeable soils. Water Resour. Res. 6(2), 478-490.

Dunne, T, Black, RD. 1970b. Partial area contributions to storm runoff in a small New England watershed. Water Resour. Res. 6(5), 1296-1311.

Dunne, T, Moore, TR, Taylor, CH. 1975. Recognition and prediction of runoff-producing zones in humid regions. Hydrol. Sci. Bull. 20(3), 305-327.

Fayer, MJ, Hillel, D. 1986. Air encapsulation: I. Measurement in a field soil. Soil Sci. Soc. Am. J. 50(3), 568-572.

Freeze, RA, Cherry, JA. 1979. Groundwater. Prentice-Hall, Englewood Cliffs, New Jersey.

Gerdel, RW. 1948. Physical changes in snow cover leading to runoff, especially to floods. IAHS-AIHS Publication 3142-53.

Gillham, RW. 1984. The capillary fringe and its effect on water-table response. J. Hydrol. 67(1-4), 307-324.

Guo, H, Jiao, JJ, Weeks, EP. 2008. Rain-induced subsurface airflow and Lisse effect. Water Resour. Res. 44(7), 136-144.

Healy, RW, Cook, PG. 2002. Using groundwater levels to estimate recharge. Hydrogeology Journal 10(1), 91-109.

Heliotis, FD, DeWitt, CB. 1987. Rapid water table response to rainfall in a Northern Peatland ecosystem. Water Res. Bull. 23(6), 1011-1016.

Hewlett, JD, Hibbert, AR. 1967. Factors affecting the response of small watersheds to precipitation in humid areas, in: Scopper, WE, HW Lull (Eds.), International Symposium on Forest Hydrology. Pergamon, Oxford, 275–290.

Horton, RE. 1933. The role of infiltration in the hydrologic cycle. Trans. Am. Geophys. Union 14446-460.

Horton, RE. 1940. An approach toward a physical interpretation of infiltration capacity. Soil Sci. Soc. Amer. Proc. 5399-417.

Jayatilaka, CJ, Gillham, RW. 1996. A deterministic-empirical model of the effect of the capillary fringe on near-stream area runoff 1. Description of the model. J. Hydrol. 184(3-4), 299-315.

Jayatilaka, CJ, Gillham, RW, Blowes, DW, Nathan, RJ. 1996. A deterministic-empirical model of the effect of the capillary fringe on near-stream area runoff 2. Testing and application. J. Hydrol. 184(3-4), 317-336.

Kendall, KA, Shanley, JB, McDonnell, JJ. 1999. A hydrometric and geochemical approach to test the transmissivity feedback hypothesis during snowmelt. J. Hydrol. 219(3-4), 188-205.

Khaled, IM, Tsuyoshi, M, Kohei, N, Taku, N, Hiromi, I. 2011. Experimental and modeling investigation of shallow water table fluctuations in relation to reverse Wieringermeer effect. Open Journal of Soil Science 1(2), 17-24.

Kirchner, JW. 2003. A double paradox in catchment hydrology and geochemistry. Hydrol. Process. 17(4), 871-874.

Linden, DR, Dixon, RM. 1975. Water table position as affected by soil air pressure. Water Resour. Res. 11(1), 139-143.

Lorentz, SA, Thornton-Dibb, S, Pretorius, C, Goba, P. 2004. Hydrological systems modelling research programme: Hydrological processes, Phase I:I Quantification of hillslope, riparian and wetland processes. WRC Report No. K5/1061 & K5/1086. Water Research Commission, Pretoria, South Africa.130 pp.

Marui, A, Yasuhara, M, Kuroda, K, Takayama, S. 1993. Subsurface water movement and transmission of rainwater pressure through a clay layer. IAHS Publ.463-463.

McDonnell, JJ. 1990. A rationale for old water discharge through macropores in a steep, humid catchment. Water Resour. Res. 26(11), 2821–2832.

McWhorter, DB. 1971. Infiltration affected by flow of air. Hydrol. Pap. 49. Colo. State Univ. Fort Collins, Colorado, USA.

Midgley, JJ, Scott, DF. 1994. Use of stable isotopes of water (d and o-18) in hydrological studies in the Jonkershoek valley. Water SA 20(2), 151-154.

Mosley, MP. 1982. Subsurface flow velocities through selected forest soils, South Island, New Zealand. J. Hydrol. 55(1-4), 65-92.

Nolan, KM, Hill, BR. 1990. Storm-runoff generation in the Permanente Creek drainage basin, west central California--An example of flood-wave effects on runoff composition. J. Hydrol. 113(1-4), 343-367.

Novakowski, KS, Gillham, RW. 1988. Field investigations of the nature of water-table response to precipitation in shallow water-table environments. J. Hydrol. 97(1-2), 23-32.

Ogunkoya, OO, Jenkins, A. 1993. Analysis of storm hydrograph and flow pathways using a three-component hydrograph separation model. J. Hydrol. 142(1), 71-88.

Peck, AJ. 1965. Moisture profile development and air compression during water uptake by bounded porous bodies: 3. Vertical columns. Soil Sci. 100(1), 44-51.

Powers, WL. 1934. Soil-water movement as affected by confined air. J. Agric. Res. 49(12), 1125-1134.

Sklash, MG, Farvolden, RN. 1979. The role of groundwater in storm runoff. J. Hydrol. 43(1-4), 45-65.

Sklash, MG, Stewart, MK, Pearce, AJ. 1986. Storm runoff generation in humid headwater catchments, 2, A case study of hillslope and low-order stream response. Water Resour. Res. 22(8), 1273–1282.

Torres, R, Dietrich, WE, Montgomery, DR, Anderson, SP, Loague, K. 1998. Unsaturated zone processes and the hydrologic response of a steep, unchanneled catchment. Water Resour. Res. 34(8), 1865-1879.

Touma, J, Vachaud, G, Parlange, JY. 1984. Air and water flow in a sealed, ponded vertical soil column: experiment and model. Soil Sci. 137(3), 181-187.

Turton, DJ, Barnes, DR, de Jesus Navar, J. 1995. Old and new water in subsurface flow from a forest soil block. J. Environ. Qual. 24(1), 139-146.

Turton, DJ, Haan, CT, Miller, EL. 1992. Subsurface flow responses of a small forested catchment in the Ouachita Mountains. Hydrol. Process. 6(1), 111-125.

Vachaud, G, Gaudet, JP, Kuraz, V. 1974. Air and water flow during ponded infiltration in a vertical bounded column of soil. J. Hydrol. 22(1-2), 89-108.

Waddington, JM, Roulet, NT, Hill, AR. 1993. Runoff mechanisms in a forested groundwater discharge wetland. J. Hydrol. 147(1-4), 37-60.

Wang, Z, Feyen, J, Nielsen, DR, van Genuchten, MT. 1997. Two-phase flow infiltration equations accounting for air entrapment effects. Water Resour. Res. 33(12),

Wang, Z, Feyen, J, van Genuchten, MT, Nielsen, DR. 1998. Air entrapment effects on infiltration rate and flow instability. Water Resour. Res. 34(2), 213-222.

Weeks, EP. 2002. The Lisse effect revisited. Ground Water 40(6), 652-656.

Wenninger, J, Uhlenbrook, S, Lorentz, SA, Leibundgut, C. 2008. Identification of runoff generation processes using combined hydrometric, tracer and geophysical methods in a headwater catchment in South Africa. Hydrol. Sci. J. 53(1), 65-80.

Wenninger, J, Uhlenbrook, S, Tilch, N, Leibundgut, C. 2004. Experimental evidence of fast groundwater responses in a hillslope/floodplain area in the Black Forest Mountains, Germany. Hydrol. Process. 18(17), 3305-3322.

Whitham, GB. 1974. Linear and nonlinear waves. Wiley-interscience

Wilson, LG, Luthin, JN. 1963. Effect of air flow ahead of the wetting front on infiltration. Soil Sci. 96(2), 136-143.

CHAPTER 2[†]

TRANSIENT PRESSURE WAVES IN THE VADOSE ZONE AND THE RAPID WATER TABLE RESPONSE

2.1   Abstract

The behaviour of a water table is important in understanding groundwater dynamics. In this paper, results are presented of a disproportionate response of a water table in two distinct transient pressure wave mechanisms that occurred during the rainfall events of the 2000/2001 summer season and in two different hillslope zones in the Weatherley research catchment of South Africa. The first type of pressure wave mechanism was a groundwater ridging pressure wave, which frequently occurred at the low-lying wetland zone and when the capillary fringe was very close to the ground surface. Results from this zone indicated that groundwater ridging water table responses were caused by rainfall events that had a threshold total rainfall of 10 mm and the magnitude of the responses had a linear relationship with the peak rainfall intensities. It was also found that the release of tension forces in the capillary fringe, due to the downward pressure wave, was 2.5 to 22.5 times faster than the subsequent rise of the water table (the upward pressure wave). This later finding, according to the law of conservation of energy, indicated an on-set of a lateral flow of water, below the rising water table. The second pressure wave mechanism, which exhibited the characteristics of the Lisse Effect (pneumatically pressurized water table response), occurred at an elevated zone of the catchment, where bedrock is overlain by a shallow soil profile and a perched groundwater. This second pressure wave mechanism was particularly evident during a certain rainfall event that occurred in the early part of the season. During this rainfall event, a peak rainfall intensity of 228 mm/h generated a pressure

---

wave from the ground surface towards the water table, where it rapidly and disproportionately elevated the hydraulic head in groundwater by 106 cm-H$_2$O, at the toe of the slope and without the recharge of the groundwater by the infiltration profile. The elevated hydraulic head at the toe of the slope rapidly overturned the hydraulic gradients, from 0.0100, in the downslope direction, to 0.0105, in the upslope direction, in just 24 minutes. The overturned hydraulic gradients reversed the flow of water from a downslope direction to an upslope direction. The overturning wave, which originated with an elevated pressure potential of 106 cm-H$_2$0, at the downslope observation nest, travelled with an average velocity of 2 m/h and arrived at an adjacent observation nest, 46 m up the slope, with an attenuated pressure potential of 31 cm-H$_2$O. A laboratory experiment was performed to verify this second transient pressure wave mechanism and to investigate the involved processes. Results from the laboratory experiment verified that the second pressure wave was the Lisse Effect and that, as in the groundwater ridging, the capillary fringe plays a significant role in the rapid response of the water table. In conclusion, both the Lisse Effect and groundwater ridging may result in disproportionate groundwater fluxes, which is successively caused by the conversion of the capillary fringe and a disproportionately rapid water table rise.

2.2　　　Introduction

Previous studies (e.g. Pinder and Jones 1969, Sklash and Farvolden, 1979 and Wenninger *et al.*, 2004) have shown that during a rainfall event, pre-event water, which is predominantly groundwater, may appear in significant amounts in the stream stormflow hydrograph. Therefore, a comprehensive understanding of the dynamics of groundwater fluxes is important. However, in order to understand groundwater dynamics and the appearance of pre-event water in the stormflow hydrograph, it is necessary to understand the behavior of the groundwater table response during a rainfall event.

Mechanisms that have been reported in literature of a rapid water table response during a rainfall event, include: (1) the cessation of the water uptake by plants, which might occur, as a result of the reduction in evapotranspiration caused by cooler temperatures, wet leaf and long diminished sunlight hours (White, 1932 cited in Heliotis and DeWitt, 1987); (2) macropores, which enhance the rapid delivery of rain water to the water table (McDonnell, 1990); (3) groundwater ridging (Gillham, 1984); (4) the Lisse Effect (Heliotis and DeWitt, 1987; Weeks, 2002); and (5) the near-zero pressure-head-range pressure wave (Torres *et al.*, 1998). The latter three mechanisms are caused mainly by pressure waves, generated from the ground surface and transmitted through the vadoze zone to the water table. Consequently, the water table responds rapidly to the changes in pressure and not to the recharge from the infiltration profile. Furthermore, these three mechanisms have also been proposed to account for the rapid mobilization of pre-event water from hillslopes (Gillham, 1984; Torres *et al.*, 1998; Lorentz *et al.*, 2004).

The groundwater ridging has been commonly observed in environments, where the water table is shallow and the capillary fringe, or the zone of tension saturation, extends to, or intersects with, the ground surface. In such environments, it has been found (e.g. Gillham, 1984 and Abdul and Gillham, 1989) that the addition of a small amount of water results in a disproportionate rise of the water table, compared with the expected rise from the specific yield concept. Gillham (1984), for instance, reported a field experiment, in which an addition of 0.3 cm of water in an area with a shallow water table resulted in a 30 cm rise of the water table in 0.25 minutes. Later, Abdul and Gillham (1989) carried out field experiments on a plot measuring 18 m wide by 90 m long and traversed by a stream channel. These researchers applied a simulated rainfall over the plot, using a sprinkler irrigation system and observed a disproportionate rise of the water table, which was attributed to the initial proximity of the capillary fringe to the ground surface. Apart from

field experiments, laboratory experiments (Abdul and Gillham, 1984; Heliotis and DeWitt, 1987 and Khaled *et al.*, 2007) and theoretical and numerical modeling approaches (Jayatilaka and Gillham, 1996; Jayatilaka *et al.*, 1996 and Khaled *et al.*, 2011) have been used to evaluate groundwater ridging. It seems that most of the studies on groundwater ridging have been limited mainly to partially-controlled field experiments, fully-controlled laboratory experiments and theoretical/numerical simulations. Lack of observations of groundwater ridging in the field conditions has generated skepticism among researchers regarding its practicability under natural rainfall (Buttle and Sami, 1992 and McDonnell and Buttle, 1998).

The Lisse Effect may occur in environments, where the water table is deep enough to allow an unsaturated zone, with a sufficient and continuous volume of pore air, above the capillary fringe. During an intense rainfall, or a flooding event, on the ground surface, an infiltration profile is generated, which may cap the ground surface and engulf air ahead of the wetting front. If the lateral escape routes of air are limited, due to the tortuosity of the pathways; and the vertical counterflow of air is impeded by an infiltration profile; further downward movement of the wetting front compresses and increases the pore air pressure ahead of the wetting front. The increased pressure in air is immediately transferred; in an action process, to the water table below and; in a reaction process, to the wetting front above. The reaction effect of compressed pore air on infiltration has been widely studied (Adrian and Franzini, 1966; McWhorter, 1971; Touma *et al.*, 1984; Wang *et al.*, 1998).

The action of compressed pore air on the water table contributes to the pressure potential term in the groundwater, which is reflected in the rapid rise of a water level in a well, screened below the water table (Weeks, 2002). The action of compressed pore air influences the flow of water by way of total potential gradient (Bond and Collis-George, 1981). It has been noted that the Lisse Effect occurs in areas with rainfall of high magnitude and intensity, which may result in disproportionate rises in water levels that are 50-250 % higher than predicted from the specific yield (Heliotis and DeWitt, 1987; Weeks, 2002). Nevertheless, the physical processes, by which the Lisse Effect rapid water table response occurs, are not yet clear.

The near-zero pressure head range pressure wave was first observed in the field experiments and described in detail by Torres *et al.*, (1998), and latter observed in column experiments by (Rasmussen *et al.*, 2000). By the application of steady irrigation rates on the ground surface, Torres *et al.* (1998) maintained dynamic equilibrium conditions between

groundwater discharge, saturated zone and the unsaturated zone, which was at near-zero pressure head. Under these conditions, an application of a spiked intensity rainfall, caused a rapid pressure wave through the unsaturated zone, followed by a disproportionately rapid response in the saturated zone and groundwater discharge. Torres *et al.* (1998) explained that the rapid pressure wave may have elevated the hydraulic head gradient that caused a rapid effusion of stored pre-event water from the unsaturated zone. The effused pre-event water caused the rapid rise in the saturated zone and thus, increased groundwater discharge.

This paper distinguishes between a deep water table and a shallower water table by the position of the capillary fringe, with respect to the ground surface. A deep water table occurs, where the capillary fringe is sufficiently below the ground surface, to allow a sufficient depth of unsaturated zone, with a continuous pore air, in that the Lisse Effect may occur during an intense rainfall. Previous studies e.g. Heliotis and DeWitt (1987) and Weeks (2000) indicate that the Lisse effect may occur where the depth of the unsaturated zone is between 0.5 to 2.0 m. A shallow water table occurs, where the capillary fringe is close to, or intersects with, the ground surface. Furthermore, in this paper, a capillary fringe is defined as a zone of tension saturation. That is, the zone immediately above a water table, in which all the soil pores are filled with water, which is under tension pressure.

The objectives of this paper are: (1) to describe and analyze the rapid response of a water table in a groundwater ridging transient pressure wave mechanism that frequently occurred at a wetland zone of the study catchment; (2) to describe and analyze the rapid response of a water table to a transient pressure wave mechanism (which exhibited the characteristics of the Lisse Effect) that occurred during a certain rainfall event and in a raised zone of the study catchment; and (3) using a laboratory experiment, to verify the nature of the second transient pressure wave mechanism (in 2 above) and evaluate the involved physical processes.

2.3   Methodology

2.3.1   Field study site

2.3.1.1.   Field set-up

The field data were from observations made in two different hillslope zones of the Weatherley research catchment, which is located in the uMzimvubu Water Management Area (WMA) in the northern Eastern Cape Province of South Africa (Figure 2.1). The catchment lies at a latitude of 31° 06' 00'' S, a longitude of 28° 20' 10'' E and at an altitude of approximately 1300 m. The average annual rainfall in the catchment is about 740 mm, of which 82 % is received between October and March (summer period) (Lorentz *et al*., 2001). The catchment, which covers an area of 1.5 km^{2} and drains in a northerly direction, contains a wetland that lies along the entire reach of the stream.
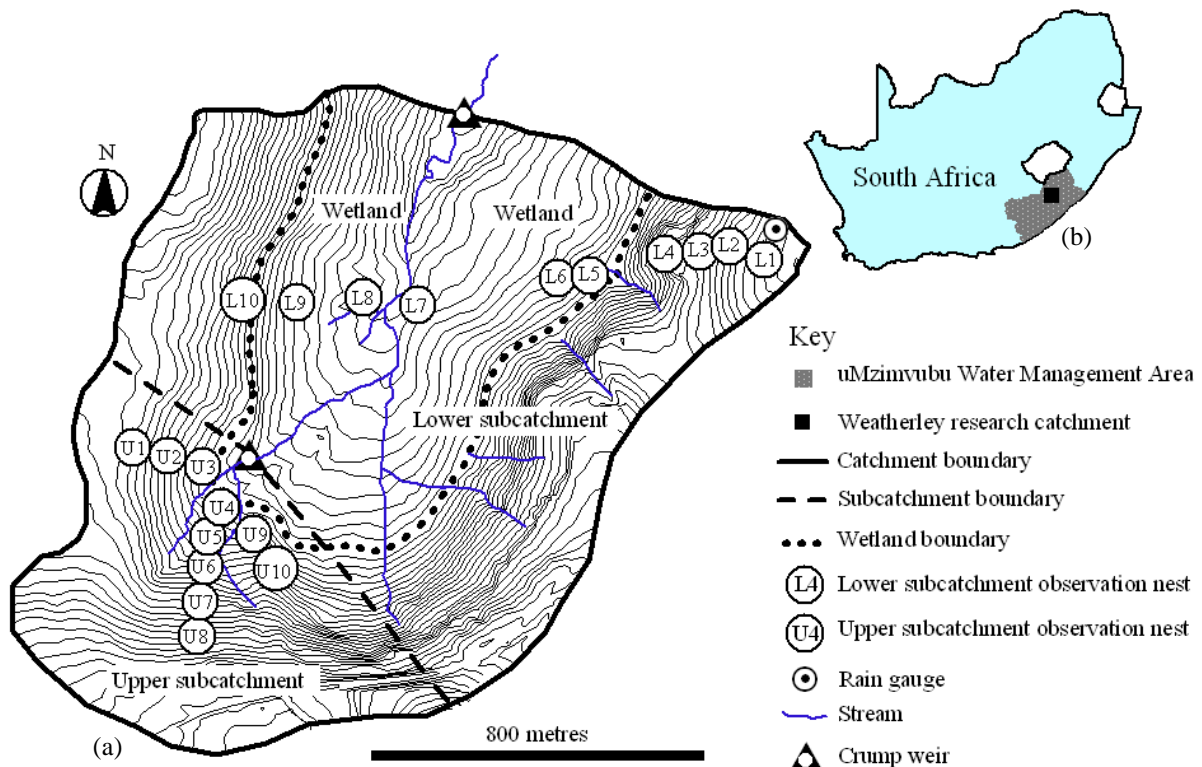
Figure 2.1 (a) The Weatherley research catchment and (b) its location in South Africa (from Lorentz *et al*., 2001).

About 200 m from the stream, in an easterly direction, there is a bedrock outcrop (between observation nests L4 and L5, in Figure 2.1), which runs almost parallel to the stream. The bedrock outcrop is about 12 m in altitude above the stream bed. This bedrock forms a shelf, over which lies a varying depth of soil. This area, henceforth referred to as 'a hillslope zone,' is one of the two zones, from where a water table response to a transient pressure wave was analyzed. The data used in the analysis were from the observation nests L2, L3 and L4 (also shown in Figure 2.2). At this zone, the average depth of the soil profile to bedrock varies from 2.5 m at the peak of the hillslope (near L1), to about 3.5 m in the middle of the slope (at L3) and thins out to zero at the bedrock outcrop (a few metres in the downslope of L4). The absolute length of the bedrock, and thus of the hillslope zone, is about 250 m (Figure 2.2). The second zone used in the analysis of rapid water table response is the wetland zone. This zone was selected because, according to the literature (e.g. Gillham, 1984; Heliotis and DeWitt, 1987), groundwater ridging rapid water table response is most likely to occur at the wetland or swampy areas. At the wetland zone, for this part of the study, data from observation nests U3, U4 and the stream discharge over the upper weir, were used.

At the present time, the land-cover over the catchment consists of patches of trees, which were planted in 2002, and patches of highland sourveld grassland. Typical grass species include *Themeda triandra* and *Tristachya leuctthrix*. Succulent species of the group *Aloe* and *Crassula* are common at shallow slopes. Generally, these grass species have shallow root systems. At the hillslope zone, the forested area covers observation nests L2 and L3, while ground cover at observation nest L1 and L4 is mainly grass. Recent observations indicate that the establishment of trees in this zone of the catchment has resulted in the depletion and complete absence of groundwater in some areas, especially at L3. The entire wetland zone is covered by shallow rooted grass.

2.3.1.2. Soil physical properties

At the hillslope zone, the soils are generally sandy loam in the upper horizons and sandy clay in the lower horizons. The dominant infiltration mechanism in the areas that are covered by grass is through the soil matrix. There were small macropores, due to small holes left by rotten vegetation roots, but they hardly extend below 10 cm below the ground surface (this was observed in the present study during the excavation of the soil profile for

samples from L4 and U3). Therefore, infiltration by preferential flow is generally insignificant. At the upper sub-catchment wetland zone, sandy loam soil and loamy clay soil appear at U1-U3 nest-axis and U4-U8 nest-axis, respectively. The specific physical soil properties i.e. hydraulic conductivities, bulk densities and porosity at each of the selected observational nests, are shown in Table 2.1
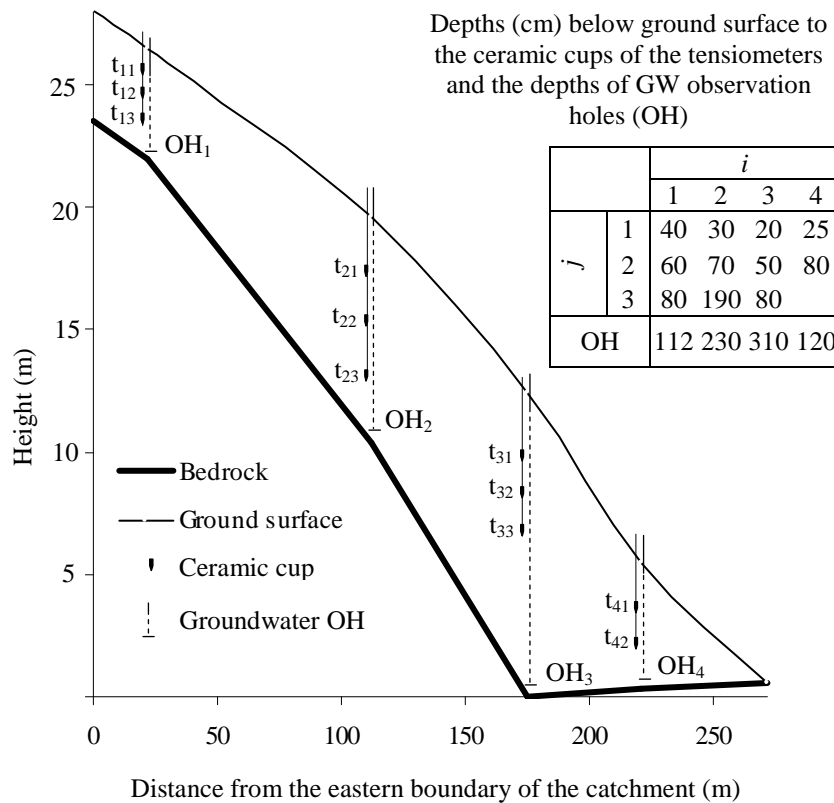
Figure 2.2 Positions of the tensiometers and groundwater observation holes (GWOH) in the soil profile at the raised hillslope zone (vertical scale is exaggerated 4 times). i = observation nest; j = tensiometer number; OH = groundwater observation hole; t_{ij} = tensiometer number j below the ground surface and at the observation nest Li; and OH$_i$ is the groundwater observation hole at observation nest Li.

The hydraulic properties, specifically water retention characteristics and hydraulic conductivities, were determined both in the field and in the laboratory (Klute and Dirksen, 1986 and Bruce and Luxmore, 1986). Field measurements at each of the indicated depths (Table 2.1) of the soil profile were carried out by tension disc and double ring infiltrometers. Undisturbed cores of soils were sampled from the indicated depths for laboratory tests, which included water retention characteristics, saturated hydraulic conductivities, bulk

densities and particle size distribution. This set of data was obtained from Lorentz *et al.* (2001). During the present investigation, tests of particle size distribution of the soil samples, from observations nests U3 and L4, were determined in the laboratory (Table 2.1).

Table 2.1 The physical properties of the soils at the selected observation nests (obtained from Lorentz *et al.*, 2001) and of the soil used in the laboratory experiments.

Site	Depth (m)	K_s (cm/h)	h_a (cm)	Soil texture	Porosity	Density (Kg/m^3)	*CS (%)	*MS (%)	*FS (%)	*S&C (%)
L2	0.00	38.81	39.20	SaLm	0.37	1750				
	0.40	3.97	21.46	SaLm	0.33	1775				
	0.80		49.75	SaLm	0.30	1850				
L3	0.00	32.94		SaLm						
	0.50	3.97	10.14	SaLm	0.32	1791				
	0.70		0.61	Lm	0.34	1760				
	1.50		71.94	ClLm	0.30	1871				
L4	0.00	29.24		SaLm						
	0.20	0.50	78.74	SaLm	0.286	1892	18.3	29.0	42.4	10.2
	0.50	0.72	8.70	SaLm	0.352	1717	21.8	26.3	44.7	7.2
	0.90	0.72		SaSiCL			23.8	30.3	41.0	4.8
*U3	0.00-0.40	2.35	43.25	SaLm		1818	12.9	16.4	36.5	34.1
	0.40-0.80	11.32		SaLm		1410				
U4	0.00			ClLm	0.468	1410				
	0.20			ClLm	0.428	1516				
*Lab	0-1.7	45	20	Sa	0.44	1500	26.0	72.0	2.0	

K_s = Saturated hydraulic conductivity, h_a = pore air entry pressure head, CS = coarse sand (0.50 – 2.00 mm), MS = medium size sand (0.25 – 0.50 mm), FS = fine sand (0.053 – 0.25 mm), S&C = Silt & Clay (< 0.053 mm). *Data determined during the present study.

2.3.1.3.   Instrumentation

The instrumentation and observations programme in the Weatherley research catchment started in 1995 to provide necessary data for the evaluation of the impact of forestation on the hydrological processes in the catchment (Wenninger *et al.*, 2008). The catchment was monitored in its pristine state up to 2002, when a section of the catchment's area was afforested (*Pinus Patula*, *Pinus Elliotti* and *Ecalyptuc Nitens*). Each observation nest at the hillslope zone consisted of a groundwater observation hole, installed to bedrock, for monitoring groundwater levels, as well as ceramic-cup tensiometers installed at different depths in the soil profile (Figure 2.2), for the measurement of the soil pore water pressure.

The observation nests U3 and U4 did only have tensiometers. Therefore, the water table responses at these nests were analyzed based on the soil pore water pressure, in which positive and negative pressure potentials imply a water table above and below the point of measurement, respectively. At U3, the ceramic cups of the shallower and deeper tensiometers were installed at 20 cm and 100 cm below the ground surface, respectively. At U4, the ceramic cup of the shallower tensiometer was at 30 cm and that of the deeper tensiometer was at 110 cm, below the ground surface.

Rainfall data were recorded via a tipping-bucket rain gauge, with an accumulation of 0.2 mm of rainfall per tip. The rain gauge logger recorded the data at one minute intervals. A detailed description of the catchment is found in Lorentz *et al.* (2001), Lorentz *et al.* (2004) and Wenninger *et al.* (2008).

Between November 1999 and April 2005, the data of tensiometric pore water pressure and water levels were monitored, recorded and stored automatically on Onset HOBO loggers. Both the data of pore water pressure, as well as of the water level, were transmitted and temporarily stored on Onset HOBO loggers via I bar Motorola MPX5100DP differential pressure transducers. This set of data was recorded with a time resolution of 12 minutes. The field data used in the present study was of the summer season of 2000/2001, when the observation programme was fully automated and prior to the establishment of trees. The summer season of 2000/2001 was selected because it had the best data in terms of continuity, compared to other observation periods.

2.3.1.4. Rainfall events

The responses of the water table were analyzed, based on rainfall events, which were based on the period above a minimum threshold of rain. Six hours, with less than 1.2 mm of rainfall, was chosen as the boundary between sequential rainfall events. For each rainfall event, hourly rainfall depths, as well as one-minute rainfall intensity, were computed.

2.3.2   Laboratory experiment

2.3.2.1.   Laboratory apparatus

The physical laboratory model consisted of a column of soil in a vertical PVC pipe with an internal diameter of 30 cm and a height of 300 cm. The soil was graded silica quartz (SiO_2), which was uniform in shape and the individual grains were stable and clean, free of organic matter. The particle size distribution, the saturated hydraulic conductivity and the water retention characteristics of sand were determined in the laboratory following the methods and procedures of Gee and Bauder (1986), Klute (1986) and Klute and Dirksen (1986), respectively. The values of the physical properties of the soil used, are shown in Table 2.1.

Seven data takeoff ports were installed along the pipe, at 60, 90, 120, 130, 140, 150 and 160 cm below the soil surface, which was at 40 cm below the top of the PVC pipe. Each data takeoff port consisted of three probes: a 0.5 bar miniature tensiometer for the measurement of soil pore water pressure, a Time Domain Reflectometry (TDR) for the measurement of volumetric water content and a pore air pressure probe for the measurement of pore air pressure. A drainage/discharge tube and a piezometer were attached to the column at a depth of 170 cm below the soil surface, for groundwater discharge and monitoring of the water table, respectively.

The TDR probes used, were made of three parallel stainless steel rods with, an exposed length of 100 mm, a diameter of 5 mm, impeded in a PVC block and at a separation distance of 17 mm. The soil water content data, measured by TDR, were recorded and temporarily stored on a CR1000 Campbell Scientific data logger via a SDMX50 Multiplexer and Campbell Scientific TDR100 wave generator. Miniature tensiometers consisted of a 15 mm-long ceramic-cup, with an outer diameter of 5 mm. The open end of the ceramic cup was joined to one end of a PVC tube with the same outer diameter. The other end of the PVC tube was connected to a differential pressure transducer. The data of pore-water pressure and pore-air pressure were recorded and temporarily stored on a CR1000 Campbell Scientific data logger via differential pressure transducers of 1 bar Motorola MPX5100DP and 0.1 bar Motorola MPX5010DP, respectively.

The pore-air pressure probe was developed for the measurement of compressed pore air. The probe was made of a PVC cylindrical solid rod, 14 cm long and 2 cm in diameter and with a hydrophobic membrane (see Figure 2.3). Holes, of 5 mm diameter, were drilled

across the PVC cylindrical solid. These transverse holes, which were drilled over a 5 cm length-portion of the cylindrical solid, were orthogonally traversed by a 2 mm diameter hole made in the longitudinal centre of the rod. The 2 mm diameter longitudinal hole only penetrated the cylindrical solid at the back end. The section of the probe, over which the transverse holes were made, was recessed and wrapped in a hydrophobic membrane, which allowed only the passage and flow of air. The hydrophobic membrane only allowed the passage of water at very high pressures, >5 cm-H_2O. A short, 5 mm diameter PVC tube, linked the probe from its back end to the differential pressure transducer. For ease of installation, the front end of the probe was made pointed.
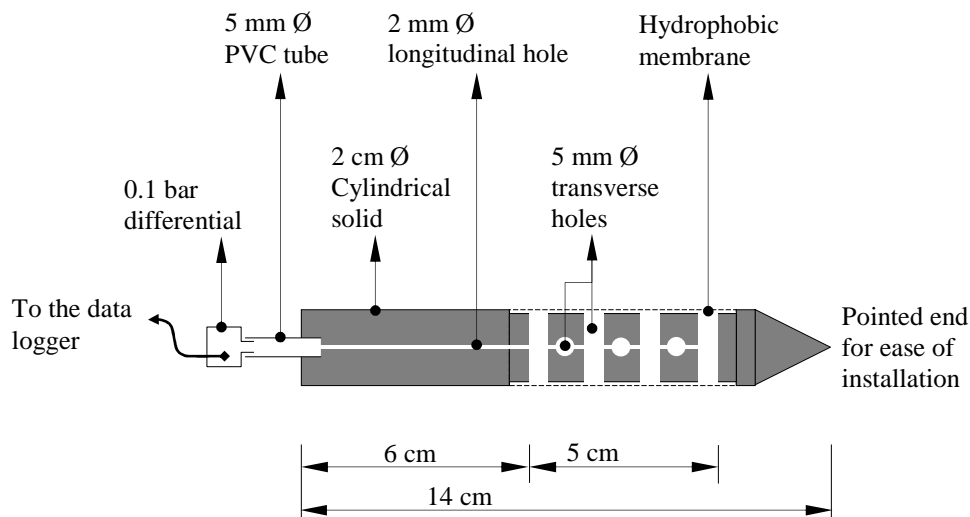
Figure 2.3 Schematic presentation of the pore-air pressure probe.

In the remaining part of this paper, for brevity and ease of reference, a specific data-takeoff port will be referred to as 'Port', followed by its depth, below the soil surface. For example, 'Port 60' refers to the data take-off port, which is also located at 60 cm below the soil surface. All the pressures reported in this paper are in height of water, specifically cm-H_2O.

2.3.2.2.   Experimental procedure

The PVC cylindrical pipe was packed with dry silica sand, in layers of ~55 cm high. After each layer, the wall of the pipe was tapped with the same number of blows, in order to

achieve uniform maximum density and packing. The TDRs and the pore-air pressure probes were inserted in the wall of the PVC pipe before being packed with sand. The ceramic-cup miniature tensiometers, due to their fragility, were inserted after packing the column. All the probes were inserted into the column of soil and the entire wall of the pipe was sealed to an air-tight state. The column of soil was instrumented as shown in Figure 2.4.

Water was introduced in the packed column of soil from the bottom to minimize the entrapment of pore air, which has been found to contribute to disproportionate water table responses (Peck, 1960; Weeks, 1979). By adjusting the level of the nozzle of the discharge tube, the initial water table was set at Port 160, as shown in Figure 2.4. The capillary fringe, of which the height was taken as equivalent to the air-entry pressure value, or the bubbling pressure, of the soil (Brooks and Corey, 1964, 1966), extended to about 20 cm above the water table. The bubbling pressure of the soil is the pressure at which a continuous non-wetting phase exists in a porous media. The initial conditions of the soil column were, as shown in Figure 2.4.
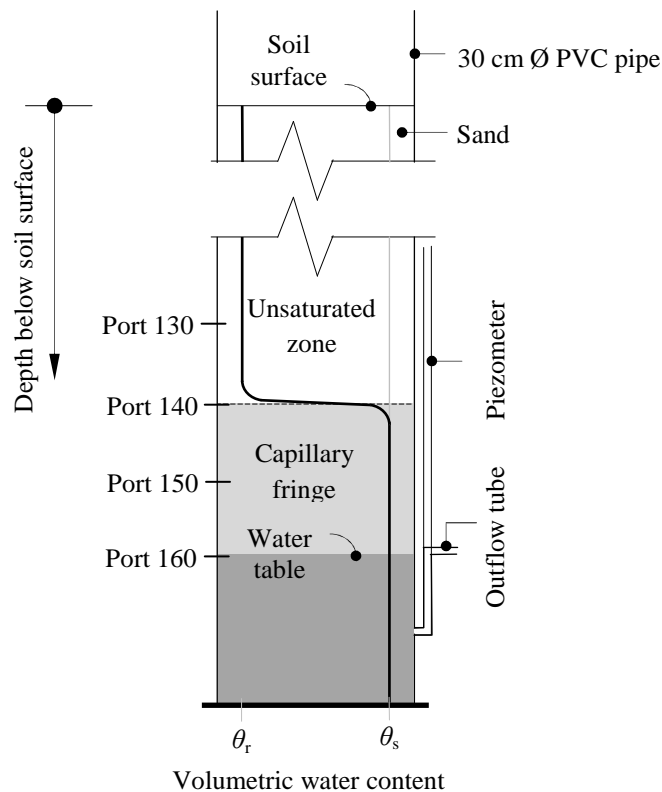
Figure 2.4 The initial conditions (pre-simulations conditions) for the laboratory experiment. θ_r = residual soil water content, θ_s = saturated soil water content.

With the described set up, the experiment was initiated by ponding the soil surface with 15 cm of water. Groundwater fluxes, tensiometric pore water pressure, volumetric water content and pore air pressure were monitored and recorded at a time-resolution of 20 seconds, starting from the moment the soil surface was ponded.

2.4 Results

2.4.1 Rainfall events

The total of 96 rainfall events occurred during the summer season of 2000/2001 in the Weatherley research catchment. The general characteristics of the rainfall events are summarized in Table 2.2. Only the rainfall events that caused rapid water table response, at the selected observation nests at the wetland zone or/and at the hillslope zone are included. The events are ordered according to their dates of occurrence. The total rainfall amount recorded during this period was 947 mm, which was significantly above the mean annual precipitation amount of 740 mm in this catchment (Lorentz *et al.*, 2004; Wenninger *et al.*, 2008). 70% of the rainfall events were less than 10 mm. Event 19 had the highest rainfall, namely 67.8 mm, as well as the highest peak 1-minute intensity, namely 228 mm/h. These high intensities may have an error of about 20-30%, since tipping bucket rain gauges have been found (Habib *et al.*, 2001) to overestimate the intensities of rainfall as the bucket cannot be emptied completely.

Table 2.2 Rainfall events that caused rapid water table responses in the Weatherley research catchment during the summer season of 2000-2001.

Event No.	Date	Start time (h)	End time (h)	Event duration (h, m)	Total rainfall (mm)	Max. 1-min intensity (mm/h)	Time of max intensity (h)
	2000						
19	8 Nov.	1541	1705	1, 24	67.8	228	1633
20	12 Nov.	1638	1655	0, 18	4.6	60	1642
22	18 Nov.	1040	2343	13, 03	11.4	24	1751
28	28 Nov.	1343	1836	4, 53	16	84	1356
32	3 Dec.	1432	1751	3, 19	10.8	66	1439
34	7 Dec.	1732	2358	6, 26	12.4	18	1914
36	10-11 Dec.	1309	2232	33, 23	42.8	24	1316
38	20 Dec.	1722	2037	3, 15	29.4	78	1834
39	24-25 Dec.	1359	1435	24, 36	31.2	90	1647
	2001						
42	1-2 Jan.	0001	0653	30, 52	27	30	0707
43	8 Jan.	1350	2304	9, 14	20	18	2100
46	13-14 Jan.	1406	1108	21, 02	28	84	1812
47	18 Jan.	1804	1941	1, 37	11.2	30	1815
48	19 Jan.	1550	2111	5, 21	4.6	12	1557
49	20 Jan.	1537	1555	0, 18	6.8	48	1543
54	28-29 Jan.	1207	0058	12, 51	39.8	42	1252
58	7 Feb.	1742	2039	2, 57	15	48	1756
60	13-15 Feb.	1640	0451	36, 11	56.4	60	1721
62	19 Feb.	1556	2010	4, 14	16.2	84	1600
65	23 Feb.	1351	2126	7, 35	21.8	48	1451
70	10 Mar.	1316	2028	7, 12	47.2	102	1405
75	17 Mar.	1410	1924	5, 14	26.6	132	1532
80	23 Mar.	1645	2219	5, 34	17.6	66	1637
88	8 Apr.	1931	2048	1, 17	8.6	66	2040
89	10 Apr.	1908	1938	0,30	32	156	1925
93	23 Apr.	1847	2231	3, 44	12.6	90	2032

2.4.2 Field observations of rapid water table responses to transient pressure waves

2.4.2.1. Rapid water table response to groundwater ridging transient pressure wave at a wetland zone

Responses of the soil pore water pressure at the observation nests U3 and U4, at the wetland zone, are shown in Figure 2.5. The water table at U4 seems to have remained at the ground level, starting from December 2000, until April 2001. This is attributed to the type of soil at U4, the heavy clay soil that did not easily drain, after saturation. The type of soil at U4 did not easily allow the passage of pressure due to the rainfall on the ground surface down the soil profile.

On the other hand, at U3, three main temporal phases are noted in the responses of the pore water pressure to the rainfall events. Phase 1 occurred during the months of September and October, in which the water table (capillary fringe) was still deep and the upper tensiometer recorded extremely dry conditions. The tensiometric pore water responses, to the rainfall events in Phase 1, are generally characterized by very large changes in pressure potential. In Phase 3, the water table was nearly always above the shallower tensiometer. Phase 2 begins from mid-November to mid-March and is characterized by the oscillation of the water table (zero pressure head) around the shallower tensiometer. It is worth noting that the two tensiometers exhibited a more uniform pattern during Phase 2 than in the other two phases. From the position of the shallower tensiometer below the ground surface, resonance of the water table around this shallower tensiometer, the water retention characteristics of the soil at this nest (h_a = 45 cm, Table 2.1) and the rapid and simultaneous responses of the two tensiometers, groundwater ridging transient pressure wave water table response may have occurred frequently during Phase 2. A close similarity can also be seen in the responses to the rainfall events, of the tensiometers at U3 (Phase 2) and the stream discharge over the upper weir.
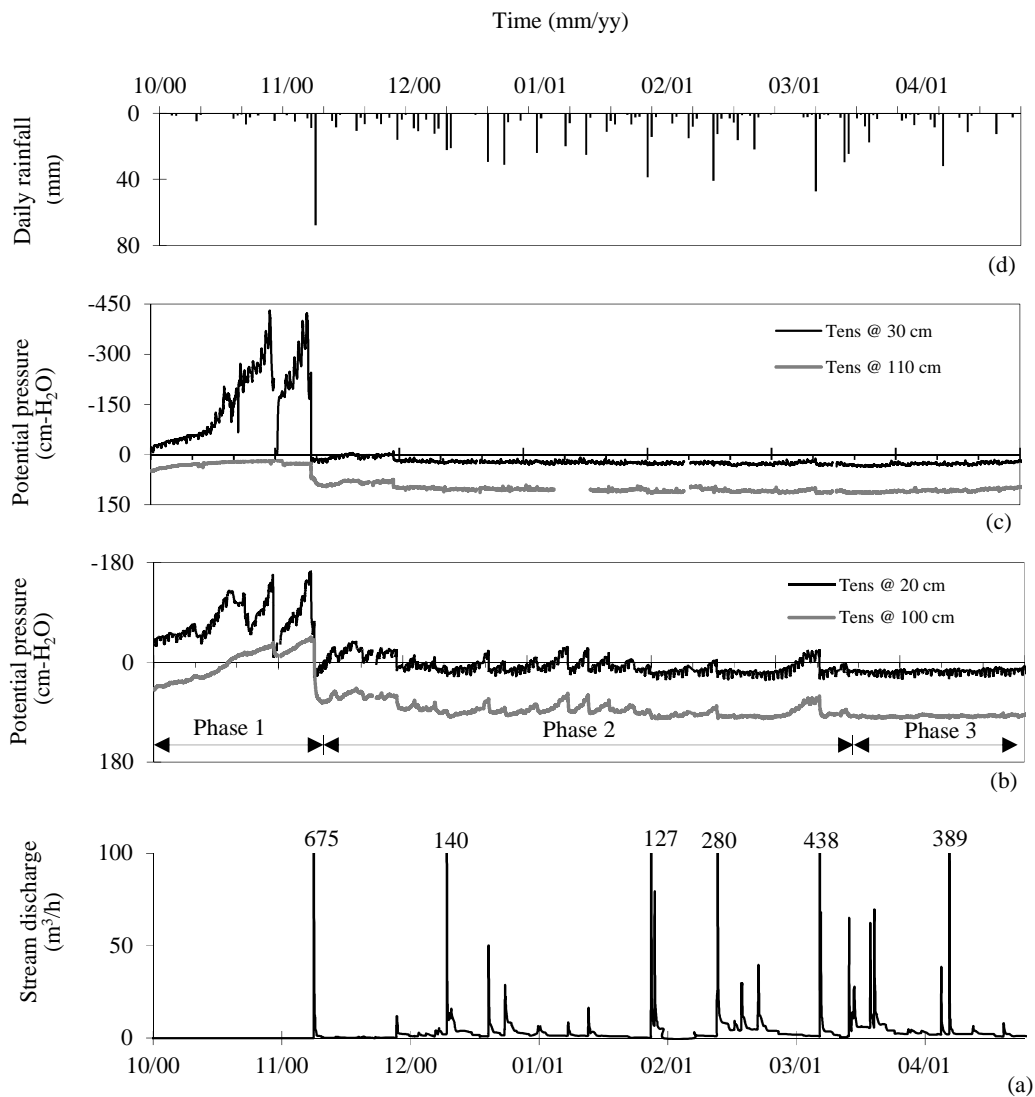
Figure 2.5 The response of (a) the stream discharge over the upper weir, (b) the tensiometric pore water pressure at U3 and (c) the tensiometric pore water pressure at U4 to (d) the daily rainfall during the summer season of 2000/2001. The stream discharge axis in (a) is truncated at 100 m³/h. The values on the discharge curve are the respective temporal maximum flow rate for discharges > 100 m³/h.

Factors that control the groundwater ridging water table response

An analysis was carried out to assess the effect of peak rainfall intensity and total rainfall depth on the pore water pressure responses, indicated by the shallower tensiometer at the observation nest U3. It was found that groundwater ridging only occurred in the rainfall events that had a minimum total rainfall depth of 10 mm (Figure 2.6).
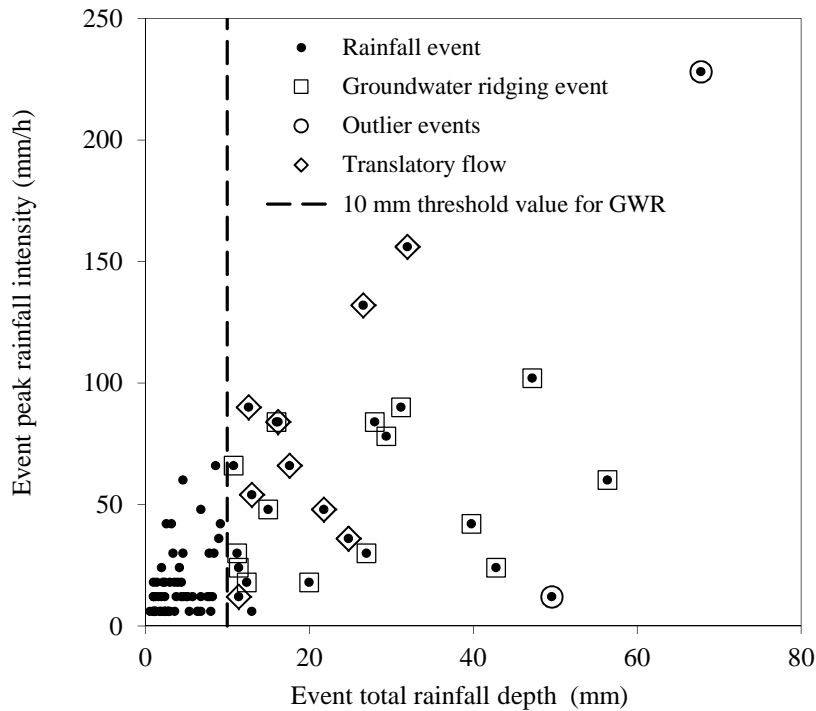
Figure 2.6 The influence of peak rainfall intensity and total rainfall depth on the water table response to groundwater ridging (GWR) transient pressure wave at U3.

A separate analysis of the position of the water table, via the pressure potential values of the deeper tensiometer, indicated that in addition to the threshold rainfall amount, groundwater ridging pressure wave occurred only, when the water table was between 43.4 and 18.9 cm below the ground surface (Table 2.3). This requirement of the initial position of the water table explains the presence of the two outlier rainfall events (in Figure 2.6), which yielded more than 10 mm of rainfall, but did not cause groundwater ridging water table response. In these two events, the initial water table was below the deeper tensiometer (>100 cm below the ground surface). This implies that the capillary fringe was too deep, for groundwater ridging to occur.

Similarly, the initial water table requirement indicates the significant role played by the soil water content, which can be inferred from; the time interval the end-time of one rainfall event and the start-time of the next rainfall event, as well as from the pre-event values of the pressure potentials. It was observed that all the events that caused groundwater ridging had a minimum separation time of 3.72 days between events (Table 2.3). This minimum separation time was required for drainage and recovery of the capillary fringe, before the

subsequent groundwater ridging pressure wave could occur. The role of the initial soil water content in groundwater ridging was also inferred from initial values of pressure potential recorded by the shallower tensiometer. For the events that caused groundwater ridging, the shallower tensiometer recorded pre-event pressure potential values of between -1.30 and -27.20 cm-H2O. In events, where the total rainfall depth was greater than 10 mm and the shallower tensiometer recorded higher values of pressure potential, a translatory or a piston flow (Lischeid *et al.*, 2002; Becker and Kaden, 2003) type of pressure wave might have occurred (Figure 2.6). The water table might have been very close to the ground surface, or at the ground surface (entire soil profile is under positive pressure), and any disturbances on the ground surface only generated a pressure wave that was transmitted through the saturated zone, without any effect on the water table.

Table 2.3 Rainfall events in which the water table response to a groundwater ridging transient pressure wave occurred at observation nest U3. The pre-event water table (WT) was estimated from the pressure potential (PP) values of the deeper tensiometer.

Rainfall					Response of the shallower tensiometer (at 20 cm)			Pre-event WT below ground surface	Time since previous event with rainfall >10 mm
Event No.	Start time		Total depth	Max. intensity	Start PP	End PP	Total PP		
	Date	(h)	(mm)	(mm/h)	(cm-H$_2$O)			(cm)	(d)
28	28 Nov. 2000	1343	16	84	-23.85	15.68	39.53	32.54	19.86
32	3 Dec. 2000	1432	10.8	66	-1.30	8.72	10.02	23.63	4.83
34	7 Dec. 2000	1732	12.4	18	-10.49	12.06	22.55	26.97	3.99
38	20 Dec. 2000	1722	29.4	78	-20.80	17.08	37.88	34.50	8.78
39	24 Dec. 2000	1359	31.2	90	-2.14	20.70	22.84	18.90	3.72
42	1 Jan. 2001	0001	27	30	-9.38	15.12	24.50	23.40	6.39
43	8 Jan. 2001	1350	20	18	-27.20	12.62	39.82	43.40	6.29
46	13 Jan. 2001	1406	28	84	-24.41	15.96	40.37	40.89	4.63
47	18 Jan. 2001	1804	11.2	30	-18.29	9.83	28.12	31.43	4.29
60	13 Feb. 2001	1640	56.4	60	-5.20	27.38	32.88	20.85	5.83
70	10 Mar. 2001	1316	47.2	102	-23.57	30.44	54.01	39.22	14.66

A general linear relationship was identified between the intensity of rainfall and the total reaction of the shallower tensiometer (Figure 2.7). This linear relationship implies that the higher the rainfall intensity, the larger the response of the water table. The influence of rainfall depth and intensity on groundwater ridging water table response, for two representative rainfall events, is schematically shown in Figure 2.8.
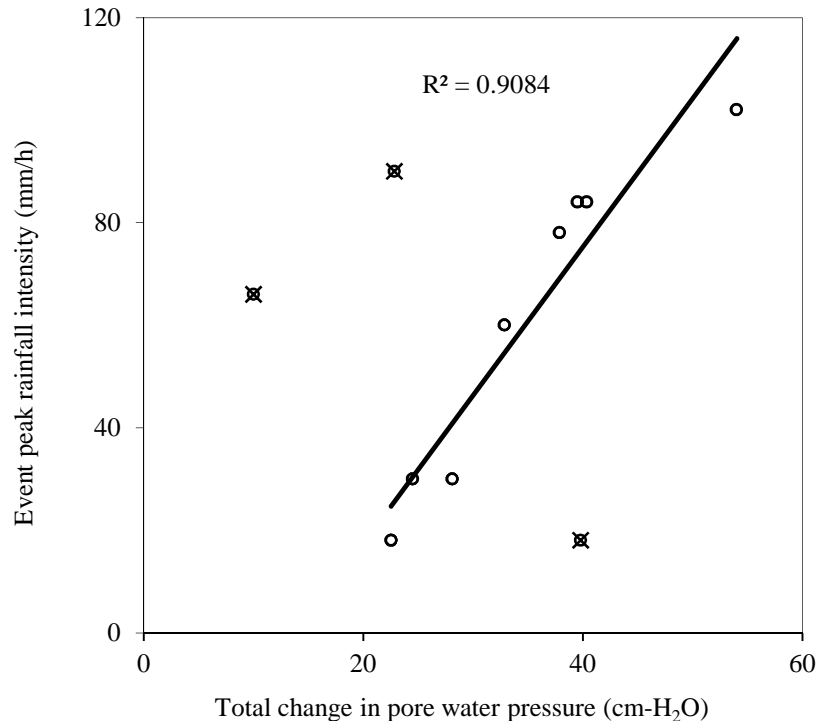
Figure 2.7 General linear relationship between events' peak rainfall intensities and the total changes in pore water pressure within the capillary fringe (at the shallower tensiometer) during the groundwater ridging transient pressure waves at U3. The R^2 of 0.9084 is achieved, when the three crossed events are excluded. In the three events, the tensiometer recorded the most extreme values of pre-event pressure potential; the upper two events had the highest values, while the lower single event had the lowest value (see Table 2.3).

Figure 2.8 (a) is the response of the tensiometers to the rainfall Event No. 43, which had a total rainfall depth of 20 mm and a peak intensity of 18 mm/h. Figure 2.8 (b) is the response of the tensometers to the rainfall Event No. 70, which had a total rainfall depth of 47.2 mm and a 1-minute peak intensity of 102 mm/h. The pre-event pressure potential values of the shallower tensiometer, in the two events, were -27.2 cm-H_2O and -23.6 cm-H_2O, respectively. The rate of and the total response of the shallower tensiometer, however, were proportional to the total rainfall depth and peak intensity (Figure 2.8). Furthermore, in Figure 2.8, a very important feature is noted: the refraction (the rate of change in response) in the pressure curves of the shallower tensiometer, as soon as they cross the zero pressure line. Bearing in mind that the shallower tensiometer was within the capillary fringe, which

extended close to the ground surface, the section of the pressure curve before the zero pressure line represents the release of the tension forces (caused by the downward pressure wave) in water within the capillary fringe, while the section after the zero pressure line represents the rising water table (upward pressure wave). An analysis of the pressure curves of the shallower tensiometer, for all the events that caused the groundwater ridging water table response, indicated that its rate of reaction to the downward pressure wave was 2.5 to 22.5 times its rate of reaction to the upward pressure wave.
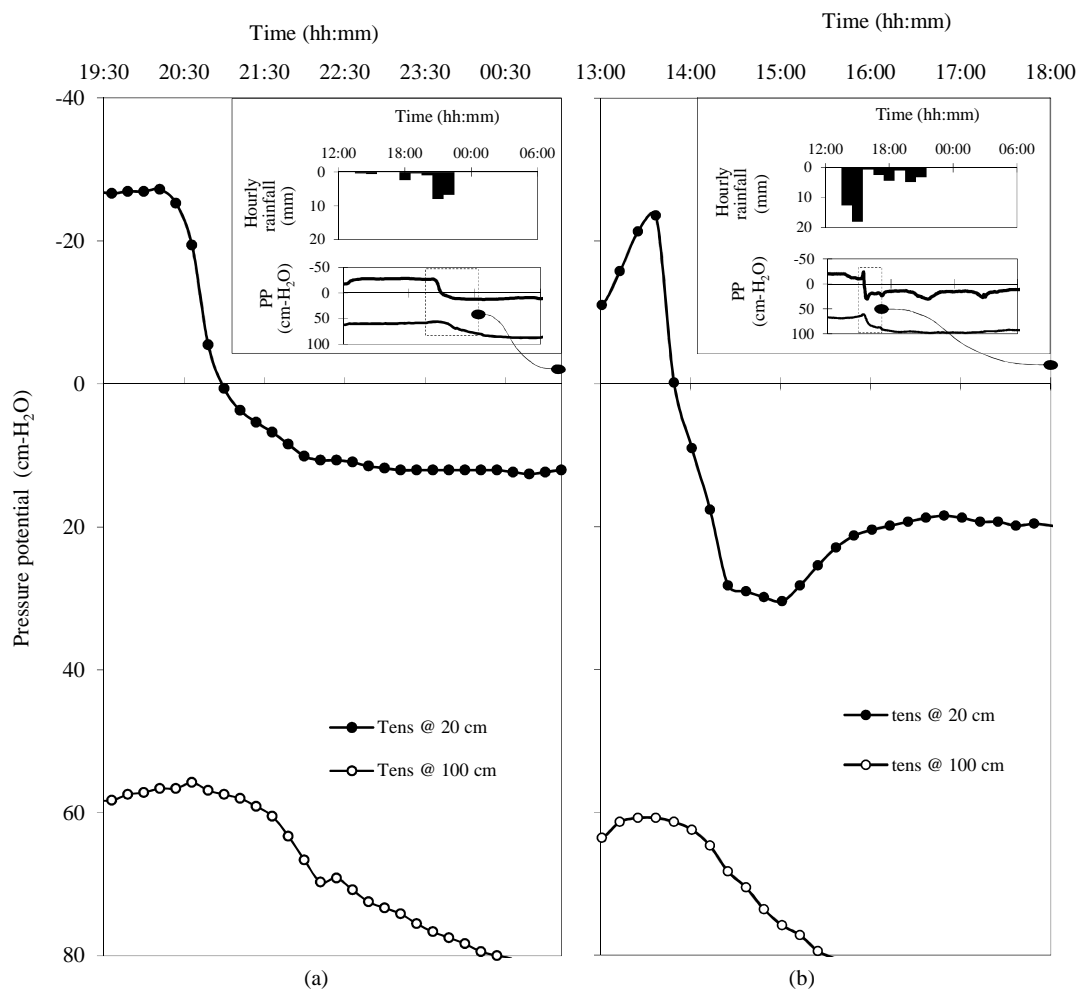
Figure 2.8 The responses of the tensiometers at U3 to (a) the rainfall Event No. 43 that occurred on 8th January 2001 and (b) the rainfall Event No. 70 that occurred on 10th March 2001. PP is pressure potential.

2.4.2.2.   Rapid water table response to a transient pressure wave at a hillslope zone

The results of soil pore water pressure and water level responses to the rainfall events of the summer season of 2000/2001 at the observational nests L2, L3 and L4 at the hillslope zone, are shown in Figure 2.9. From the responses of the water level and tensiometric pore water pressure at L2, in Figure 2.9 (e) and Figure 2.9 (f), respectively, it can be seen that the lower horizons of the soil profile at this nest remained at constant saturation throughout the season. This observation is made from the nearly constant pore water pressure recorded by the deepest tensiometer and the nearly constant water level in the observation hole. This implies no recharge of the groundwater. However, the two shallower tensiometers responded, more often, in a uniform pattern consistent with the rainfall events.

Down the slope, at L3, the water level responses displayed fluctuations in the water table (Figure 2.9 c), which indicated recharge and drainage of the groundwater. However, there seems to be no common pattern in the responses of the water level and the responses of the tensiometric pore water pressure at L3 (Figure 2.9 d). This implies that the water table fluctuations at L3 might not have been caused by the recharge from above. This can also be noted in the disconnection between the responses of the two shallower tensiometers (tensiometer at 20 cm and tensiometer at 50 cm) and the deepest tensiometer (tensiometer at 80 cm) at L3 (Figure 2.9 d). While the two shallower tensiometers rapidly and uniformly responded to the rainfall events, the magnitude of these responses diminished with depth; the deepest tensiometer responding only to fewer rainfall events. This implies that the infiltration front, to which the two shallower tensiometers responded, did not, in many rainfall events, reach the deepest tensiometer. These observations concur with those of Lorentz *et al.* (2004), who found that the percolation to the water table, of the infiltration front at L3 is generally slow. It is also worth noting that, while the two shallower tensiometers reacted almost at the same rate, their recovery rates were noticeably distinct, the lower one recovering more rapidly.

Figure 2.9 Responses of the water levels in the groundwater observation holes (GWOH) and tensiometric pore-water pressure at observation nests L2, L3 and L4 to daily rainfall during the summer season of 2000-2001. Missing data was caused by mechanical breakdown in the logging system.

Further down the slope, at L4, the two tensiometers (Figure 2.9 b), positioned at 25 cm and 80 cm below the ground surface; and the water level in the groundwater observation holes (Figure 2.9 a), all responded in a uniform, simultaneous and similar pattern to the rainfall events that occurred between the beginning of the season to about mid-February, when the water level seemed to have reached the ground surface. This implies a rapid propagation of a pressure wave through the soil profile at this observation nest (L4). It is necessary to point out that, when a rainfall event of high intensity and magnitude impinged the ground surface, with the subsurface conditions of a deep water table and a dry soil profile above, the responses of pore water pressure and water level were relatively rapid and large in magnitude. This was particularly noticeable, for instance, during the rainfall events 19 and 54, which occurred on 8th November 2000 and 28th January 2001, respectively. A critical consideration of the responses of the water level and tensiometric pore water pressure at L3 and L4 indicates that, the water level responses at L3 followed more, although with some lag time, into the pattern of water level responses at L4, than in the pattern of its counterpart tensiometers at L3. This phenomenon was again more evident during the rainfall events 19 and 54. It will suffice to present in detail just one of these two events, Event 19, of which the results, are shown in Figure 2.10.

In Figure 2.10(a) the water levels were plotted with bedrock, as a zero datum. The geology of this zone indicates that the bedrock gradient dips from L2 and L4, converging at L3 (see Figure 2.2). This configuration of the bedrock topography explains the presence of 40 cm of water in the observation hole at L3 and the absence of water in the observation hole at L4, in the pre-event period of Event 19 (Figure 2.10a). Since the gradient of bedrock between L4 and L3 is small, a horizontal bedrock datum was assumed, from which the water levels in Figure 2.10 were plotted.

At L4, before Event 19, the tensiometer at 25 cm and 80 cm below the ground surface indicated the pre-event pressure potential values of about 70 cm-H_2O and 45 cm-H_2O, respectively (Figure 2.10b), while the observation hole indicated dry conditions (Figure 2.10a).

Time (dd/mm)

(d) Rainfall Event No. 19

(c) Tensiometric pore water pressure at L3

(b) Tensiometric pore water pressure at L4

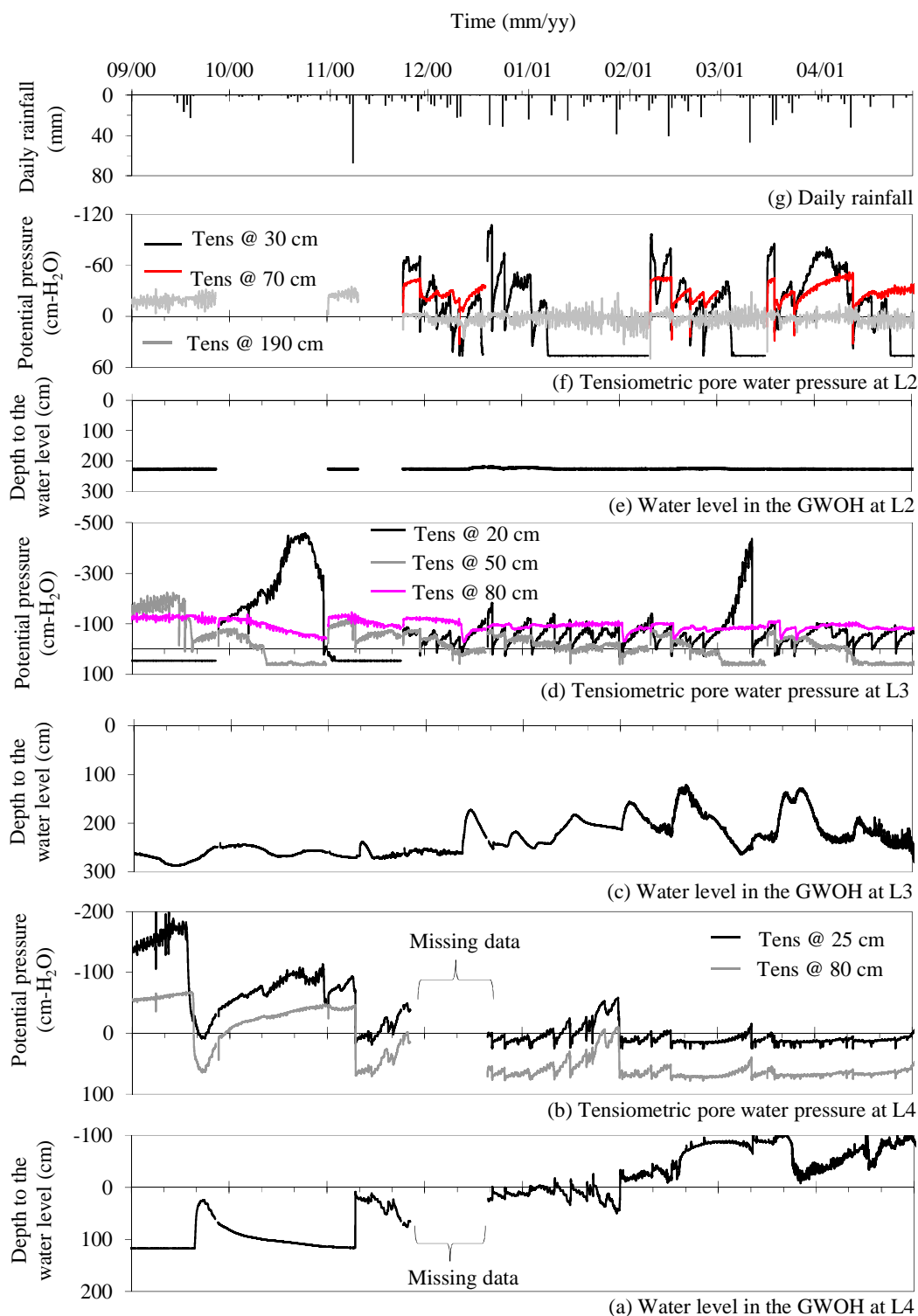(a) Water levels in the GWOH at L3 and L4
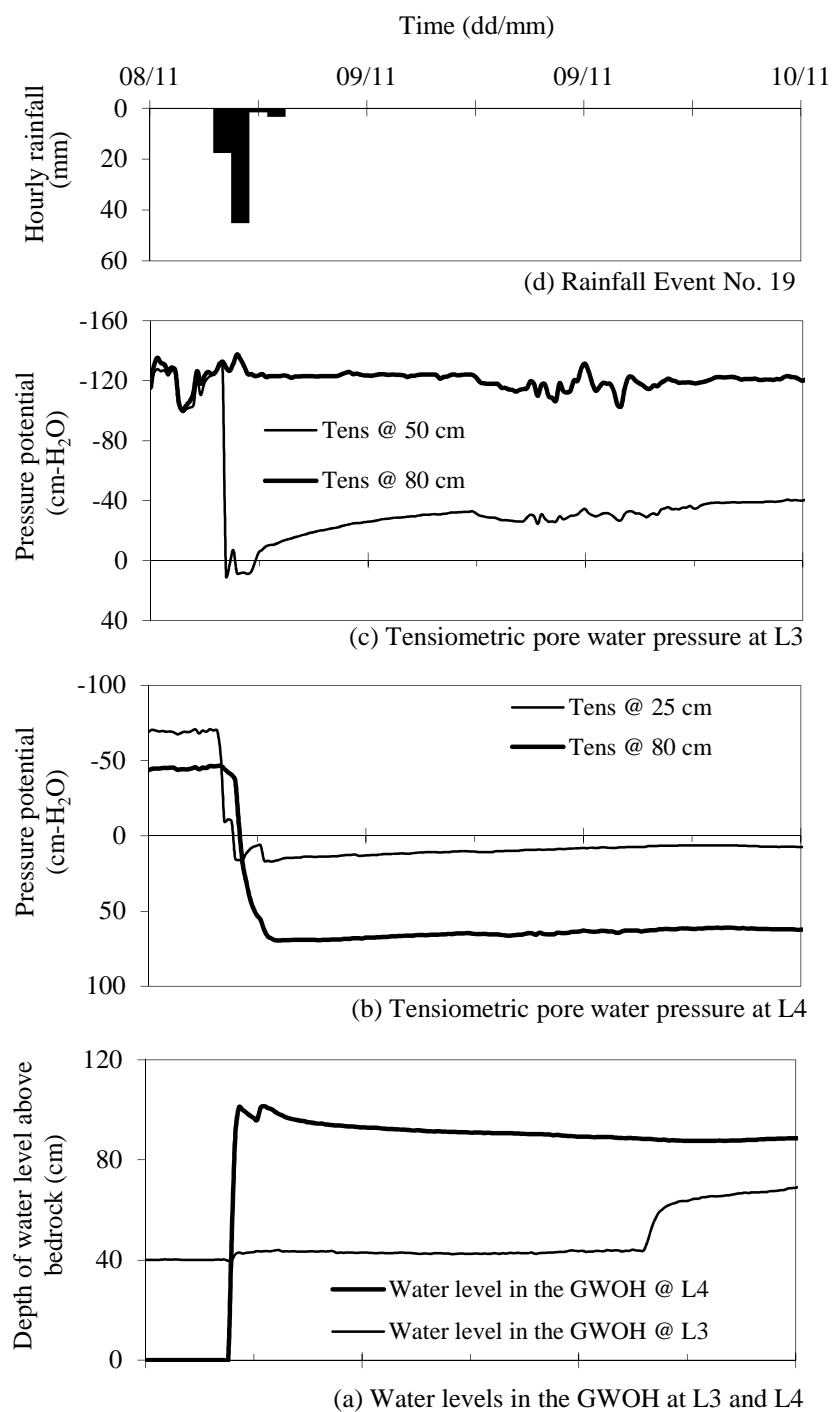
Figure 2.10 The responses of the water levels in groundwater observation holes (GWOH) and the tensiometric soil pore water pressure at observation nests L3 and L4 to rainfall Event No. 19.

During Event 19, the middle tensiometer at L3 (tensiometer at 50 cm) reacted rapidly, while the deeper tensiometer (tensiometer at 80 cm) did react only slightly. At L4, the pore water

pressure at the two tensiometers and the water levels started to react at 16h35, 2 minutes after the peak rainfall intensity impinged the ground surface (Table 2.2). Given that the logging time resolution of the data was 12 minutes, the lag time between the peak rainfall intensity and the responses of the tensiometric pore water pressure and the water level might have been less than 2 minutes. The deeper tensiometer recorded a change of 110.4 cm-H_2O in the soil pore water pressure, while the water level was elevated by 106.1 cm; both within two-and-a-half hours, but the former reacting more slowly than the latter. This simultaneous and almost equivalent magnitude of the change in the water level and the tensiometric pore water pressure indicates signals of a pressure wave, which might be of the Lisse Effect. Torres *et al*. (1998) observed a similar simultaneous response in tensiometric pore water pressure at different soil depths and two different observation points, when they applied intense irrigation rates (between 370 and 5725 mm/h) on the ground surface. Torres *et al*. (1998) speculated compressed pore air ahead of the wetting front (Lisse Effect).

2.4.3   Laboratory experimental results

In the pre-simulation period, in the laboratory experiment, all the tensiometers indicated unsaturated conditions (negative pressure potential). The pre-simulation piezometric water level was at Port 160, which corroborates with the pressure potential value at this port (0 pressure head). However, the volumetric water content at Port 160 and Port 150 indicated maximum saturation, while Port 140 indicated partially saturated conditions. Therefore, from the tensiometric pore water pressure, volumetric water content and pore air-entry value of the soil used (Table 2.1), Port 160 was on the water table, Port 150 was right in the middle of the capillary fringe and Port 140 was close to the upper boundary of the capillary fringe.

During the simulation, pore air pressure, tensiometric pore water pressure and piezometric water levels responded, as soon as water was ponded on the soil surface. The volumetric water content of the shallowest sensor, i.e., Port 60, responded almost 44 minutes after the start of the experiment (Figure 2.11). These observations indicate that the tensiometric pore water pressure and piezometric water levels responded to the compressed pore air pressure, before the arrival of the wetting front. The decrease in the volumetric water content at Port 140 and Port 150, were caused by groundwater depletion, as a result of groundwater discharge (results not shown).
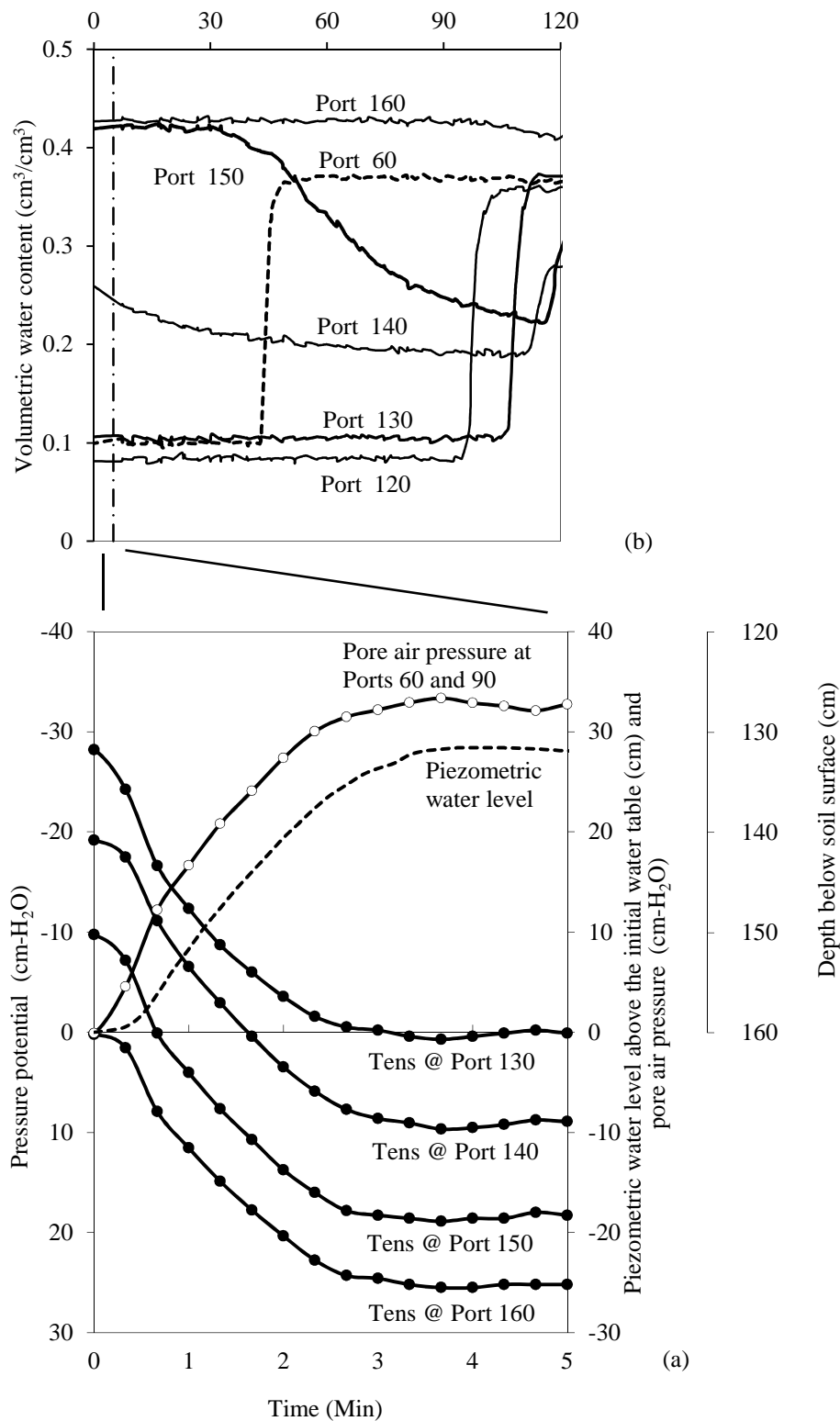
Figure 2.11 The responses of (a) the piezometric water level, tensiometric pore water pressure and compressed pore-air pressure, and (b) volumetric soil water content during the laboratory experiment. The results in (a) are only for the first 5 minutes and those in (b) are for the first 120 minutes of the experiment.

The rise in the piezometric water level was nearly always on a par with the increase in the fluid pressure in the soil pore water (ψ) inside the column, as indicated by the tensiometer at Port 160. The increase in ψ was proportional to the increase in compressed pore air. It is also worth noting that, the tensiometers, which were above the water table, reacted from their initial more-negative pressure potential values to their less-negative pressure potential values in a gradual manner.

2.5   Discussion

2.5.1   The role of the capillary fringe in the transient pressure waves

The Lisse effect transient pressure wave
Results from the hillslope zone showed that, in the pre-event period of Event 19, there was completely no water in the observation hole at L4. Conversely, during Event 19, it was noted that there were rapid and disproportionate responses in tensiometric pore water pressure, as well as the water level at L4. The rapidly elevated pore water pressure and water level remained at their new elevated values, for several days, after the rainfall event (Figure 2.10). This phenomenon is the Lisse Effect, which is described as: "initially rapid, 2-4 days for full recovery," (Table 1 of Heliotis and DeWitt, 1987).

In the pre-event period of Event 19, there was 40 cm of water above the bedrock in the observation hole at L3. From the water levels at L3 and L4, and the configuration of the bedrock topography, the profiles of the water table and the capillary fringe, between the two nests and prior to Event 19, can be extrapolated, as shown in Figure 2.12. With Figure 2.12, the processes that occurred at L4 can be explained clearly with the aid of the laboratory results.

The laboratory results revealed that the Lisse Effect water table response is mainly caused by the release of tension forces in water within the capillary fringe, and that the total rise in the piezometric water level was caused by the cumulative effect of two main processes. First, the pressure energy injected into the capillary fringe, due to the compressed pore air pressure, releases the tension forces in the water within the capillary fringe, hence subjecting it (water within the capillary fringe) to gravity forces. This elevates the hydraulic head that results in the initial rapid rise of the piezometric water level (see Figure 2.13 a, b,

and c). Secondly, if the injected pressure energy is significantly large, the excess pressure energy adds to the already raised hydraulic head (caused by the first process) (see Figure 2.13 d). The first process explains the sudden appearance of water in the observation hole at the field's observation nest L4. The downward pressure wave increased the fluid pressure in the water within the capillary fringe (Figure 2.12), hence, rapidly causing the effusion of the stored pre-event water as it (pressure wave) propagated downward. The effused pre-event water accounts for the sudden appearance of water in the observation tube, which was dry in the pre-event period of the rainfall Event No. 19. Similar processes of the conversion of the capillary fringe (as shown in Figure 2.13) might have occurred at the observation nest U3, at the wetland zone.
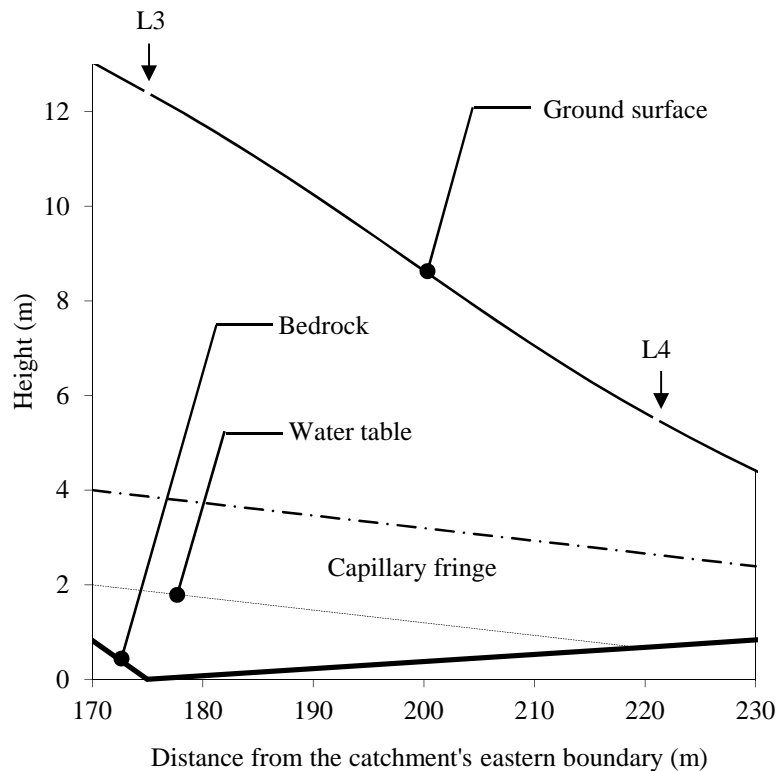
Figure 2.12 Extrapolated profiles of the water table and the capillary fringe between L3 and L4, prior to the rainfall Event No. 19. The extrapolation was based on the water levels at L3 (40 cm) and at L4 (0 cm) prior to the event and the topography of the bedrock. The vertical scale is exaggerated four times.

| | (a) $t = 0$ | (b) $0 < t < 0.33$ | (c) $t = 0.67$ | (d) $t = 1.67$ | (e) $t = 3.00$ |
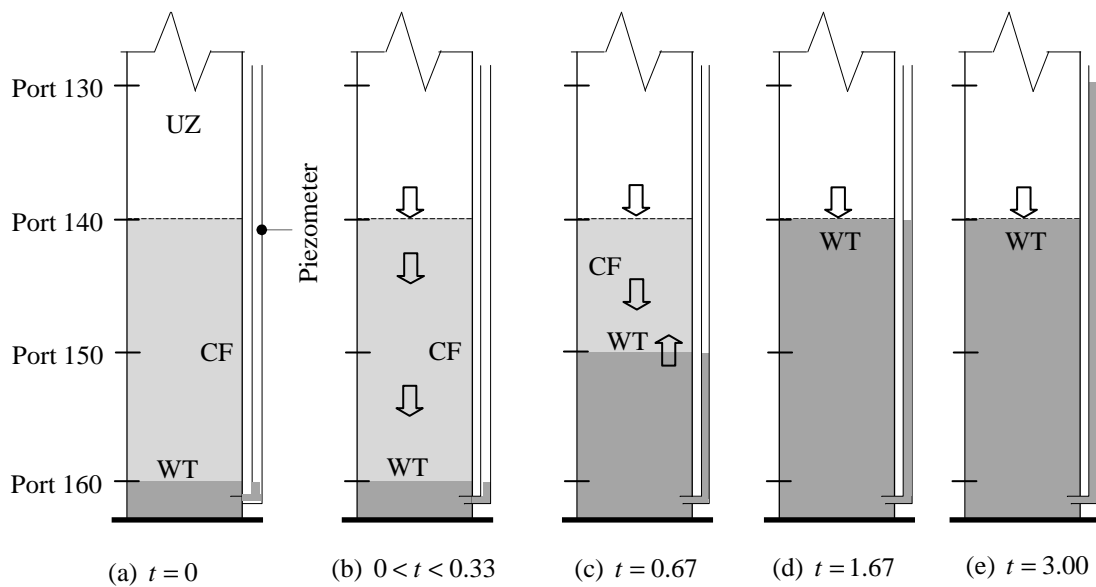
Figure 2.13 Temporal and discrete evolution of the water table (WT) caused by the release of tension forces in water within the capillary fringe (CF) in the Lisse Effect laboratory experiment. The arrow on top of the CF represents the compressed pore air in the unsaturated zone (UZ), the downward arrow within the CF represents positive pressure propagating downwards (downward pressure waves) towards the water table (WT) and the upward arrow represents the rising WT (upward pressure wave). Time, t, is in minutes and with reference to Figure 2.11. (a) is before the start of experiment, (b) is the downward pressure wave through capillary fringe, but just before it arrives on the WT, (c) the WT through capillary fringe, (d) the WT has just arrived on top of the CF and (e) the water level in the piezometer rises above the top of the saturated zone inside the column of soil (this is caused by the excess compressed pore air).

Groundwater ridging transient pressure wave

Field results from the observation nest U3, at the wetland zone, revealed that groundwater ridging occurred only in the rainfall events that had a minimum total rainfall depth of 10 mm (Figure 2.6)). The point of discussion here is that this threshold amount also depends on the position of the tensiometer, within the capillary fringe, or below the ground surface. For instance, had the tensiometer been in a shallower position, the value of the minimum total rainfall amount could have been higher, and vice-versa. However, the minimum total rainfall amount suggests that, in a given suitable environment, any small amount of water can not cause groundwater ridging, as indicated by (Gillham, 1984)Gillham (1984); instead, a threshold amount is required. Our observations, on the other hand, support those of (Heliotis and DeWitt, 1987)Heliotis and DeWitt (1987), who found that a critical amount of rainfall was required to cause a rapid water table response.

An interesting feature was identified in the pressure curves of the shallower tensiometer at U3. The pressure curves indicated a more rapid reaction of the tensiometer, before the zero pressure-head value, than after the zero pressure-head value. This feature, according to the law of conservation of energy, implies an onset of lateral flow of water below the rising water table. We discuss this feature with reference to Figure 2.14, which was developed from Figure 2.8(a).

(a) 1930   (b) 2030   (c) 2130
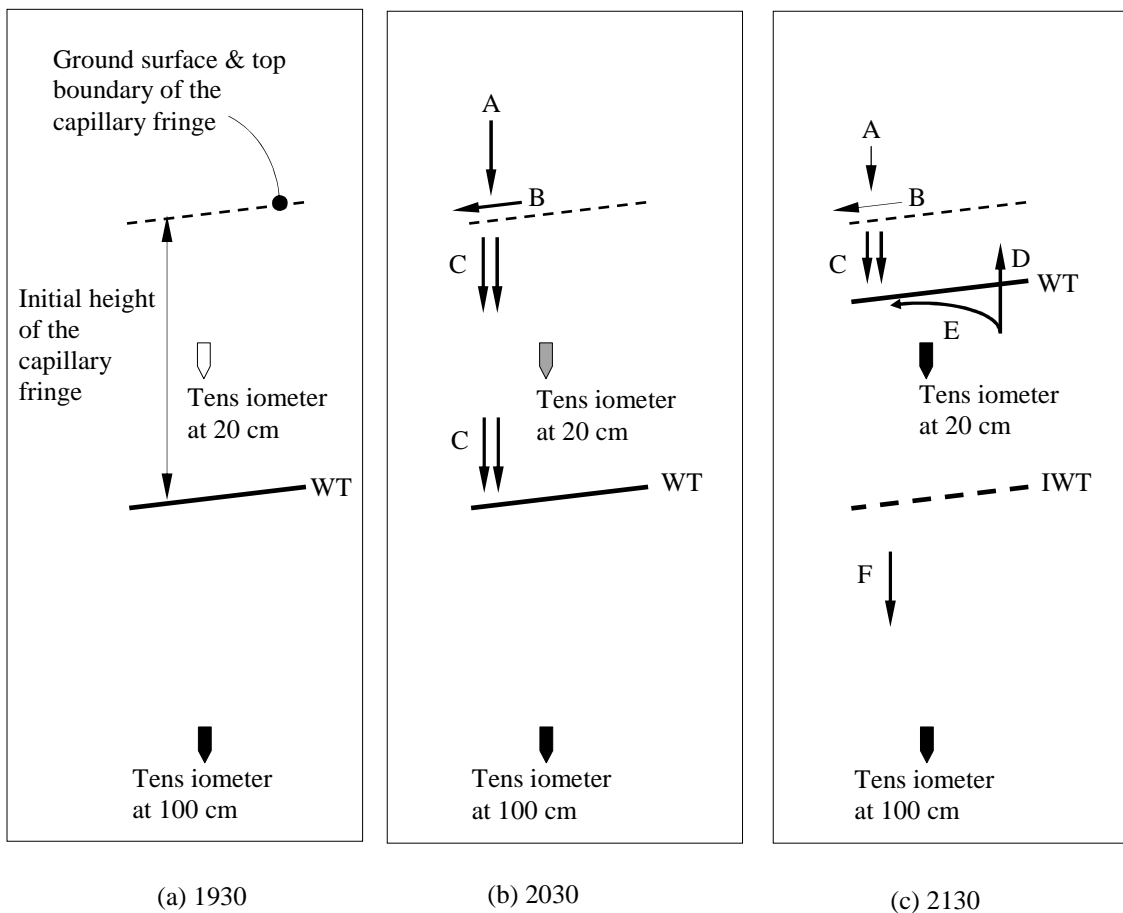
Figure 2.14 Schematic presentation of (b) the release of tension forces in water within the capillary fringe, (c) the subsequent rising water table and the simultaneous lateral flow of water, below the rising water table, during groundwater ridging water table response. (a) is the pre-event state. Arrows: A = rainfall, B = saturated overland flow, C = downward pressure wave through capillary fringe, D = rising water table (upward pressure wave), E = ensuing lateral flow, as the negative pressure in the water within the capillary fringe is turned into positive pressure, F = pressure wave, under the water table (and due to the rising water table), propagating toward the deeper tensiometer. WT = water table, IWT = initial water table. The three states (times) of the water table are with reference to Figure 2.8(a).

Figure 2.14 (a) represents the state of the system in the pre-event period. The shallower tensiometer indicated negative pressure potential (-27.2 cm-H_2O), while the deeper tensiometer indicated positive pressure potential (56.5 cm-H_2O). However, from the soil water retention information (h_a = 45 cm-H_2O, Table 2.1), the shallower tensiometer was within the capillary fringe, which extended to the ground surface, as idealized in Figure 2.14(a). It is important to keep in mind that the water within the capillary fringe is usually under tension forces and cannot flow by gravity. Only the water below the water table can flow by gravity.

Figure 2.14 (b) represents the state of the system, during the initial period of the rainfall event. Since the capillary fringe is saturated, no infiltration of the rainwater is anticipated. Therefore, formation of saturated overland flow (SOF), or ponding, is expected at the on-set of a rainfall event. The impact of rainfall on the ground surface (Arrow A) and the ensuing SOF, or ponding, (Arrow B) injects positive pressure into the soil profile (the capillary fringe). This injected pressure energy propagates through the capillary fringe, as a downward pressure wave (Arrow C), releasing tension pressure in water within the capillary fringe. As soon as the initial downward pressure wave-front arrives on the water table, the water table starts to ascend, as shown in Figure 2.14 (c) (Arrow D). The water that was initially under tension, within the capillary fringe, is now under positive pressure and subjected to gravity flow, below the rising water table. As the water table rises, therefore, the converted water, underneath the water table, flows laterally, as shown in Figure 2.14 (c) (Arrow E). Consequently, due to this lateral flow, the rate of the rising water table (upward pressure wave) would be lower than the rate of the downward pressure wave, a phenomenon that results in the decrease in the rate of response of the pressure curve, after crossing the zero pressure line (Figure 2.8a). For completeness, where there is no provision for lateral flow, the refraction in the pressure curve at zero pressure head is expected not to occur.

2.5.2 Response of groundwater fluxes at a hillslope zone

The response in the water level at L3, located in the upslope of L4, occurred, after the response in the water level at L4, located near the toe of the slope. This delayed water level response at L3 is caused, neither by the recharge of the water table from the infiltration profile, nor by the subsurface groundwater flow from the upslope direction. This is based on a number of reasons. Although, as it has been mentioned above, there seem to be preferential flows at L3, the infiltration profile through this mechanism (preferential flows)

did not reach the deeper soil horizon, to recharge the water table. This is from the lack in response of the deeper tensiometer at L3 (Figure 2.10c). Furthermore, since no change was recorded in the water level at L2 (Figure 2.9), the rapid response of the water level at L3 was not caused by the groundwater flow from the upslope direction. Therefore, the rapid response of the water level at L3 was caused by the reversed groundwater flow from the downslope direction, after the rapid elevation of the hydraulic head in groundwater at the toe of the slope (L4).

The general direction of groundwater fluxes between L3 and L4 at any time was determined from the hydraulic gradient between the two nests. In Figure 2.15, the hydraulic grade lines are shown for five specific times, during and immediately after Event 19. The hydraulic grade lines in Figure 2.15 were plotted by joining the hydraulic heads between L3 and L4 at the specified times. The value of the hydraulic gradient for each hydraulic grade line for the specified times are also indicated in Figure 2.15.
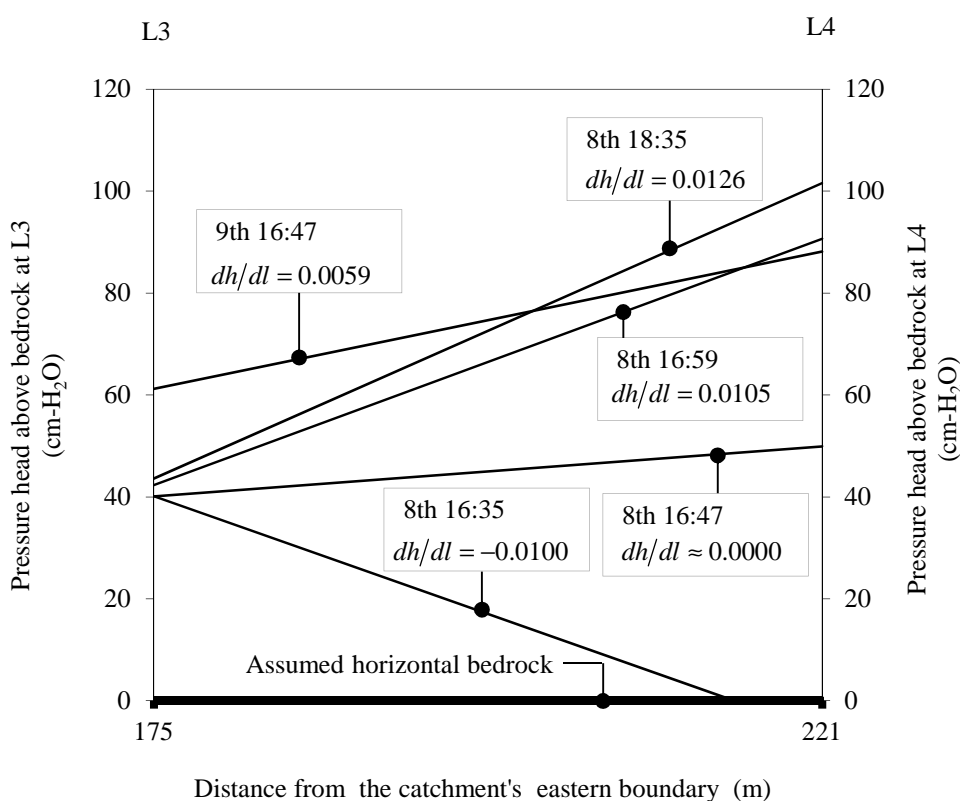
Figure 2.15 The temporal and discrete evolution of the hydraulic gradient between L3 and L4, as a result of a transient pressure wave at L4 during the rainfall Event No. 19.

Just before the rapid response of the water level at L4, to the peak rainfall intensity, which occurred at 16h33, the hydraulic gradient between L3 and L4 was 0.0100, towards the downslope direction (Figure 2.15). Immediately the peak intensity rainfall impinged the ground surface, the water level at L4 (right hand vertical axis of Figure 2.15) was rapidly elevated, attaining the maximum change of 106 cm in two hours, and of which 90 cm was recorded in the initial 24 minutes. On the other side (left hand vertical axis of Figure 2.15), the water level at L3 did not immediately respond to this intense rainfall, except for a small rise of about 3 cm that might have been caused by a shock or vibration wave (Amiaz *et al.*, 2011)(Amiaz *et al.*, 2011). Therefore, due to the rapid increase of the difference in fluid pressures between the two nests, there was about 205 % (181.2^o) overturn in the hydraulic gradient from 0.0100, in the downslope direction, to 0.0105, in the upslope direction, in just 24 minutes. The overturned hydraulic gradient consequently caused an overturn in the direction of groundwater fluxes. The overturning wave, which developed and attained a pressure potential of 90 cm-H_2O at L4 at 16h59 on the 8th November; arrived at L3, 46 m in the upslope direction, on the 9th November 16h23, almost 24 hours later, with an attenuated pressure potential of 31 cm-H_2O.

2.5.3 The role of transient pressure wave water table responses in stream generation

The results presented in this paper adds to the numerous proposed answers (e.g. Bishop *et al.*, 2004), to the questions that have been raised, regarding the storage of the pre-event water in a catchment and its subsequent rapid mobilization during a rainfall event (Kirchner, 2003). The results from the present study support earlier arguments (e.g. Buttle, 1994) that, in the pre-event period, a substantial amount of pre-event water is stored in an immobilized form, within the capillary fringe. During a rainfall event, this stored pre-event water may be rapidly mobilized by, either the groundwater ridging or the Lisse Effect. Furthermore, the pre-event water, stored in the capillary fringe, due to its proximity to the ground surface, may be chemically and isotopically distinct from the pre-event water, stored under the phreatic surface and forms the baseflow (Buttle, 1994). Therefore, when the pre-event water within the capillary fringe is mobilized into the stream, it introduces an isotopic and a chemical signature that is distinct from that of the new event water, derived from the rainfall event, as well as the pre-event water, derived from the baseflow (groundwater). The stormflow hydrograph, therefore, may consist of three chemically and isotopically distinct types of water (Ogunkoya and Jenkins, 1993).

The results presented in this study demonstrate that the groundwater ridging and the Lisse Effect are among the predominant mechanisms responsible for mobilization of pre-event water from hillslopes to the stream in the Weatherley research catchment. This supports the findings of Wenninger *et al.* (2008), who observed that even during flood events; groundwater component formed at least 62% of the total event runoff.

2.6   Conclusions and Recommendations for Further Research

Groundwater ridging transient pressure wave mechanism occurs, where and when the capillary fringe is very close to, or intersects, with the ground surface. Groundwater ridging mechanism can rapidly mobilize pre-event water from the soil profile and account for its (pre-event water) significant appearance in the stream stormflow hydrograph. This conclusion is made from field observations and should, therefore, serve to alleviate any skepticism, regarding the practicability of groundwater ridging in the field conditions.

Owing to the characteristics of the capillary fringe, or the zone of tension saturation, any small amount of water introduced on the ground surface, in an environment that is suitable for groundwater ridging, cannot cause a rapid water table response. Instead, the groundwater ridging water table response depends on the intensity, with which water is applied on the ground surface. The applied water intensity introduces additional energy, which releases tension forces in water within the capillary fringe, hence, enabling the water table to rise. Therefore, the total water response, in the groundwater ridging mechanism, is proportional to the intensity of rainfall.

The capillary fringe plays a central role, not only in the groundwater ridging, but also in the Lisse Effect. In both mechanisms, the water table responses occur, as a result of an introduction of additional energy into the capillary fringe. In the groundwater ridging, due to the proximity of the capillary fringe to the ground surface, an additional energy is derived directly from the rainfall intensity. In the Lisse Effect, the additional energy is derived from compressed pore air, in the unsaturated zone and ahead of a wetting front.

In both mechanisms, the introduced energy propagates towards the water table, as a downward pressure wave, releasing tension forces in water within the CF. As soon as the downward pressure wave front arrives on the water table (WT), the WT begins to ascend, as an upward pressure wave. The ascending WT contributes to the pressure potential in

groundwater, hence elevating the hydraulic head, which disproportionately increases the groundwater fluxes. Further studies are recommended to develop a mathematical theory for the physical processes involved in groundwater ridging and the Lisse Effect water table responses.

2.7   References

Abdul, AS, Gillham, RW. 1984. Laboratory studies of the effects of the capillary fringe on streamflow generation. Water Resour. Res. 20(6), 691-698.

Abdul, AS, Gillham, RW. 1989. Field studies of the effects of the capillary fringe on streamflow generation. J. Hydrol. 112(1-2), 1-18.

Adrian, DD, Franzini, JB. 1966. Impedance to infiltration by pressure build-up ahead of the wetting front. J. Geophys. Res. 71(24), 5857-5862.

Amiaz, Y, Sorek, S, Enzel, Y, Dahan, O. 2011. Solute transport in the vadose zone and groundwater during flash floods. Water Resour. Res. 47(10), W10513.

Becker, A, Kaden, S. 2003. The role of pressure wave translatory flow in subsurface stormflow generation. Geophysical Research Abstracts, Vol. 5, 14434.

Bishop, K, Seibert, J, Köhler, S, Laudon, H. 2004. Resolving the double paradox of rapidly mobilized old water with highly variable responses in runoff chemistry. Hydrol. Process. 18(1), 185-189.

Bond, WJ, Collis-George, N. 1981. Ponded infiltration into simple soil systems: 3. The behavior of infiltration rate with time. Soil Sci. 131(6), 327-333.

Brooks, RH, Corey, AT. 1964. Hydraulic properties of porous media. Colorado State University, Fort Collins, CO, 27 pages.

Brooks, RH, Corey, AT. 1966. Properties of porous media affecting fluid flow. J. Irrig. Drain. Div., ASCE 92(IR2), 61-88.

Bruce R. R., Luxmoore R. J. 1986. Water retention: Field methods, in: Ed. Klute, A (Eds.), Methods of soil analysis. Part 1. Physical and mineralogical methods. American Society of Agronomy, Madison, Wisconsin, 663-686.

Buttle, JM. 1994. Isotope hydrograph separations and rapid delivery of pre-event water from drainage basins. Prog. Phys. Geog. 18(1), 16-41.

Buttle, JM, Sami, K. 1992. Testing the groundwater ridging hypothesis of streamflow generation during snowmelt in a forested catchment. J. Hydrol. 135(1-4), 53-72.

Gee, GW, Bauder, JW. 1986. Particle-size analysis, in: Klute, A (Eds.), Methods of soil analysis. Part 1. Physical and mineralogical methods. American Society of Agronomy, Madison, Wisconsin, 383–411.

Gillham, RW. 1984. The capillary fringe and its effect on water-table response. J. Hydrol. 67(1-4), 307-324.

Habib, E, Krajewski, WF, Kruger, A. 2001. Sampling errors of tipping-bucket rain gauge measurements. Journal of Hydrologic Engineering 6(2), 159-166.

Heliotis, FD, DeWitt, CB. 1987. Rapid water table response to rainfall in a Northern Peatland ecosystem. Water Res. Bull. 23(6), 1011-1016.

Jayatilaka, CJ, Gillham, RW. 1996. A deterministic-empirical model of the effect of the capillary fringe on near-stream area runoff 1. Description of the model. J. Hydrol. 184(3-4), 299-315.

Jayatilaka, CJ, Gillham, RW, Blowes, DW, Nathan, RJ. 1996. A deterministic-empirical model of the effect of the capillary fringe on near-stream area runoff 2. Testing and application. J. Hydrol. 184(3-4), 317-336.

Khaled, IM, Kohei, N, Taku, N, Hiromi, I, Tsuyoshi, M. 2007. Laboratory investigations of short-term fluctuations of shallow groundwater in response to recharge events.

Khaled, IM, Tsuyoshi, M, Kohei, N, Taku, N, Hiromi, I. 2011. Experimental and modeling investigation of shallow water table fluctuations in relation to reverse Wieringermeer effect. Open Journal of Soil Science 1(2), 17-24.

Kirchner, JW. 2003. A double paradox in catchment hydrology and geochemistry. Hydrol. Process. 17(4), 871-874.

Klute, A. 1986. Water retention: Laboratory methods, in: Ed. Klute, A (Eds.), Methods of soil analysis. Part 1. Physical and mineralogical methods. American Society of Agronomy, Madison, Wisconsin, 635-662.

Klute, A, Dirksen, C. 1986. Hydraulic conductivity and diffusivity: Laboratory methods, in: Klute, A (Eds.), Methods of soil analysis. Part 1. Physical and mineralogical methods. American Society of Agronomy, Madison, Wisconsin, 687-734.

Lischeid, G, Kolb, A, Alewell, C. 2002. Apparent translatory flow in groundwater recharge and runoff generation. J. Hydrol. 265(1-4), 195-211.

Lorentz, SA. 2001. Hydrological systems modelling research programme: Hydrological processes, Phase I: Processes definitions and database. WRC Report No. 637/1/01. Water Research Commission, Pretoria, South Africa.102 pp.

Lorentz, SA, Thornton-Dibb, S, Pretorius, C, Goba, P. 2004. Hydrological systems modelling research programme: Hydrological processes, Phase II: Quantification of

hillslope, riparian and wetland processes. WRC Report No. K5/1061 & K5/1086. Water Research Commission, Pretoria, South Africa.130 pp.

McDonnell, JJ. 1990. A rationale for old water discharge through macropores in a steep, humid catchment. Water Resour. Res. 26(11), 2821–2832.

McDonnell, JJ, Buttle, JM. 1998. Comment on "A deterministic--empirical model of the effect of the capillary-fringe on near-stream area runoff. 1. Description of the model" by Jayatilaka, C. J. and Gillham, R. W. (Journal of Hydrology vol. 184 (1996) 299-315). J. Hydrol. 207(3-4), 280-285.

McWhorter, DB. 1971. Infiltration affected by flow of air. Hydrol. Pap. 49. Colo. State Univ. Fort Collins, Colorado, USA.

Ogunkoya, OO, Jenkins, A. 1993. Analysis of storm hydrograph and flow pathways using a three-component hydrograph separation model. J. Hydrol. 142(1), 71-88.

Peck, AJ. 1960. The water table as affected by atmospheric pressure. J. Geophys. Res. 65(8), 2383-2388.

Pinder, GF, Jones, JF. 1969. Determination of the ground-water component of peak discharge from the chemistry of total runoff. Water Resour. Res. 5(2), 438-445.

Rasmussen, TC, Baldwin Jr, RH, Dowd, JF, Williams, AG. 2000. Tracer vs. pressure wave velocities through unsaturated saprolite. Soil Sci. Soc. Am. J. 64(1), 75-85.

Sklash, MG, Farvolden, RN. 1979. The role of groundwater in storm runoff. J. Hydrol. 43(1-4), 45-65.

Torres, R, Dietrich, WE, Montgomery, DR, Anderson, SP, Loague, K. 1998. Unsaturated zone processes and the hydrologic response of a steep, unchanneled catchment. Water Resour. Res. 34(8), 1865-1879.

Touma, J, Vachaud, G, Parlange, JY. 1984. Air and water flow in a sealed, ponded vertical soil column: experiment and model. Soil Sci. 137(3), 181-187.

Wang, Z, Feyen, J, van Genuchten, MT, Nielsen, DR. 1998. Air entrapment effects on infiltration rate and flow instability. Water Resour. Res. 34(2), 213-222.

Weeks, EP. 1979. Barometric fluctuations in wells tapping deep unconfined aquifers. Water Resour. Res. 15(5), 1167-1176.

Weeks, EP. 2002. The Lisse effect revisited. Ground Water 40(6), 652-656.

Wenninger, J, Uhlenbrook, S, Lorentz, SA, Leibundgut, C. 2008. Identification of runoff generation processes using combined hydrometric, tracer and geophysical methods in a headwater catchment in South Africa. Hydrol. Sci. J. 53(1), 65-80.

Wenninger, J, Uhlenbrook, S, Tilch, N, Leibundgut, C. 2004. Experimental evidence of fast groundwater responses in a hillslope/floodplain area in the Black Forest Mountains, Germany. Hydrol. Process. 18(17), 3305-3322.

2.8   Appendices

Pressure head, h_c, (cm-H$_2$O)
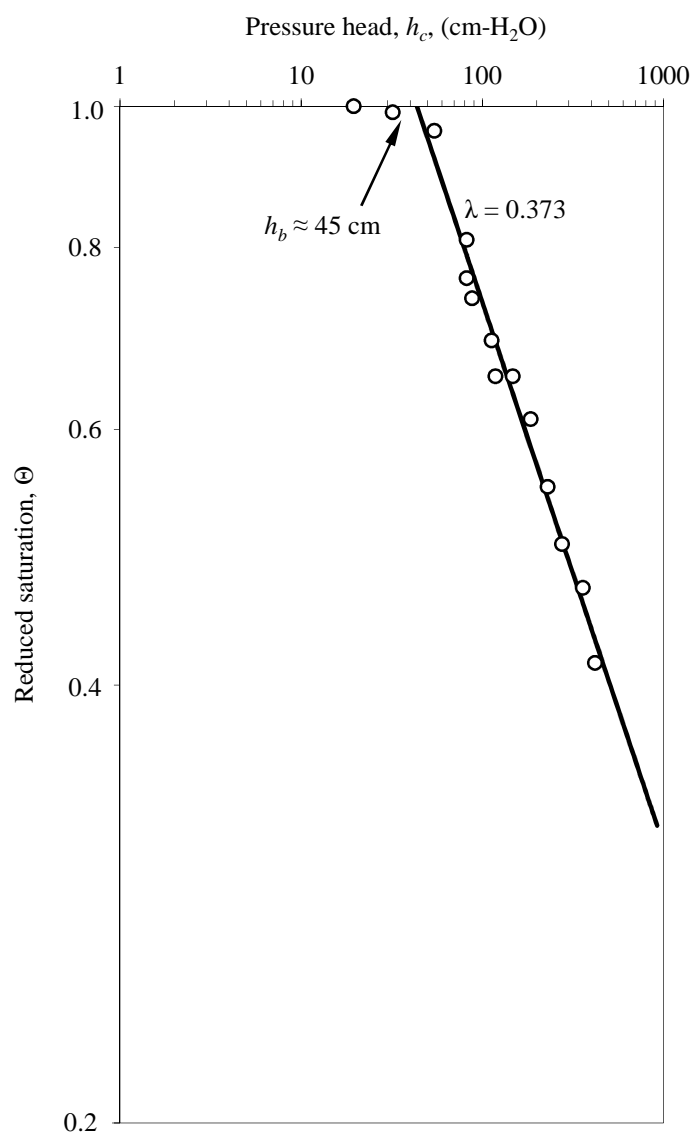
Figure A2.1 Capillary pressure head as a function of reduced saturation for the soil sample from the observation point U3 in the Weatherley research catchment. h_b is the air entry pressure head of the sample.

Figure A2.2 The responses of the tensiometers at U3 to the rainfall Event No. 28, which occurred on 28th November 2000. PP is pressure potential.
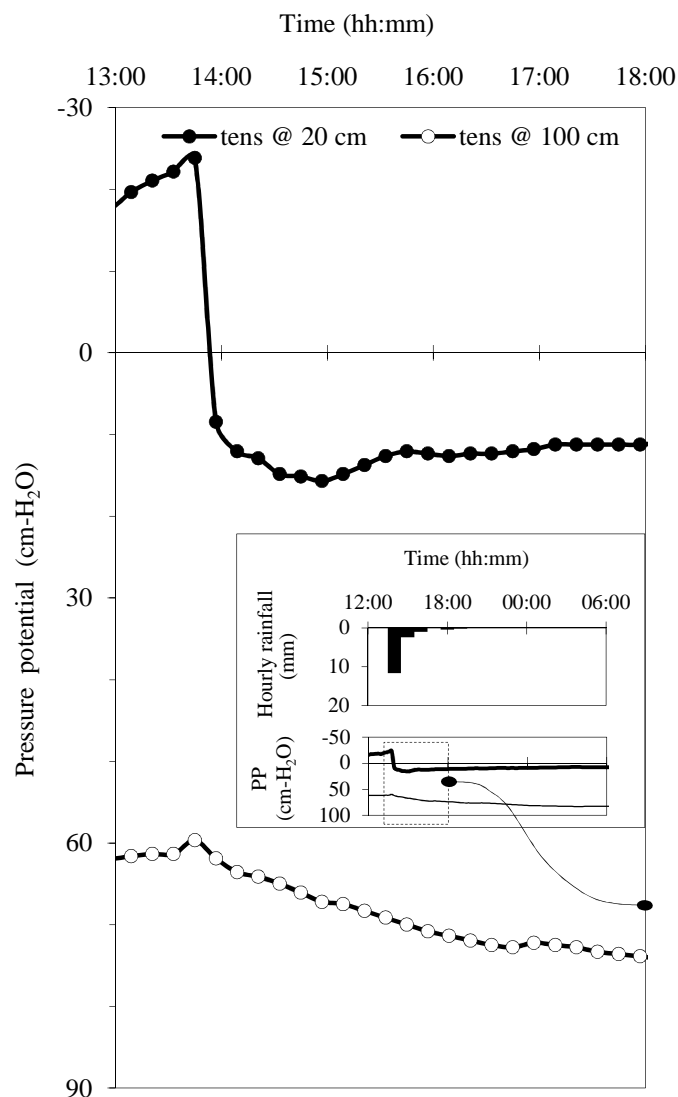
Rainfall event No.	28
Maximum 1-minute rainfall intensity (mm/h)	84
Rate of response of Tensiometer at 20 cm, before 0 PP, [a]	161.5
Rate of response of Tensiometer at 20 cm, after 0 PP, [b]	7.2
[a]/[b]	22.3
Total response of Tensiometer at 20 cm	39.5

Figure A2.3 The responses of the tensiometers at U3 to the rainfall Event No. 32, which occurred on 3rd December 2000. PP is pressure potential.
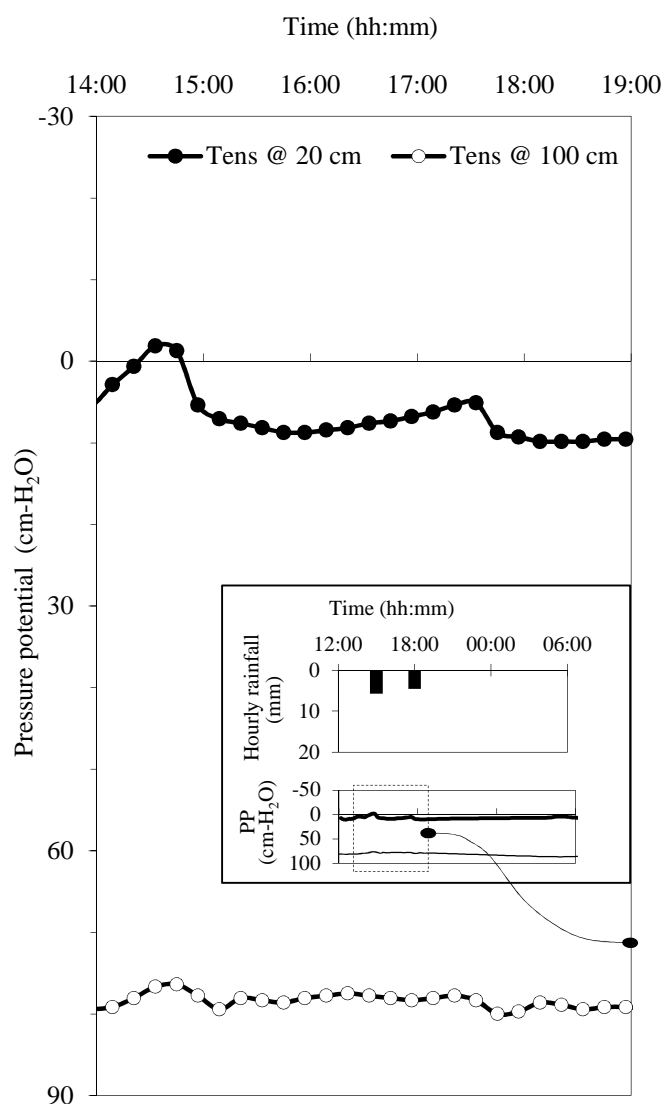
Rainfall event No.	32
Maximum 1-minute rainfall intensity (mm/h)	66
Rate of response of Tensiometer at 20 cm, before 0 PP, [a]	33.4
Rate of response of Tensiometer at 20 cm, after 0 PP, [b]	2.8
[a]/[b]	12.0
Total response of Tensiometer at 20 cm	10.0

Rainfall event No.	34
Maximum 1-minute rainfall intensity (mm/h)	18
Rate of response of Tensiometer at 20 cm, before 0 PP, [a]	8.0
Rate of response of Tensiometer at 20 cm, after 0 PP, [b]	0.8
[a]/[b]	10.5
Total response of Tensiometer at 20 cm	22.6

Figure A2.4 The responses of the tensiometers at U3 to the rainfall Event No. 34, which occurred on 7th December 2000. PP is pressure potential.

Rainfall event No.	38
Maximum 1-minute rainfall intensity (mm/h)	78
Rate of response of Tensiometer at 20 cm, before 0 PP, [a]	59.9
Rate of response of Tensiometer at 20 cm, after 0 PP, [b]	22.6
[a]/[b]	2.7
Total response of Tensiometer at 20 cm	37.9

Figure A2.5 The responses of the tensiometers at U3 to the rainfall Event No. 38, which occurred on 20th December 2000. PP is pressure potential.

Rainfall event No.	39
Maximum 1-minute rainfall intensity (mm/h)	90
Rate of response of Tensiometer at 20 cm, before 0 PP, [a]	51.5
Rate of response of Tensiometer at 20 cm, after 0 PP, [b]	3.4
[a]/[b]	15.1
Total response of Tensiometer at 20 cm	22.8

Figure A2.6 The responses of the tensiometers at U3 to the rainfall Event No. 39, which occurred on 24th December 2000. PP is pressure potential.

Figure A2.7 The responses of the tensiometers at U3 to the rainfall Event No. 42, which occurred on 1st January 2001. PP is pressure potential.

Figure A2.8 The responses of the tensiometers at U3 to the rainfall Event No. 43, which occurred on 8th January 2001. PP is pressure potential.

Rainfall event No.	43
Maximum 1-minute rainfall intensity (mm/h)	18
Rate of response of Tensiometer at 20 cm, before 0 PP, [a]	69.6
Rate of response of Tensiometer at 20 cm, after 0 PP, [b]	3.2
[a]/[b]	22.1
Total response of Tensiometer at 20 cm	39.8

Figure A2.9 The responses of the tensiometers at U3 to the rainfall Event No. 46, which occurred on 13th January 2001. PP is pressure potential.
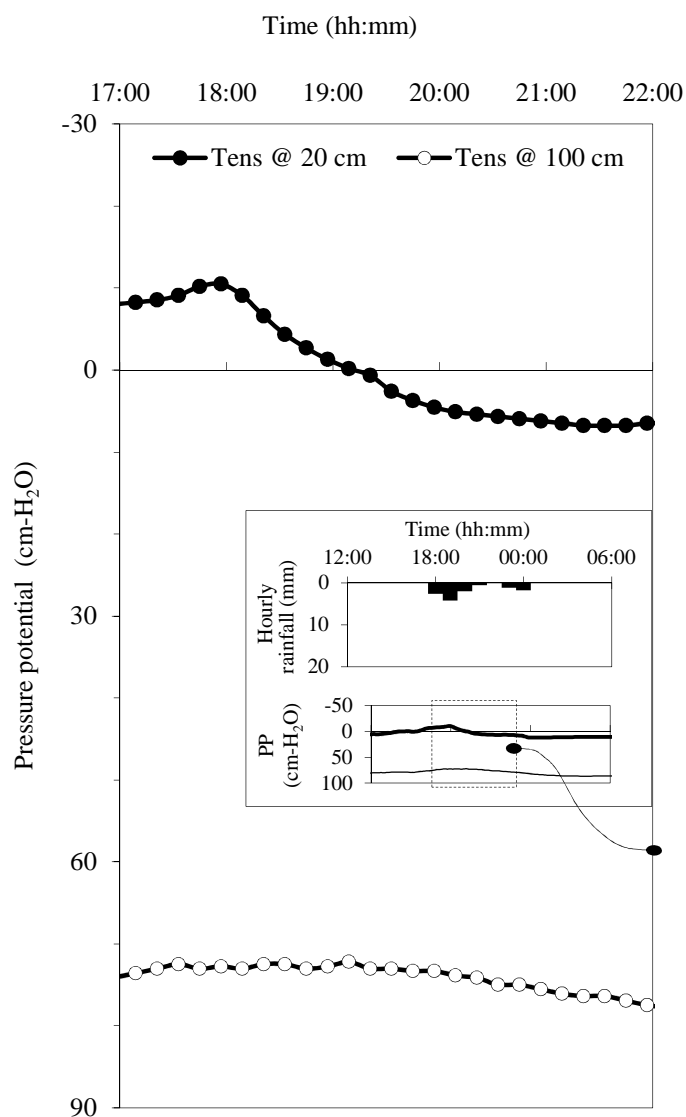
Rainfall event No.	46
Maximum 1-minute rainfall intensity (mm/h)	84
Rate of response of Tensiometer at 20 cm, before 0 PP, [a]	118.3
Rate of response of Tensiometer at 20 cm, after 0 PP, [b]	7.8
[a]/[b]	15.2
Total response of Tensiometer at 20 cm	40.4

Figure A2.10 The responses of the tensiometers at U3 to the rainfall Event No. 47, which occurred on 18th January 2001. PP is pressure potential.
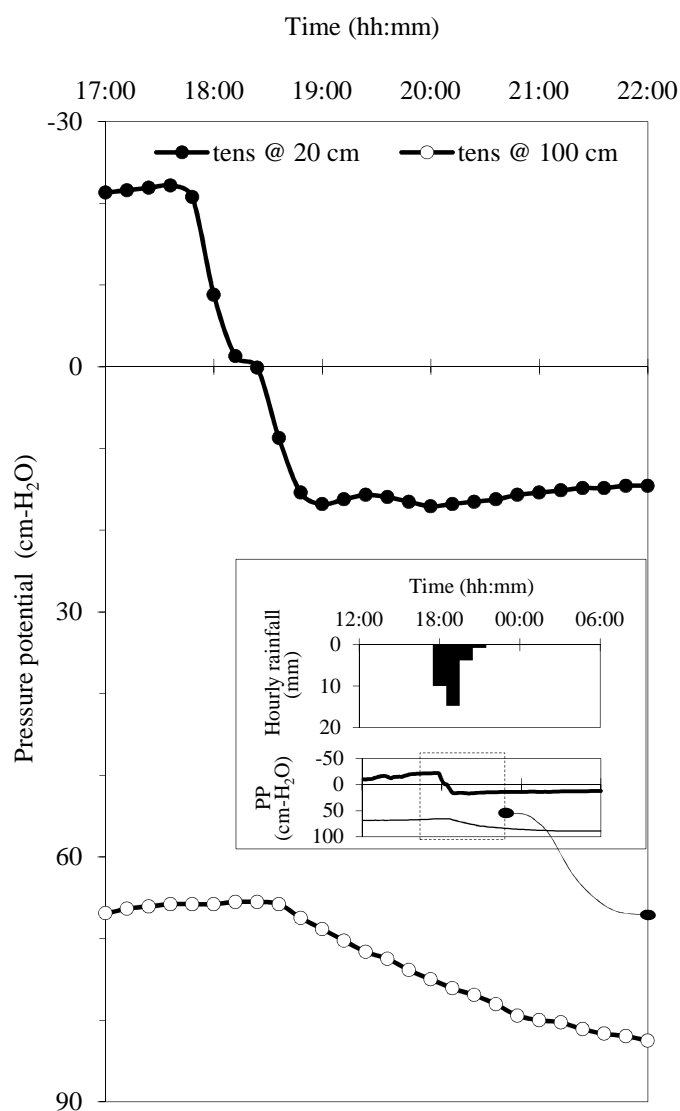
Rainfall event No.	47
Maximum 1-minute rainfall intensity (mm/h)	30
Rate of response of Tensiometer at 20 cm, before 0 PP, [a]	53.6
Rate of response of Tensiometer at 20 cm, after 0 PP, [b]	3.4
[a]/[b]	15.9
Total response of Tensiometer at 20 cm	28.1

Figure A2.11 The responses of the tensiometers at U3 to the rainfall Event No. 60, which occurred on 13th February 2001. PP is pressure potential.

Rainfall event No.	60
Maximum 1-minute rainfall intensity (mm/h)	60
Rate of response of Tensiometer at 20 cm, before 0 PP, [a]	30.2
Rate of response of Tensiometer at 20 cm, after 0 PP, [b]	1.7
[a]/[b]	17.3
Total response of Tensiometer at 20 cm	32.6

Figure A2.12 The responses of the tensiometers at U3 to the rainfall Event No. 70, which occurred on 10th March 2001. PP is pressure potential.
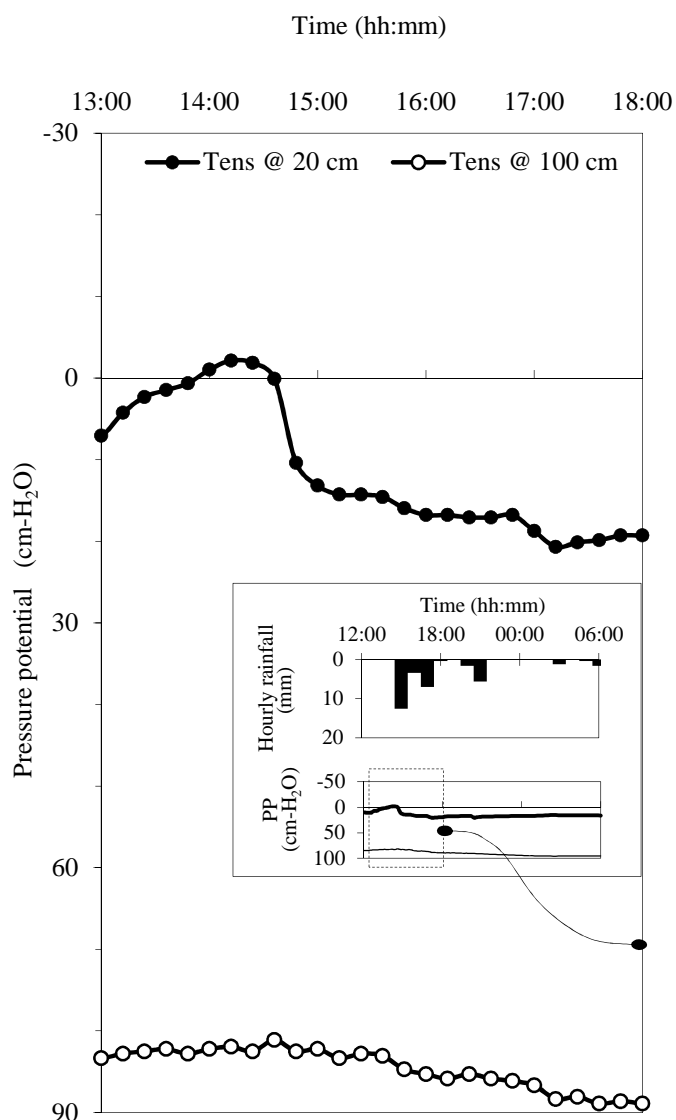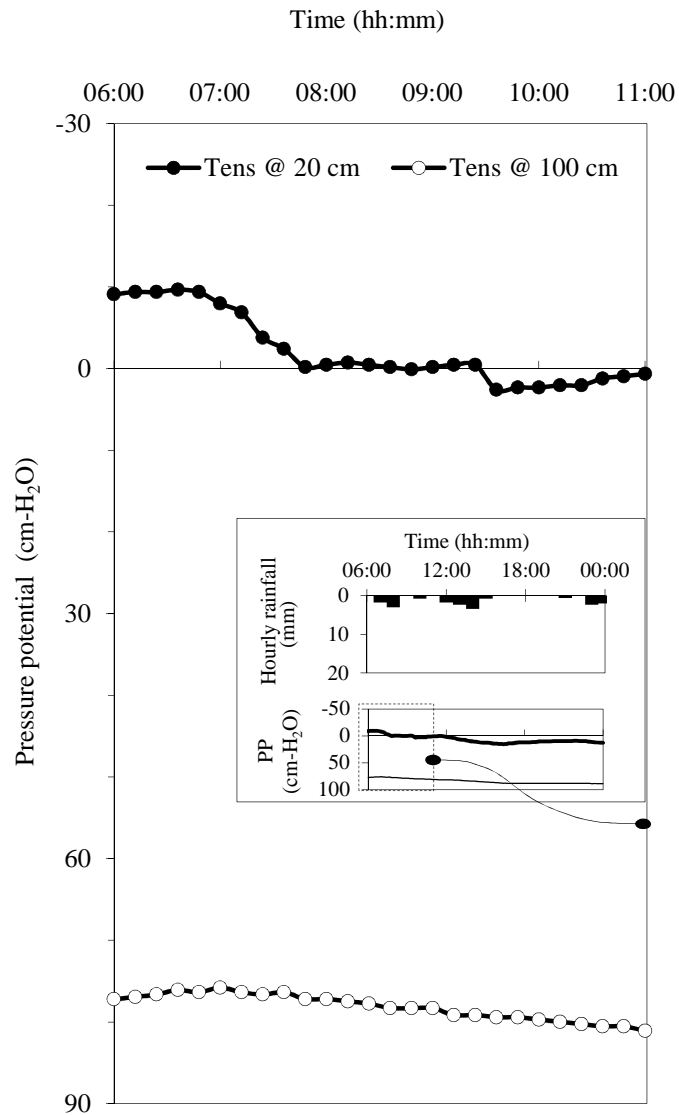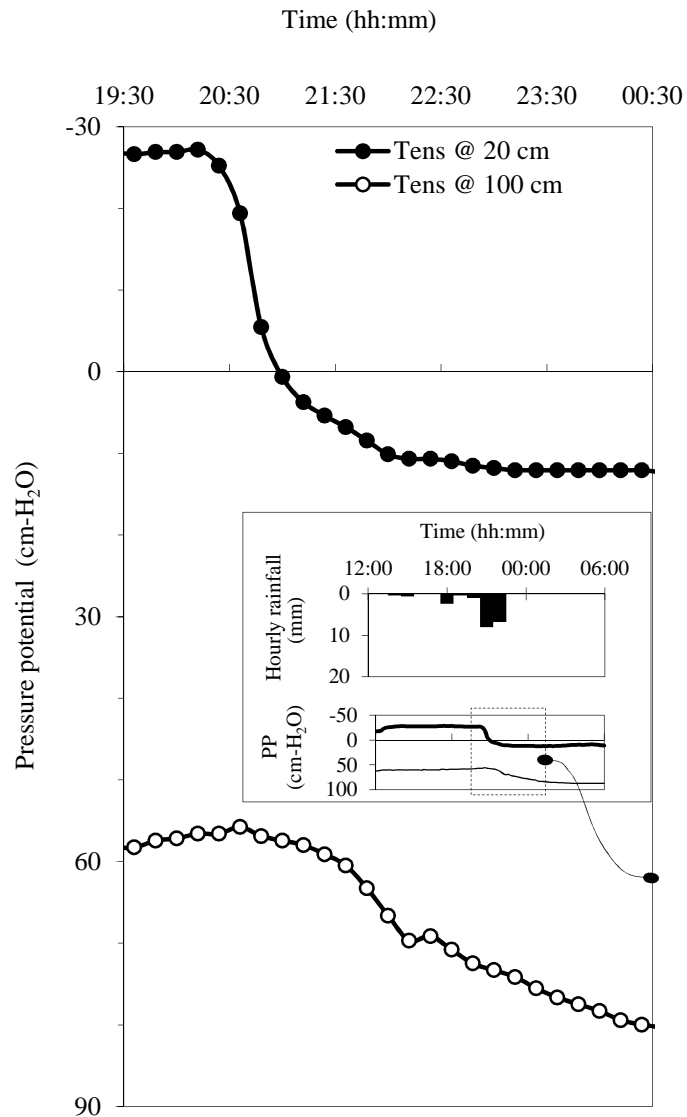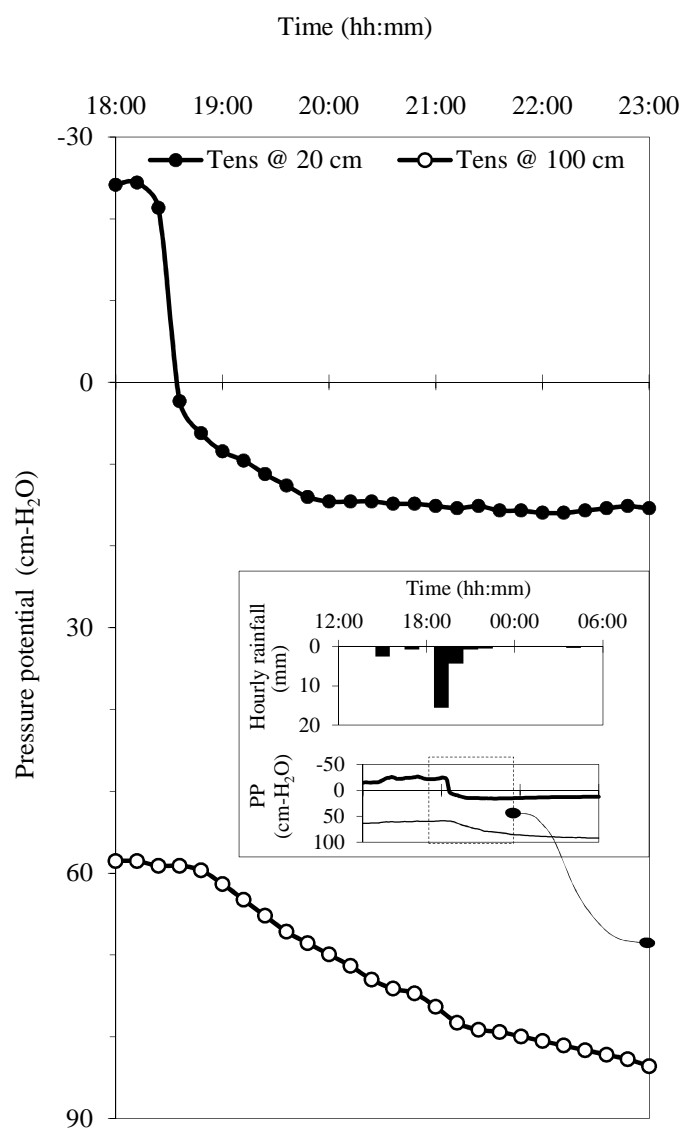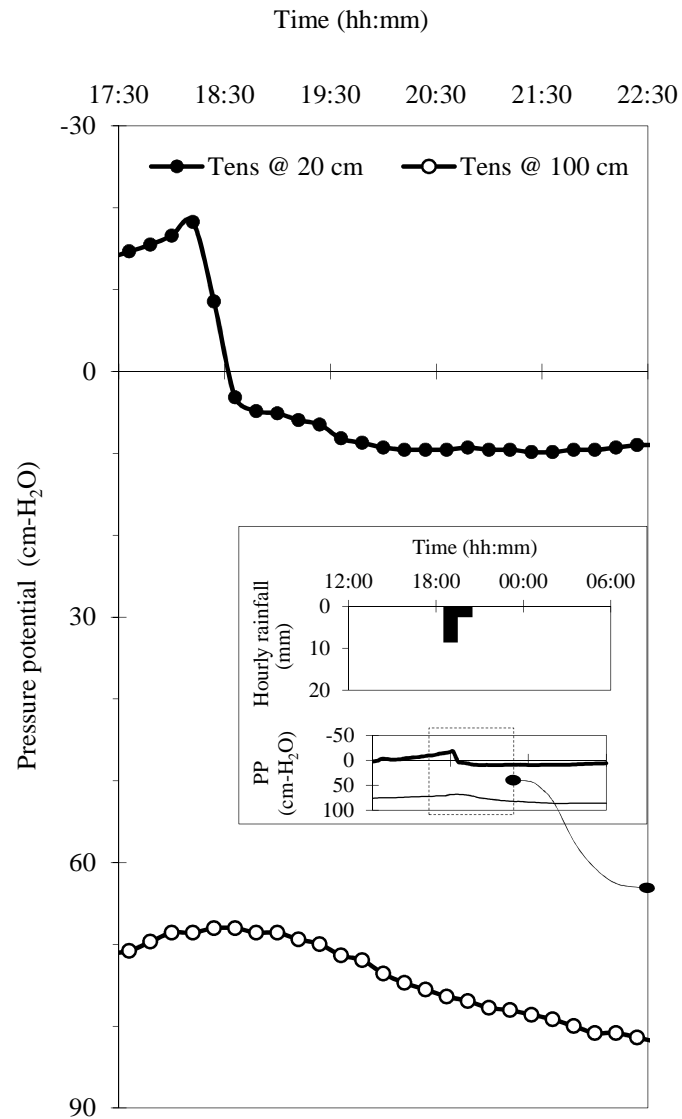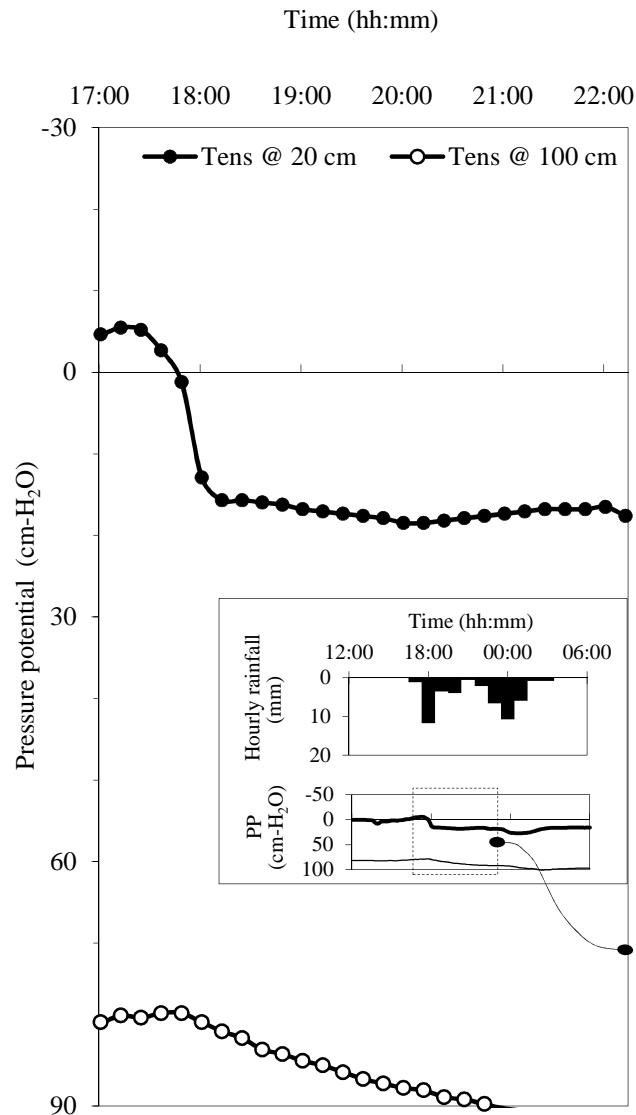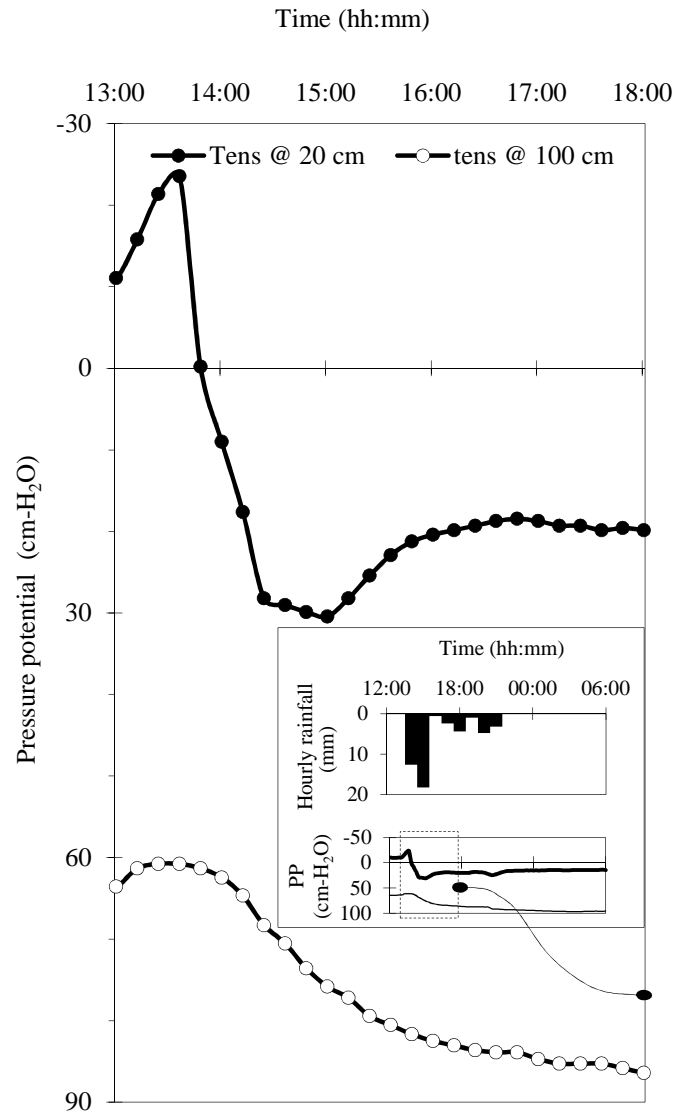
Rainfall event No.	70
Maximum 1-minute rainfall intensity (mm/h)	102
Rate of response of Tensiometer at 20 cm, before 0 PP, [a]	117.0
Rate of response of Tensiometer at 20 cm, after 0 PP, [b]	48.0
[a]/[b]	2.4
Total response of Tensiometer at 20 cm	54.0

TRANSIENT PRESSURE WAVES IN HILLSLOPES

PhD thesis

Waswa GW

School of Engineering, University of KwaZulu-Natal, South Africa

CHAPTER 3[†]

THEORY OF DIFFUSION OF ENERGY THROUGH CAPILLARY FRINGE AND A WATER TABLE RISE IN THE LISSE EFFECT PHENOMENON

3.1   Abstract

Previous studies have demonstrated that during a rainfall event, a stream stormflow hydrograph may consist of pre-event and event water. In most catchments, pre-event water, which exists in the catchment before the rain event, is predominantly groundwater. The Lisse Effect, i.e. the rapid response of a water level to pressurized pore air in the unsaturated zone, is one of the mechanisms that have been proposed to account for the rapid mobilization of pre-event water from hillslopes. Recent results have revealed that the capillary fringe (CF) plays a central role in the Lisse Effect. When compressed pore air is imposed on the upper boundary of the CF, two types of pressure waves are sequentially generated within the CF. First, there is a downward pressure wave that releases the tension forces in water within the CF. As soon as the downward pressure wave front arrives on the water table (WT), the WT begins to ascend, as an upward pressure wave. The ascending water table (increased energy content) contributes to the pressure potential in groundwater, hence elevating the hydraulic head. In this paper, the problem of conduction of energy through a capillary fringe, and hence, the rapid rise of a water table in the Lisse effect, is investigated, both theoretically and experimentally. Theoretically, from the law of conservation of energy and continuity equation, a one-dimensional diffusion equation, $d_e.\partial^2 h_w / \partial y^2 = \partial h_w / \partial t$, is derived for the conduction of pressure energy through a CF. The solution, $h_w(t, y)$, to the equation, is the pressure potential at any space coordinate $y > 0$

---

† This Chapter is based on the Manuscript: "Waswa GW and Lorentz SA (under review): Theory of diffusion of energy through capillary fringe and a water table rise in the Lisse effect phenomena. Vadose Zone Journal

and at any time coordinate $t > 0$, when an external positive pressure (e.g. compressed pore air pressure in the unsaturated zone) is instantly imposed on the upper boundary of the CF, $y = 0$, via the Heaviside unit step function, $u(t)$. The key parameter, which determines the behavior of conduction of pressure energy through capillary fringe, is the energy diffusivity coefficient, d_e. Experimentally, a laboratory soil column apparatus is used to investigate the transmission of energy through the CF in three physically distinct types of soils, classified as: Coarse, Medium and Fine. Both the theoretical and experimental results are fairly in agreement, with regard to the changes in pressure potentials in the CF and WT rise in all the three soils, due to compressed pore air pressure on the upper boundary of the CF. The results indicate that the total rise in the piezometric water levels is inversely proportional to the height of the CF (or the pore air entry pressure value) of the material and directly proportional to, but less than, the magnitude of compressed pore air pressure. This was mainly caused by energy losses within the capillary fringe.

Key words: *compressed pore air pressure, diffusion equation, mathematical model, pressure potential, pre-event water*

3.2   Introduction

3.2.1   Background studies and problem statement

Previous studies have demonstrated that a stream stormflow hydrograph may consist of pre-event and event water (Pinder and Jones, 1969; Sklash and Farvolden, 1979). Pre-event water, also called "old water' (Collins *et al.*, 2000; Bishop *et al.*, 2004; Kienzler and Naef, 2008), is the water that exists in the catchment prior to a rainfall event. In many catchments, pre-event water is predominantly groundwater that is held in the saturated zone, as well as in the unsaturated zone. Since it is widely understood that groundwater travels at a low velocity, the appearance of a significant amount of the pre-event water (groundwater) in the stream stormflow hydrograph is a paradox (Kirchner, 2003) that calls for the investigation into the mechanisms that may enhance the rapid effusion and delivery of groundwater from hillslopes into a stream.

Mechanisms that have been proposed to explain the rapid mobilization of pre-event water (groundwater) from hillslopes include: preferential flow (McDonnell, 1990), groundwater ridging (Gillham, 1984), translatory flow (Lischeid *et al.*, 2002), transmissivity feedback (Kendall *et al.*, 1999), and pressurized pore air in the unsaturated zone (Torres *et al.*, 1998; Lorentz *et al.*, 2004). While most of these mechanisms have been extensively studied, the role of compressed pore air pressure in the rapid mobilization of groundwater has only been speculated (Torres *et al.*, 1998; Lorentz *et al.*, 2004).

However, studies have been undertaken on the rapid response of a water table to compressed pore air pressure in the unsaturated zone, a phenomenon referred to as the Lisse Effect. For instance, Heliotis and DeWitt (1987) developed qualitative characteristics of the Lisse Effect, after observations in northern Michigan peatland during intense rainfall events. In his revisit to the Lisse Effect, Weeks (2002) has detailed the relationship between the characteristics of the infiltration profile and the development of compressed pore air ahead of a wetting front. Linden and Dixon (1975) carried out a detailed field irrigation experiment, from which they observed increased hydraulic heads in groundwater, as a result of compressed pore air ahead of a wetting front. Marui *et al.* (1993) observed a rapid groundwater discharge that was caused by increased pore air pressure above the water table.

Most recently, Waswa *et al.* (2013) demonstrated that the capillary fringe plays a significant role in the rapid response of a water table in the Lisse Effect. These researchers observed

that, when a positive pressure is imposed on the upper boundary of the capillary fringe, two types of pressure waves occur within the capillary fringe. First, a downward pressure wave, which releases tension forces in water, propagates from the upper boundary of the capillary fringe towards the water table. On the arrival of the pressure wave front on the water table, the water table starts to rise, as an upward pressure wave. It was observed that the upward pressure wave contributes to the pressure potential in the groundwater, steepening the hydraulic gradient and thus increasing groundwater fluxes. However, there is still need for a theory that can explain or represent these processes.

The overall aim of the present study, therefore, is to develop and present a mathematical theory that can explain the processes involved in the response of a water table, as a result of the action of compressed pore air on the upper boundary of a capillary fringe. However, before the presentation of the model, a summary of some fundamental principles and a brief overview of some of the existing models are presented.

3.2.2 Some fundamental principles and definitions

3.2.2.1 Soil water potential energy

Soil water potential is the energy state of soil water, defined by its equivalent potential energy, as determined by the various forces on the water per unit quantity, and relative to a reference potential zero. Forces acting on soil water are: (1) capillary forces; (2) adsorptive forces (adhesion of water to solid soil surface); (3) gravitational forces; (4) drag, or shear forces (at soil surface-water interface); and (5) osmotic forces (Childs and George, 1948). Capillary and adsorptive forces are collectively referred to as soil matric potential and pre-dominate the unsaturated zone, or more precisely, the vadose zone. However, when dealing with both saturated and unsaturated zones, the preferred term is the pressure potential (Hillel, 1971), the values of which, in the respective zones, are positive and negative.

A static pure liquid in a porous media (e.g. soil water) possesses two types of energy: (1) potential energy, due to its position; and (2) pressure energy exerted on the sideways of the containing media. The pressure energy and potential energy are convertible, one into the other, and therefore, their sum for a liquid at rest is constant (Mathur, 2003). The fluid energy considered in this study is the pressure energy in the pore fluid, within a porous media. This pressure energy may also be expressed,

with reference to a water table, as the potential energy; taking negative values above a water table and positive values below a water table. Soil water potential can be expressed in three units: (1) potential energy per unit mass of water, $mgh/m = gh$, e.g. Nm/kg [L^2T^{-2}]; (2) potential energy per unit volume of water, $mgh/V = \rho gh$, e.g. N/m^2 [$ML^{-1}T^{-2}$] which is the water pressure units; and (3) potential energy per unit weight of water, mgh/mg, e.g. m [L], which is the height of water. In this paper, energy in soil water and soil air will be expressed by the last unit.

3.2.2.2   Capillary pressure

Capillary pressure, h_c [L], is the difference in pressure across the interface between two immiscible fluids (Scheidegger, 1960) e.g. air and water in soil:

$$h_c = h_a - h_w \qquad\qquad [3.1]$$

where, h_a [L] is the pressure in the air phase (non-wetting phase) and h_w [L] is the pressure in the water phase (wetting phase). The capillary pressure can also be estimated from the relationship of the soil pressure head and volumetric water content. Brooks-Corey (B-C) equation (Brooks and Corey, 1964),

$$h_c = h_b \Theta^{-1/\lambda}, \qquad\qquad [3.2]$$

is one of the models commonly used in estimating the capillary pressure head. In Eq. [3.2], h_b [L] is the air entry pressure head (Figure 3.1), λ is the pore size distribution index of the material and Θ [-] is the normalized water saturation, given as $\Theta = (\theta - \theta_r)(\theta_s - \theta_r)^{-1}$, θ [L^3L^{-3}] is the measured soil water content, θ_r [L^3L^{-3}] is the residual water content and, θ_s [L^3L^{-3}] is the saturation water content.

3.2.2.3   The capillary fringe

The air entry pressure head, h_b, in the B-C's equation, Eq. [3.2], has widely been adopted in defining the height of the capillary fringe (Bear, 1988; Nachabe, 2002), which usually extends above the phreatic surface. Brooks and Corey (1964) showed that, when the experimental data $h_c = h_c(\Theta)$ are plotted on a log-log paper, a straight line is obtained, except for Θ close to unit. They suggested that the negative slope of the curve λ (pore size

distribution) and the intercept h_b (the value of h_c obtained, by extending the straight line to $\Theta = 1$) be used as constants characterizing the medium. Bear (1988) noted that this approach is extremely useful, for example, when choosing sand for laboratory experiments, as the entire function $h_c = h_c(\Theta)$ is represented by two constants.
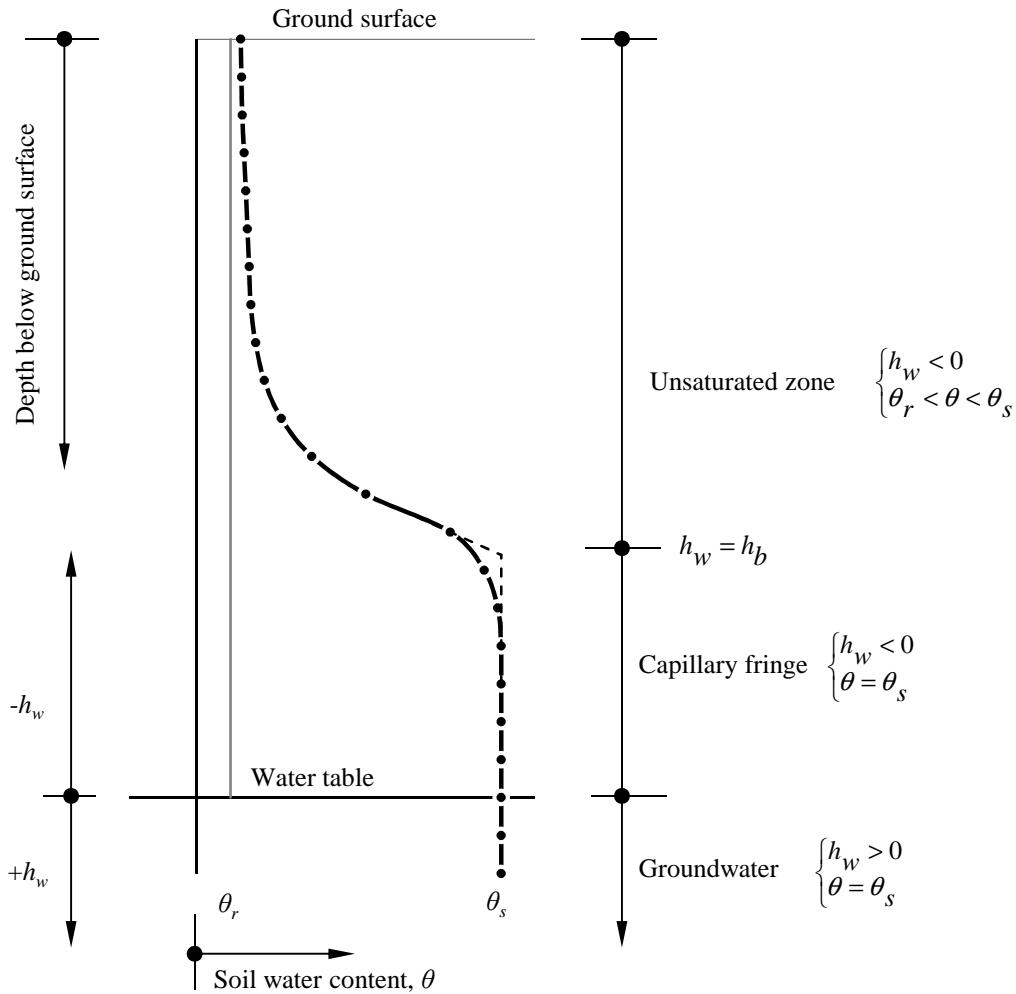
Figure 3.1 Properties and position of the capillary fringe in the structure of the groundwater. h_w is pore water pressure, h_b is air entry pressure, θ_r is residual soil water content, θ_s is saturated soil water content (modified from Gillham, 1984).

The extent of the capillary fringe above the phreatic surface depends on the wetting and drying history of the sample, the texture, the grain size, and the structural characteristics and compressibility of the material (Gillham, 1984). The ranges of the depth of a capillary fringe for various soils are: (1) for sand – 1cm to 100 cm; (2) silt soil – 100 cm to 1000 cm; and (3)

clay - > 10 m (Gillham, 1984). A capillary fringe is descriptively referred to as zone of tension saturation (Gillham, 1984) because the water within this zone is usually under tension ($h_w < 0$), as the water found in the unsaturated zone, and yet all the soil pores are completely filled with water (i.e., $\theta = \theta_s$), as in the zone under the phreatic surface (Figure 3.1).

By this definition, therefore, it follows that pressure is the only variable, between the water within the capillary fringe and the water below the water table. This implies that any phenomena that can vary the pressure within the capillary fringe may cause a water table to respond, without the recharge of the infiltration profile.

3.2.3   Review of some models

Since change in pressure potential in soils is commonly associated with the change in soil water content, many existing models of propagation of pressure energy in saturated and unsaturated porous media, e.g. Iverson (2000) and Rasmussen *et al.* (2000), are based on the Richards' Equation (Richards, 1931):

$$\frac{\partial \theta}{\partial t} = \frac{\partial}{\partial y}\left[K(\theta)\left(\frac{\partial \psi}{\partial y} - 1 \right) \right] = \frac{\partial}{\partial y}\left[D(\theta)\frac{\partial \theta}{\partial y} - K(\theta) \right] , \qquad [3.3]$$

where,

$$D(\theta) = K(\theta)\frac{\partial \psi}{\partial \theta} = \frac{K(\theta)}{C(\psi)} , \qquad [3.4]$$

is the hydraulic diffusivity, $C(\psi)$ is the specific water capacity, θ is the soil water content, $K(\theta)$ is the unsaturated hydraulic conductivity (depends on soil water content), ψ is the fluid pressure (capillary suction for unsaturated porous media), y and t are the space and time coordinates, respectively. It should be emphasized that the Richards' Equation was developed for the movement of water in the unsaturated soils.

$C(\psi)$, in Eq. [3.4], is the slope of the water retention curve and is only defined in the unsaturated zone (above the capillary fringe). That is, $C(\psi)$ quantitatively defines the relationship between the change in pressure potential and the change in water content.

From the Richards' Equation, therefore, it may be stated that, in a porous media of specified physical properties, the propagation of certain saturation carries with itself a distinct pore water pressure that is unique from other saturations. In other words, water is the pressure (energy) carrier, and therefore, without the movement of water, pressure (energy) may not be propagated.

Since a functional relationship exists between θ and ψ, diffusivity is also expressed in terms of soil water content, or pressure head. Wu (2003) noted that hydraulic diffusivity provides a measure of the rate of water movement through soil. Because diffusivity is directly proportional to hydraulic conductivity, the rate of water movement through soil is highest, when the soil is fully saturated (maximum diffusivity). It is logical, therefore, to assume that the water-flow-dependent pressure (energy) transmission will be highest during saturated hydraulic conductivity. Iverson (2000) adopted this assumption, of maximum diffusivity and minimum value of $\partial\theta/\partial\psi$ (maximum value of $\partial\psi/\partial\theta$), in the derivation of a diffusion model for predicting pore water pressure propagation through a saturated zone, under specified rainfall conditions at the ground surface. Therefore, Iverson's model may not apply in the capillary fringe, where the transmission of pressure energy is entirely a diffusive process that occurs, without water flux and the source of energy perturbation is the compressed pore air pressure.

Rasmussen *et al.* (2000) derived an advection-diffusion equation:

$$\frac{\partial\psi}{\partial t} = D(\theta)\frac{\partial^2\psi}{\partial y^2} - v\frac{\partial\psi}{\partial y} \,, \qquad\qquad [3.5]$$

for the prediction of transient pressure wave velocities in unsaturated soils, due to perturbations at the soil surface. The coefficient v in Eq. [3.5] is the wave velocity, expressed as $dK/d\theta$.

Although, Rasmussen *et al.* (2000) derived Eq. [3.5] from the Richards' Equation and the kinematic wave theory, they estimated the hydraulic diffusivity parameter, neither as defined in Eq. [3.4], nor by Iverson's approximation approach. They used an analytical

parameter estimation technique (Farlow, 1982), based on their experimental data and their equation, to estimate the diffusivity coefficient in Eq. [3.5]. Furthermore, in the implementation of their equation, Rasmussen *et al.* (2000) ignored the kinematic velocity component (i.e. $v = 0$) which effectively reduced their original equation to the diffusion equation, similar to the one derived by Iverson (2000).

Eq. [3.5] was specifically developed and solved for the unsaturated zone (conditions) and for spike (short term) pressure perturbations. Therefore, it may not apply in a saturated zone, such as the capillary fringe, in which the source of pressure perturbation (compressed pore air) lasts for an extended duration, nearly 2-4 days (Heliotis and DeWitt, 1987). Nevertheless, hitherto, Rasmussen *et al.*'s (2000) approach of estimating the diffusivity coefficient seems to be the most viable for an equation of diffusion of energy through soil water.

In conclusion, while the Richards' Equation, and more specifically, the embedded hydraulic diffusivity, sufficiently and adequately applies to the unsaturated zone, it violates the law of the conservation of energy, when applied to saturated zone, in which a fluid-pressure propagation-velocity may be much faster than the average water flow velocity (Rasmussen *et al.*, 2000 and Wenninger *et al.*, 2004). In the present chapter, an attempt is made to establish the theory of diffusion of energy through a capillary fringe, and generally, through any saturated zone, when a source of energy perturbation is instantly imposed on its upper boundary and for an extended. In doing this, the theory has been developed from first principles, because the contradictions to be avoided are inherent in the fundamental conceptions employed. The neglect of energy relationships is not permissible. The developed theory is evaluated using the laboratory experimental results.

3.3   Theoretical approach

3.3.1   Assumptions

The equations derived and presented in this section, are based on the following assumptions: (1) the porous media is homogeneous and isotropic on the averaging scale; (2) the porous media is rigid and non-deformable in space and time (the physical properties of the porous medium are spatially and temporally constant); (3) water, as a fluid, is incompressible; (4) the height of the capillary fringe, above the water table, is equivalent to the pore air entry

pressure head, h_b, of the porous media and as defined by the B-C's equation, Eq. [3.2]; (5) below the upper boundary of the capillary fringe, the pressure potential varies linearly with depth; (6) water is a continuous phase beneath the upper boundary of the capillary fringe i.e., $\theta = \theta_s$, for $h_w > h_b$. Similarly, it is assumed that air is a continuous phase above the upper boundary of the capillary fringe, i.e. $\theta = \theta_r$, for $h_w < h_b$; (7) water and air are homogeneous, immiscible and their viscosities are constant; (8) the change in pore air pressure in the unsaturated zone, above the upper boundary of the capillary fringe, is uniform and does not vary with depth.

3.3.2 Derivation of differential equation of conduction of energy through capillary fringe

An idealized capillary fringe, as shown in Figure 3.2, is considered. The capillary fringe is of uniform unit cross-sectional area, U, and uniform saturation, i.e

$$\theta(y) = \theta_s, \text{ for } y > 0. \tag{3.6}$$

The vertical space coordinate is oriented positive downwards, with its origin at the upper boundary of the capillary fringe. The energy coordinate is also oriented positive downwards, but with its origin at the water table.

Within this framework, the unsaturated zone (UZ), the zone below the phreatic surface and the capillary fringe (CF) can be defined as: -

$$\begin{aligned} h_w &< 0 \\ \theta &< \theta_s \end{aligned}, \tag{3.7}$$

$$\begin{aligned} h_w &> 0 \\ \theta &= \theta_s \end{aligned} \tag{3.8}$$

and

$$\begin{aligned} h_w &< 0 \\ \theta &= \theta_s \end{aligned} \tag{3.9}$$

respectively.

The boundaries of the capillary fringe can be defined by the space and energy coordinates. The upper boundary of the capillary fringe, β_{tcf}, is defined as:

$$\begin{aligned} y &= y_0 = 0 \\ h_w &= h_b = -y_{cf} \end{aligned}, \qquad [3.10]$$

while the lower boundary of the capillary fringe (the phreatic surface), β_{wt}, is defined as:

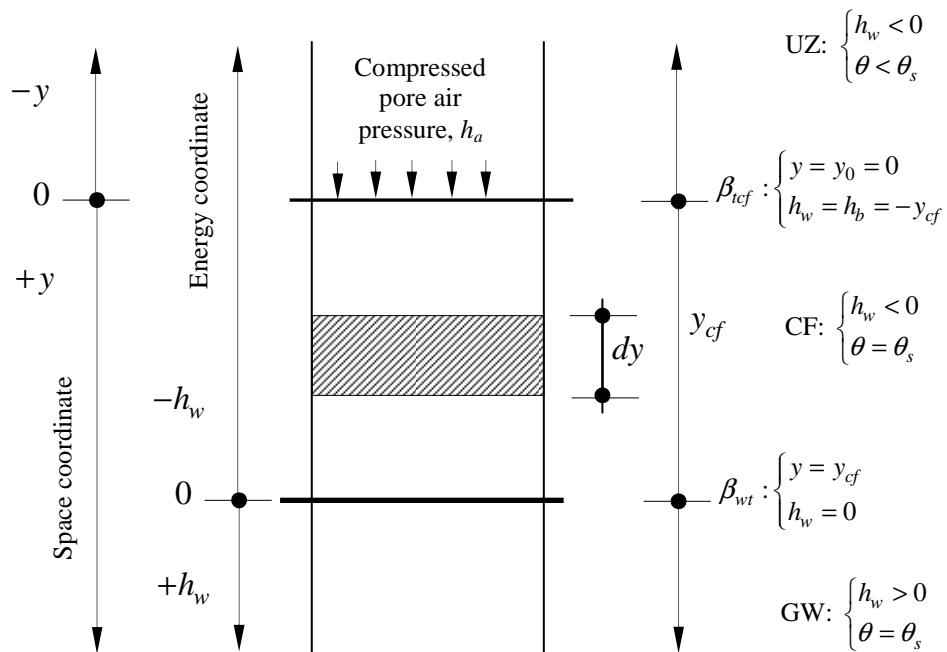$$\begin{aligned} y &= y_{cf} \\ h_w &= 0 \end{aligned}, \qquad [3.11]$$

Figure 3.2 Idealized free body diagram of a capillary fringe (CF) used in the derivation of the differential equation of diffusion of energy through soil water. UZ is unsaturated zone and GW is groundwater (under positive pressure).

Energy equation

It should be noted that the fundamental property here is energy, which cannot be described by a velocity field of water. This is because energy is propagated through water by conduction process and without the movement of water particles. Therefore, the continuity equation is conceived for the flux of energy without an association with the water velocity field. In the basic law of conservation of energy for the entire height of the capillary fringe, $y_0 \le y \le y_{cf}$, the rate of change of energy within the capillary fringe is equal to the net propagation of energy through the two boundaries, β_{tcf} and β_{wt}. Consider an infinitesimal section of height dy in the interval $y_0 \le y \le y_{cf}$. The energy content, dE_c, in this infinitesimal section is proportional to the weight of water and the fluid pressure (energy per unit weight of water), h_w:

$$dE_c = U\rho_w g\left(\phi dy\right)h_w \qquad\qquad [3.12]$$

where, U is the unit cross-sectional area (m^2), ρ_w is the density of water (kg m^{-3}), ϕ is the porosity of the porous media and g is the gravitational constant (m s^{-2}). Therefore, in the absence of work done, the total energy content in the interval $y_0 \le y \le y_{cf}$ is:-

$$E_c = \int_{y_0}^{y_{cf}} U\rho_w g\phi h_w(y,t)dy \qquad\qquad [3.13]$$

Constitutive equation

The constitutive equation is derived, based on the Fourier's law of heat conduction (Yunus, 2003),, which for our present case, can be stated as: the rate of energy propagating into a body (a capillary fringe) through a small surface element on its boundary is proportional to the area of that element and the outward normal derivative of the pressure energy at that location. In other words, the diffusion rate of energy through a surface/boundary is proportional to the negative pressure energy gradient across the surface/boundary. Therefore, the net energy through the boundaries β_{tcf} and β_{wt} is:-

$$E_r\left(t\right) = \kappa U\phi\frac{dh_w}{dy}(y_{cf},t) - \kappa U\phi\frac{dh_w}{dy}(y_0,t) \qquad\qquad [3.14]$$

where, κ is energy conductivity of the pore fluid. Energy conductivity, analogous to thermal conductivity in thermodynamics (Yunus, 2003), is the rate of energy transfer through a unit thickness of the material (capillary fringe) per unit area per unit pressure difference.

From the law of conservation of energy, it implies that:-

$$\frac{dE_c}{dt} = E_r(t), \text{or } \frac{d}{dt}\int_{y_0}^{y_{cf}} \rho_w g h_w(y,t)dy = \kappa\frac{dh_w}{dy}(y_{cf},t) - \kappa\frac{dh_w}{dy}(y_0,t).$$ [3.15]

For smooth material properties, i.e., if ρ_w and k are continuous with continuous first derivatives, the solution $h_w(y,t)$ is also continuous with continuous first partial derivatives $\partial h_w/\partial y$ and $\partial h_w/\partial t$ (Kevorkian, 1989). Hence, Eq. [3.15] can also be written in the following form, after expressing the right-hand side as the integral of a derivative:

$$\int_{y_0}^{y_{cf}} \left\{ \rho_w g \frac{\partial h_w}{\partial t}(y,t) - \frac{\partial}{\partial y}\left[\kappa\frac{\partial h_w}{\partial y}(y,t) \right] \right\} dy = 0$$ [3.16]

Since Eq. [3.16] can apply to any limits y_1 and y_2, it follows that the integrand must vanish:

$$\rho_w g \frac{\partial h_w}{\partial t} - \frac{\partial}{\partial y}\left[\kappa\frac{\partial h_w}{\partial y} \right] = 0.$$ [3.17]

Eq. [3.17] can be written simply as:-

$$\frac{\partial h_w}{\partial t} = d_e \frac{\partial^2 h_w}{\partial y^2}$$ [3.18]

in which, d_e, the energy diffusivity, is defined as:

$$d_e = \frac{\kappa}{\rho_w g},$$ [3.19]

Energy diffusivity, analogous to thermal diffusivity (Yunus, 2003), is another material property that appears in the transient energy conduction analysis. It represents how fast energy diffuses through a material.

3.3.3　　　Non-dimensionalization

In the present problem, the variables are h_w, t and y, while the parameters are d_e and y_{cf}. The variables are therefore normalized as follows:

$$H_w = \frac{h_w}{y_{cf}}, \qquad T = \frac{t.d_e}{y_{cf}^2}, \qquad Y = \frac{y}{y_{cf}} \qquad\qquad \text{[3.20a, b, c]}$$

Then Eq. [3.18] can be written in a dimensionless form as:

$$\frac{\partial H_w}{\partial T} = \frac{\partial^2 H_w}{\partial Y^2} \qquad\qquad \text{[3.21]}$$

3.3.4　　　Initial and boundary conditions

Initial conditions

Based on the assumption that the pressure potential, below the upper boundary of the capillary fringe, β_{tcf} , linearly varies with depth, the initial condition can be written as: -

$$h_w(y,0) = y - y_{cf} \qquad \text{for} \qquad y > 0 \qquad\qquad \text{[3.22]}$$

Here, the expression for space limits is for any depth of the saturated zone, below the upper boundary of the capillary fringe. Note that the initial condition Eq. [3.22] holds for any depth below the upper boundary of the capillary fringe, and is independent of the thickness of the saturated zone, or the position of the lower boundary.

Boundary conditions

The upper boundary condition is defined by:

$$h_w(0,t) = h_a . u(t), \qquad\qquad t > 0 \qquad\qquad\qquad\qquad [3.23]$$

where, h_a is the imposed compressed pore air pressure and $u(t)$ is the Heaviside unit step function (Sokolnikoff *et al.*, 1958; Trim, 1990; Riley *et al.*, 2006).

It is also important to pose the semi-infinite boundary condition, where the change in pressure potential, as a result of compressed pore air pressure at the boundary β_{tcf}, becomes negligible, as the depth increases. This can be written as:-

$$\frac{dh_w(y,t)}{dy} \to 0 \text{, as } y \to \infty \qquad\qquad\qquad\qquad [3.24]$$

It is important to note that the change in pressure energy at any point within a static, homogeneous and incompressible fluid, depends on the depth of that point relative to some reference plane, and is not influenced by the size and shape of the container (Janna, 1983). In other words, the position of the lower boundary or the shape of the container does not have any influence on the change in pressure energy at a point within the saturated porous media.

3.3.5 The solution of the differential equation

We seek the solution to Eq. [3.18], which can also satisfy the initial and boundary conditions Eq. [3.22-3.24]. Applying the Laplace transform in the time domain to Eq. [3.19], i.e.

$$d_e L \left\{ \frac{\partial^2 h_w}{\partial y^2} \right\} = L \left\{ \frac{\partial h_w}{\partial t} \right\}, \qquad\qquad\qquad [3.25]$$

yields,

$$d_e \frac{\partial^2 h_w}{\partial y^2} = s h_w - h_w(y,0) \qquad\qquad . \qquad\qquad [3.26]$$

where, s is a variable in the Laplace transform (Farlow, 1982; Trim, 1990).

Applying the Laplace transform to the boundary condition, Eq. [3.23], yields:

$$L\{h_w(0,t)\} = \frac{h_a}{s}, \qquad s > 0 \qquad\qquad [3.27]$$

With the initial condition, Eq. [3.26] can be written as,

$$d_e \frac{\partial^2 h_w}{\partial y^2} - s h_w = (y_{cf} - y) \qquad\qquad [3.28]$$

The general solution to the complementary function (CF) of Eq. [3.29] is:

$$h_w(y,s) = A(s)\exp-\left(\sqrt{\frac{s}{d_e}}\, y\right) + B(s)\exp\left(\sqrt{\frac{s}{d_e}}\, y\right), \qquad\qquad [3.29]$$

where $A(s)$ and $B(s)$ are constants, of which the values are to be determined by the boundary and initial conditions.

The solution to the particular integral of Eq. [3.28] takes the form of:

$$h_w(y,s) = C(s)\, y + D(s), \qquad\qquad [3.30]$$

which, when solved for the constants, becomes

$$h_w(y,s) = \frac{y}{s} - \frac{y_{cf}}{s} \qquad\qquad [3.31]$$

Therefore, the solution to Eq. [3.26] is:

$$h_w(y,s) = A(s)\exp-\left(\sqrt{\frac{s}{d_e}}\, y\right) + B(s)\exp\left(\sqrt{\frac{s}{d_e}}\, y\right) + \frac{y}{s} - \frac{y_{cf}}{s} \qquad\qquad [3.32]$$

On the substitution of the initial and boundary conditions, Eq. [3.32] becomes

$$h_w(y,s) = \left(\frac{h_a}{s}\right)\exp-\left(\sqrt{\frac{s}{d_e}}\,y\right) + \frac{y}{s} - \frac{y_{cf}}{s}, \qquad\qquad [3.33]$$

which, on application of the inverse Laplace transform, $L^{-1}\{h_w(y,s)\}$, yields

$$h_w(y,t) = h_a.erfc\left(\frac{y}{\sqrt{4d_e t}}\right) + (y - y_{cf}) \qquad\qquad [3.34]$$

The dimensionless counterpart of Eq. [3.34] is: -

$$H_w(Y,T) = H_a.erfc\left(\frac{Y}{\sqrt{4T}}\right) + (Y-1) \qquad\qquad [3.35]$$

Note that Eq. [3.34], which is analogous to the heat conduction solution (Carslaw and Jaeger, 1959, pp 63) and Eq. [3.36] consist of both the initial condition, $(y - y_{cf})$, as well as the change in pressure potential, as a result of the imposed compressed pore air pressure on the boundary β_{tcf}. In using the model, it will suffice to use and report only the results of the change in pressure potential at any specified depth, without including the initial pressure potential.

3.3.6   Estimation of energy diffusivity coefficient

By knowing the energy diffusivity, it is possible to understand how fast energy can be transmitted in a particular medium. In applying Eq. [3.34], values of energy diffusivity should be known. Here, this parameter is determined by fitting Eq. [3.34] to the experimental data, in a methodology similar to that employed by Rasmussen *et al.* (2000) and Flury and Gimmi (2002). The time of peak response, t_p, occurs, when the second time derivative of Eq. [3.35] is equated to zero, i.e. $\partial^2 h_w(y,t)/\partial t^2 = 0$, which yields:

$$t_p = \frac{y^2}{6d_e} \qquad\qquad [3.36]$$

Determination of the time to peak, t_p, is schematically shown in Figure 3.3.
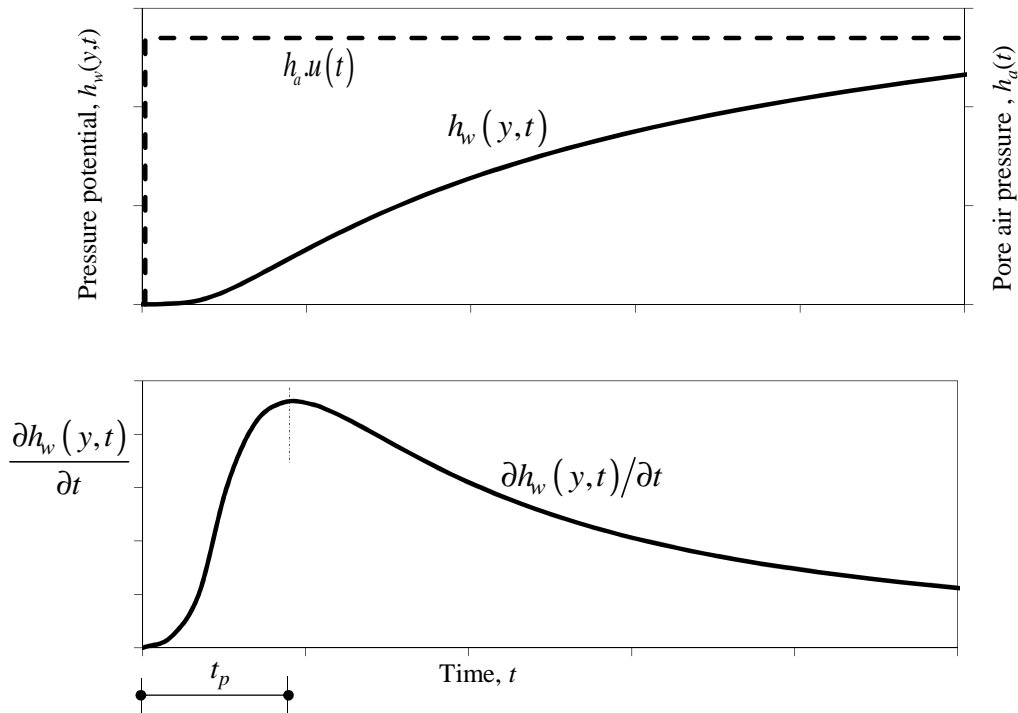
Figure 3.3 Schematic presentation of determining the time to peak, t_p, for estimation of energy diffusivity coefficient, d_e.

3.4 Experimental approach

3.4.1 Material parameters

The unconsolidated porous media, water and air are the three main materials used in the laboratory experiments. The porous media comprises a mix of graded silica quartz (SiO_2) and clay soil, both of which were obtained from a commercial supplier. The individual grains of the soils are uniform in shape, stable, clean and free of organic matter. The graded silica sand was supplied in two grades, which were predominantly medium sand and fine sand. The clay was Kaolin clay powder (China clay), comprising trace mica and quartz. The silica quartz sand and Kaolin clay powder had bulk densities of 1500 kg/m^3 and 350 Kg/m^3, respectively.

The two graded silica sands and clay soil were mixed in different ratios, to obtain three types of soils of different physical properties, as shown in Table 3.1. For ease of reference, these soils are named Coarse soil (C), Medium soil (M) and Fine soil (F).

Table 3.1 Physical properties of the soils used in the laboratory experiments

Quantity	Symbol	Value			Water
		Soil			
		C	M	F	
Bulk density	ρ_s (Kg m^{-3})	1500	1550	1700	1000
Porosity	ϕ	0.40	0.40	0.45	
Saturated hydraulic conductivity	K_{sat} (cm min^{-1})	1.68	1.02	0.52	
Pore air entry pressure head	h_b (cm)	20	30	35	
Pore size distribution index	λ	2.65	1.7	4.72	
Particle size distribution					
Coarse sand, CS (%)		25	13	13	
Medium sand, MS (%)		73	45	46	
Fine sand, FS (%)		2	40	33	
Silt, S (%)		0	2	2	
Clay, Cl (%)		0	0	6	

C is Coarse textured soil, M is medium textured soil and F is Fine textured soil. CS = coarse sand (0.50 – 2.00 mm), MS = medium size sand (0.25 – 0.50 mm), FS = fine sand (0.053 – 0.25 mm), S = silt (< 0.053 mm), Cl = clay (~2 μm)

The Coarse soil contained the highest percentage of coarse sand and medium sand, and zero percentage of clay content. The Medium soil was made of almost an equal percentage of medium sand and fine sand, and zero clay content. The Fine soil was the only soil that contained clay soil. The Medium soil and the Fine soil had nearly equal heights of capillary fringe (Figure 3.4). The particle size distribution, the saturated hydraulic conductivity and the water retention characteristics of the three soils were determined in the laboratory, following the methods and procedures of Gee and Bauder (1986), Klute (1986) and Klute and Dirksen (1986), respectively.
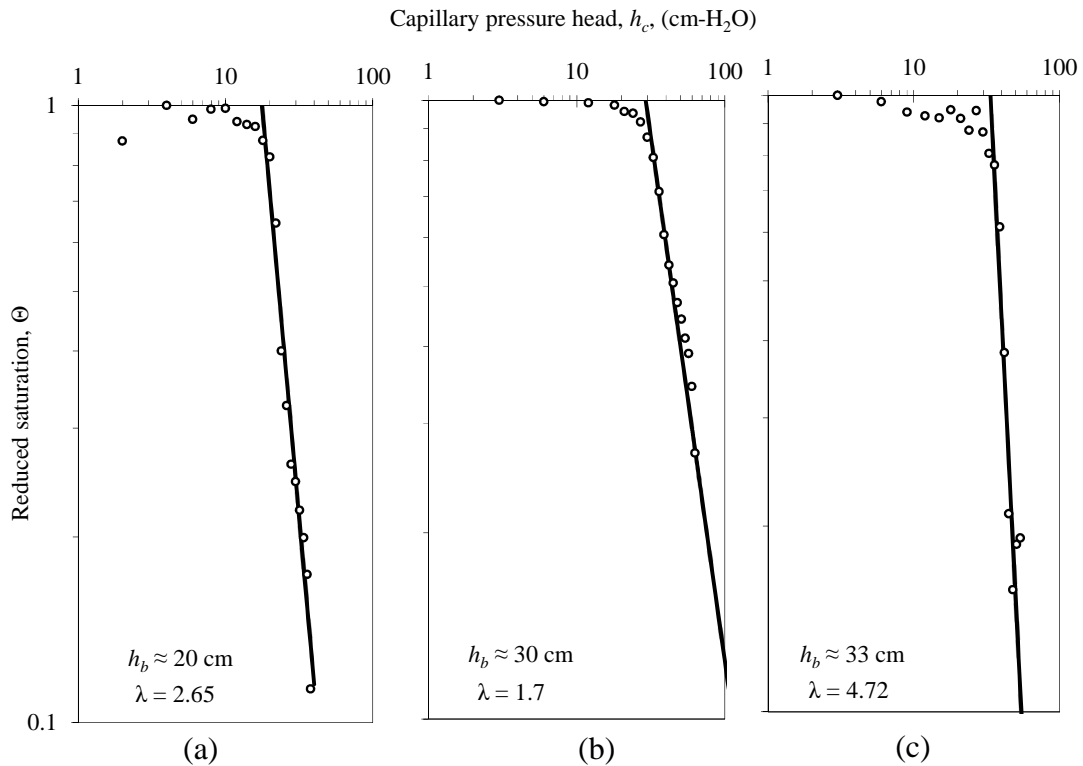
Capillary pressure head, h_c, (cm-H$_2$O)

Figure 3.4 Capillary pressure head as a function of reduced saturation for the (a) Coarse soil, (b) Medium soil, and (c) Fine soil, used in the laboratory experiments

3.4.2   Experimental apparatus and instrumentation

The physical laboratory model consisted of a column of soil in a vertical PVC pipe with an internal diameter of 30 cm and a height of 210 cm. Seven data takeoff ports were installed along the pipe, at 60, 90, 120, 130, 140, 150 and 160 cm, below the soil surface, which was at 40 cm below the top of the PVC pipe, as shown in Figure 3.5. Henceforth, a data take-off port will be referred to by its position, below the soil surface. For example, Port 60 refers to a data take-off port located at 60 cm, below the soil surface. The assumptions stated in the derivation of the theoretical equation apply in the laboratory experiment as well.

Each data takeoff port was installed with a Time Domain Reflectometry (TDR) probe, for the measurement of volumetric water content. Each of the lower five ports had a 0.5 bar miniature tensiometer, for the measurement of soil pore water pressure. Each of the upper two ports was installed with a pore air pressure probe, for the measurement of pore air pressure. A drainage/discharge tube and a piezometer were attached to the column, at a depth of 170 cm below the soil surface, for groundwater discharge and for the monitoring of the groundwater level, respectively.
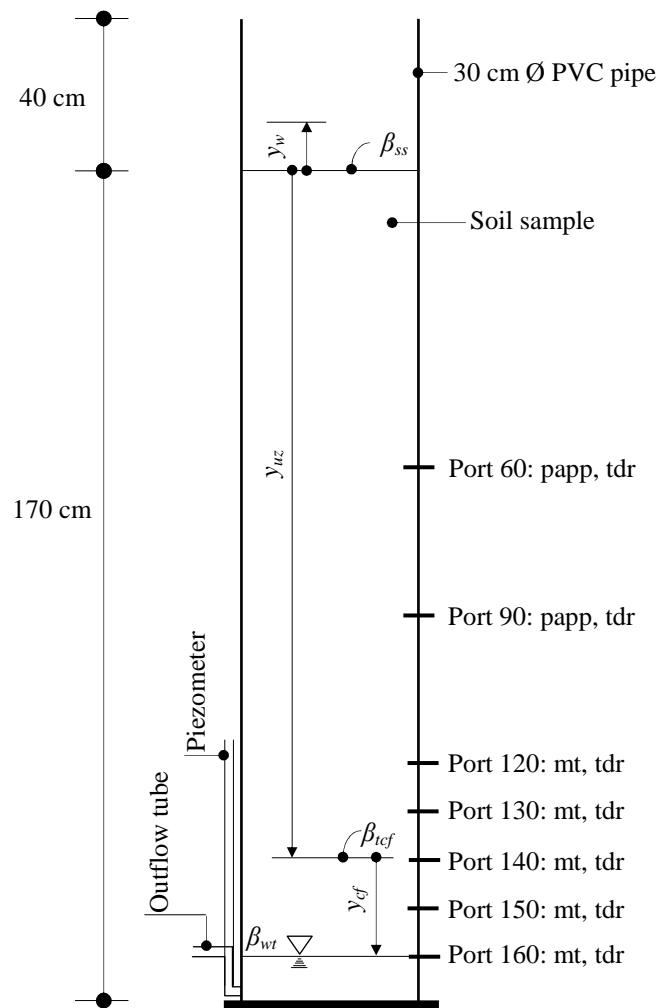
Figure 3.5(a) Laboratory experimental set up. y_{cf} is height of capillary fringe, y_{uz} is height of unsaturated zone, y_w is height of water ponding on the soil surface, β_{ss} is soil surface, β_{tcf} is top boundary of the capillary fringe, β_{wt} is water table (zero pressure line), papp is pore air pressure probe, tdr is time domain reflectometry, and mt is miniature tensiometer.

The TDR probe was made of three, 5 mm diameter parallel stainless steel rods, which were impeded into a PVC block, at a separation distance of 17 mm and exposed length of 100 mm. The soil water content data, measured by the TDRs, were recorded and temporarily stored on a CR1000 Campbell Scientific data logger via a Campbell Scientific TDR100 wave generator and a SDMX50 Multiplexer (Figure 3.5(b)). Miniature tensiometers consisted of a 15 mm-long ceramic-cup with an outer diameter of 5 mm. The open end of the ceramic cup was joined to one end of a 10 cm-long PVC tube with the same outer diameter. The other end of the PVC tube was connected to a differential pressure

transducer. The data of pore-water pressure and pore-air pressure were recorded and temporarily stored on a CR1000 Campbell Scientific data logger via differential pressure transducers of 1 bar Motorola MPX5100DP and 0.1 bar Motorola MPX5010DP, respectively (Figure 3.5(b)).
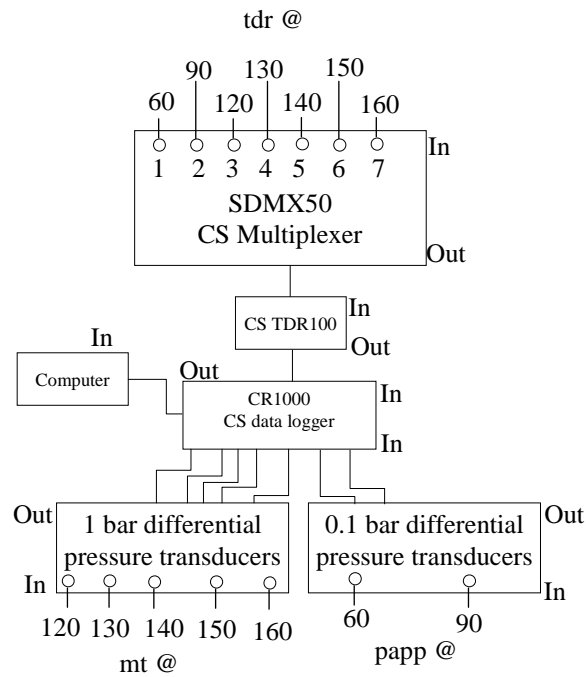
Figure 3.5(b) Instrumentation layout.

3.4.3   Experimental description

The experimental procedure described here was carried out on each of the three types of soils described in Section 3.4.1. The PVC cylindrical pipe was packed with dry soil, in layers of ~55 cm high to an average bulk density of 1530 kg/m^3. After each layer, the wall of the pipe was tapped with the same number of blows, in order to achieve uniform and maximum density and packing. The TDRs and the pore-air pressure probes were mounted in the wall of the PVC pipe, before being packed with sand. The ceramic-cup miniature tensiometers, due to their fragility, were inserted, after packing the pipe with the soil. After all the probes were seated into the column of soil, the entire wall of the pipe was sealed to an air-tight state with silicon sealant.

Water , that formed groundwater, was introduced in the packed column of soil from the bottom, to minimize the entrapment of encapsulated pore air, which has been found to contribute to disproportionate water table responses (Peck, 1960; Weeks, 1979). By adjusting the level of the nozzle of the discharge tube, the initial water table was set at the elevation of Port 160. The capillary fringe, of which the height was taken to be equivalent to the air-entry pressure value of the soil, extended above the water table.

With this initial state, the experiment was started by ponding the soil surface with water. Groundwater fluxes, tensiometric pore water pressure, volumetric water content and pore air pressure were monitored and recorded at a time-resolution of 20 seconds, starting from the moment that the soil surface was ponded. For each soil type, two experiments were performed, with different depths of surface ponded water, namely 15 cm and 30 cm.

3.5   Results

The change in pressure potential at the initial water table (lower boundary of the capillary fringe), β_{tcf} , when compressed pore air pressure is imposed on the upper boundary of the capillary fringe are as shown in Figure 3.6 and Figure 3.7

Both the theoretical and the observed results indicate that the rate of increase in pressure potential, as well as the total change in pressure potential at any time, was inversely proportional to the thickness (height) of the capillary fringe, or pore air entry pressure head, of the soil. The rate of increase in pressure potential, as recorded by the tensiometer at Port 160, was highest in the Coarse soil and lowest in the Fine soil (Figure 3.6). Likewise, at any given time, the total change in pressure potential was highest in the Coarse soil and lowest in the Fine soil (Figure 3.6). For instance, at minute 10, the total change in pressure potential in the Coarse soil, the Medium soil and the Fine soil, were approximately 35 cm-H_2O, 25 cm H_2O and 20 cm-H_2O, respectively.
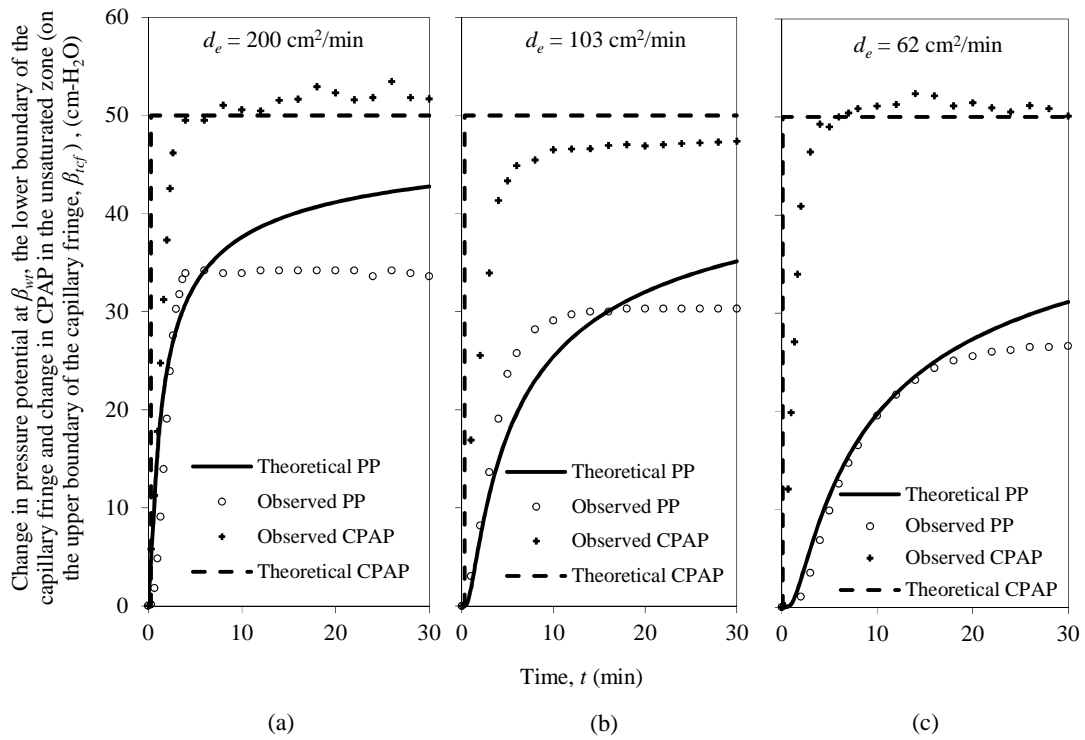
Figure 3.6 Theoretical and experimental results of pressure potential (PP) at the lower boundary of the capillary fringe (initial water table), β_{wt}, caused by compressed pore air pressure (CPAP) of 50 cm-H_2O in the unsaturated zone, in (a) Coarse textured soil (b) Medium textured soil and (c) Fine textured soil. Theoretical PP is given by Eq. [3.34] and theoretical CPAP is the Heaviside unit step function, Eq. [3.23], for h_a of 50 cm-H_2O.

The total change in pressure potential is directly proportional to, but less than, the magnitude of compressed pore air pressure (Figure 3.7)

The time lag of the pressure potential (at the water table) to respond to the imposed compressed pore air pressure on the upper boundary of the capillary fringe is observed at the origins of the pressure curves in Figure 3.6. This time lag to respond appears to increase and become more evident with the height of the capillary fringe. Whereas the response in the pressure potential in the Coarse soil appears to be instantaneous, the response in the Fine soil exhibits a more distinct time lag. However, scaling the results using the dimensionless time, T, Eq. [3.22b], the responses in all the soils are not instantaneous (Figure 3.8). Furthermore, the total change in pressure potential at the water table in all the soils only approaches the amount of compressed pore air pressure, imposed on the capillary fringe, after an extended time. This is evident in the behavior of the ratio of pressure potential to

compressed pore air pressure, i.e., h_w/h_a, which asymptotically approaches unit as time increases to infinity (Figure 3.8(c)).
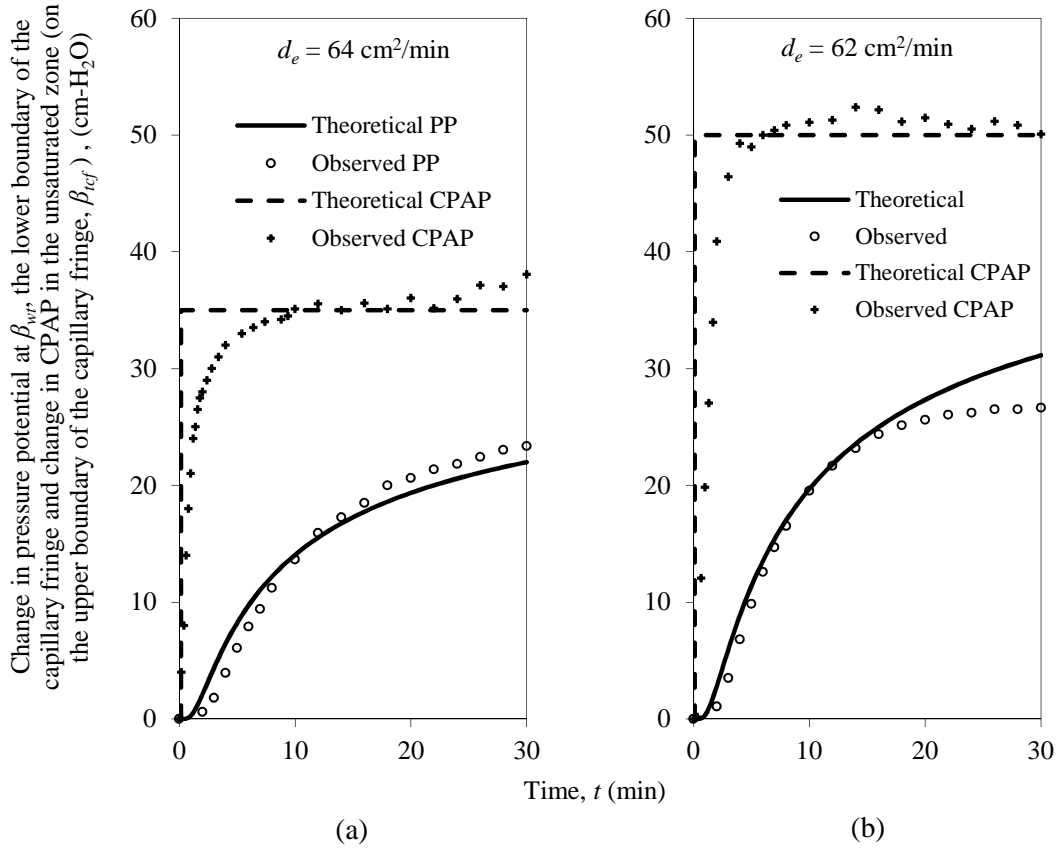

Figure 3.7 Theoretical and experimental results of pressure potential (PP) at the lower boundary of the capillary fringe (initial water table), β_{wt}, in the Fine soil, caused by caused by compressed pore air pressure (CPAP) of (a) 35 cm-H$_2$O and (b) 50 cm-H$_2$O in the unsaturated zone. Theoretical PP is given by Eq. [3.34] and theoretical CPAP is the Heaviside unit step function, Eq. [3.23].

The overlap, or the agreement, between the theoretical results and the observed results becomes stronger with the increase of the fineness of the soil. The reason for this is because of energy losses from the system, through groundwater discharge. Due to higher hydraulic conductivity of the Coarse soil than the Fine soil, there was an instantaneous and large discharge of groundwater in the experiment with the former soil as soon as pore air pressure started to increase.
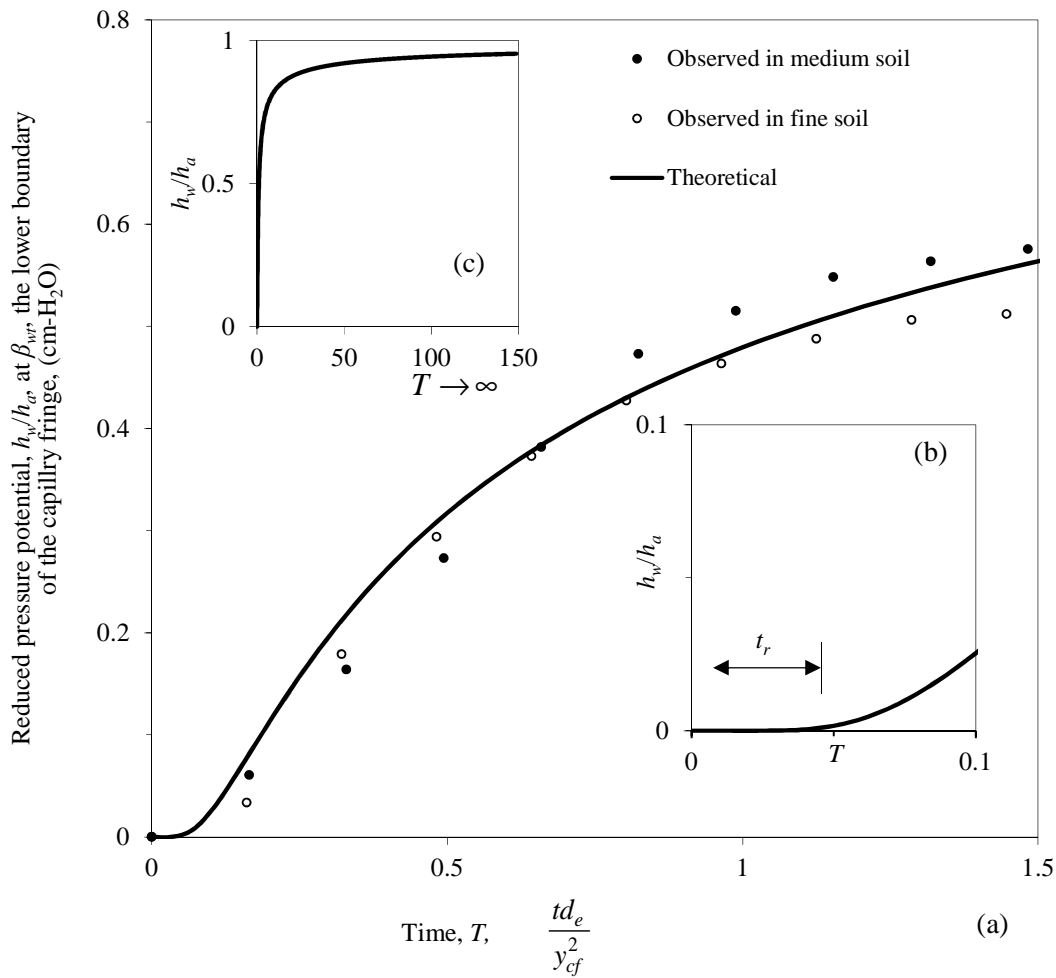
Figure 3.8 Change in pressure potential at the initial water table, β_{wt} , as a result of compressed pore air pressure imposed on the capillary fringe. (b) at the initial stage of the observation and (c) as time increases to infinity. t_r is the time lag between the moment compressed pore air is imposed on the boundary β_{tcf} and the time the water table, the boundary β_{wt}, starts to respond. Note that as time increases, the ratio of h_w/h_a approaches maximum unit asymptotically.

3.6   Discussion

Pressurized pore air, in the unsaturated zone, introduces additional energy into the capillary fringe. This imparted energy, releases the tension forces in the water within the capillary fringe, as it propagates downward (downward pressure wave) towards the water table. As soon as the first front of the downward pressure wave arrives on the water table, the water table starts to ascend (upward pressure wave). It may not be possible to precisely define a water table in the Lisse Effect, because the zero pressure line, as well as the water level in a piezometer, may rise above the saturated zone (upper boundary of the capillary fringe), as it

was illustrated by Weeks (2002) and Waswa *et al*. (2013). The results, therefore, are not discussed in terms of a water table rise, but in terms of a water level rise (piezometric water level) or change in pressure potential, with reference to the initial water table (initial water level), or the lower boundary of the capillary fringe.

The results presented here show that the rate of water level rise is more rapid in a soil with a thin capillary fringe (Coarse soil), than in a soil with a thick capillary fringe (Fine soil). Similarly, the total water level rise is higher in a soil with a thin capillary fringe (Coarse soil), than in a soil with a thick capillary fringe (Fine soil). In addition, a water table, in a soil with a thin capillary fringe (Coarse soil), responds faster to compressed pore air, than in a soil with a thick capillary fringe (Fine soil). These behaviors are caused by the variation in the height of the capillary fringe (represented by the pore air entry pressure head) and the variations in pore sizes (represented by the saturated hydraulic conductivity), between soils (Figure 3.9). In a coarse textured soil: the pore sizes are larger, the energy pathways are less tortuous and the capillary fringe is thin, compared to a fine textured soil. Therefore, the effective pathway, travelled by the introduced energy, is short and of less resistance, in a coarse textured soil, than in a fine textured soil. This, results in lower energy losses and higher energy velocities, in a coarse textured soil, than in a fine textured soil. These energy characteristics explain the variations in the rate of water level rise, total water level rise and water table (water level) response times, in different soils, as explained above. These observations contradict those reported by Guo *et al*. (2008), who indicated that the rate of, as well as the total, water level rise, is directly proportional to the air-entry pressure value (thickness of the capillary fringe) of the soil.

The preceding discussion indicates that the water level in a well, screened below the water table, may not rise to compensate fully for the compressed pore air pressure imposed on the upper boundary of the capillary fringe. This is because of the energy losses that occur during the diffusion of the injected energy through soil water, as it (energy) propagates through the capillary fringe, towards the water table. This observation contradicts the results from the simulation and analysis of the Lisse Effect by Freeze and Cherry (1979), Weeks (2002) and Guo *et al.* (2008), who indicated that the water level in an observation well rises to compensate fully for the compressed pore air pressure.

The results reported here support the earlier reported in Waswa *et al.* (2013), that the water table response, in the Lisse Effect and in the groundwater ridging, is a function of the capillary fringe, principally a pressure-dependent phenomenon and may not be as

instantaneous as reported by e.g. Gillham (1984), Heliotis and DeWitt (1987) and Weeks (2002). On the other hand, the findings reported in this paper agree with those of Gillham (1984), Novakowski and Gillham (1988) and Waswa *et al.* (2013), that the groundwater ridging, as well as the Lisse Effect, water table response, is more likely to be observed in areas with coarse textured soils than in areas with fine textured soils. The common reason that has been given for this difference is that in fine textured soils, e.g. clay soil, the macropores tend to be more and stable than in coarse textured soils. The presence of macropores results in the rapid outflow of air ahead of a wetting front, hence inhibiting the Lisse effect. Macropores also result in a fragmented capillary fringe making it difficult to interpret the groundwater ridging, if it occurs. But for the present study, the explanation for the different water table responses in coarse textured and fine textured soils is in the difference in their pore sizes. In a coarse textured soil, owing to its large pores, more energy is transmitted through the capillary fringe towards the water table and in a more rapid manner compared to a fine textured soil.
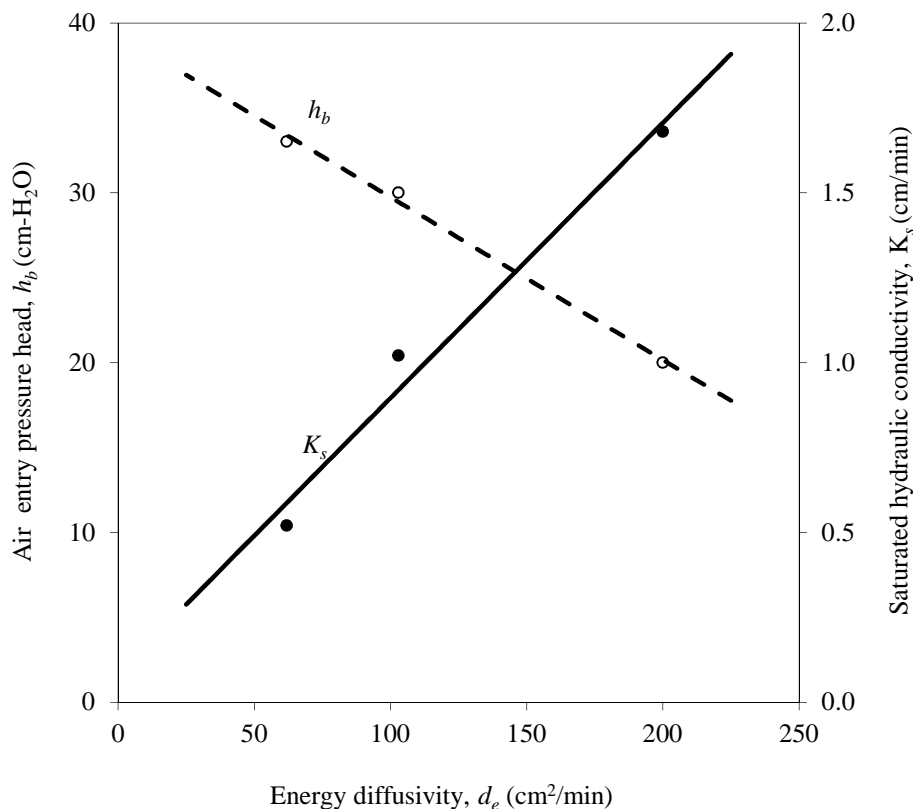

Figure 3.9 Relationship between energy diffusivity coefficient, de, and air entry pressure head (thickness of the capillary fringe) and the saturated hydraulic conductivity Ks (representing pore sizes and tortuosity) of the material.

The results reported in this paper also indicate that the total water table response depends on the amount of energy injected into the capillary fringe. In the Lisse Effect, the total water level rise is proportional to the compressed pore air pressure imposed on the upper boundary of the capillary fringe. In the groundwater ridging phenomena, the total water table rise is proportional to the intensity of rainfall on the ground surface (upper boundary of the capillary fringe), as indicated in Waswa *et al.* (2013), since these intensities are associated with different energy contents.

3.7   Conclusions and Recommendations for Further Research

From the fundamental principles of physics and mathematics, a diffusion equation that can describe the conduction of energy through soil water in a capillary fringe, or the zone of tension saturation, has been developed and successfully tested against laboratory experimental data. The key parameter in the equation is the energy diffusivity constant, which indicates the movement of energy through the soil water. The following conclusions, and suggestions of subjects for further studies, can be made from the theoretical and the experimental results.

Because of energy losses within the capillary fringe, the total rise in the water table in the Lisse Effect is less than compressed pore air pressure in the unsaturated zone. These losses are larger in fine soils, where the capillary fringe is thick, and small in the coarse textured soils, where the capillary fringe is thin. Therefore, the total water table rise will be inversely proportional to the height of the capillary fringe, or the pore air entry pressure of the material. Furthermore, because of these variations in the thickness of the capillary fringe and the soil pores, the water table rise is more rapid in the coarse soils than in the fine soils.

The energy diffusivity parameter may be related to the pore air entry pressure head, h_b, and saturated hydraulic conductivity, K_s, of the material by the relationship:

$$d_e = \omega \frac{K_s}{h_b}$$

[3.37]

where, ω is the constant of proportionality.

The physics of energy losses in a saturated porous media requires further investigation. In the derived equation, it was shown that the key parameter, energy diffusivity, is a function of energy conductivity. Note that, the terms hydraulic diffusivity and hydraulic conductivity are avoided, because they connote more, the notion of soil water movement, than propagation of energy through soil pore water. However, the energy conductivity (for conduction of energy) may be analogous to the hydraulic conductivity (for flow of fluid in porous media) and thermal conductivity (for conduction of heat in solids). The procedure for measuring and quantifying energy conductivity, for example, as a function of the fluid property (e.g. density), as well as material property (e.g. porosity and tortousity), should be developed.

This study has determined that the Lisse Effect is primarily caused by the conversion of the capillary fringe. The Lisse Effect may still be observed, even where the screened section of an observation well, extends above the water table (Weeks, 2002), or even more precisely, above the capillary fringe. Further investigations are required to determine the extent, to which a well that is screened continuously below the ground surface, may impact on the effectiveness of compressed pore air pressure in the Lisse Effect phenomenon.

3.8   References

Bear, J. 1988. Dynamics of fluids in porous media. Dover Publications, New York, USA.

Bishop, K, Seibert, J, Köhler, S, Laudon, H. 2004. Resolving the double paradox of rapidly mobilized old water with highly variable responses in runoff chemistry. Hydrol. Process. 18(1), 185-189.

Brooks, RH, Corey, AT. 1964. Hydraulic properties of porous media. Colorado State University, Fort Collins, CO, 27 pages.

Carslaw, H.S., and J.C. Jaeger. 1959. Conduction of heat in solids. Oxford Univ. Press, New York.

Childs, EC, George, NC. 1948. Soil geometry and soil-water equilibria. Discussions of the Faraday Society 378-85.

Collins, R, Jenkins, A, Harrow, M. 2000. The contribution of old and new water to a storm hydrograph determined by tracer addition to a whole catchment. Hydrol. Process. 14(4), 701-711.

Farlow, SJ. 1982. Partial differential equations for scientists and engineers. John Wiley & Sons, New York.

Flury, M, Gimmi, T. 2002. Solute diffusion, in: Ed. Dane, JH, GC Topp (Eds.), Methods of soil analysis. Part 4. Physical methods. American Society of Agronomy, Madison, Wisconsin, 1323 - 1351.

Freeze, RA, Cherry, JA. 1979. Groundwater. Prentice-Hall, Englewood Cliffs, New Jersey.

Gee, GW, Bauder, JW. 1986. Particle-size analysis, in: Klute, A (Eds.), Methods of soil analysis. Part 1. Physical and mineralogical methods. American Society of Agronomy, Madison, Wisconsin, 383–411.

Gillham, RW. 1984. The capillary fringe and its effect on water-table response. J. Hydrol. 67(1-4), 307-324.

Guo, H, Jiao, JJ, Weeks, EP. 2008. Rain-induced subsurface airflow and Lisse effect. Water Resour. Res. 44(7), 136-144.

Heliotis, FD, DeWitt, CB. 1987. Rapid water table response to rainfall in a Northern Peatland ecosystem. Water Res. Bull. 23(6), 1011-1016.

Hillel, D. 1971. Soil and water: Physical principles and processes. Academic press, New York, USA.

Iverson, RM. 2000. Landslide triggering by rain infiltration. Water Resour. Res. 36(7), 1897-1910.

Janna, WS. 1983. Introduction to fluid mechanics. Brroks/Cole Engineering Division, New York, USA.

Kendall, KA, Shanley, JB, McDonnell, JJ. 1999. A hydrometric and geochemical approach to test the transmissivity feedback hypothesis during snowmelt. J. Hydrol. 219(3-4), 188-205.

Kevorkian, J. 1989. Partial differential equations: analytical solution techniques. Wadsworth & Brooks/Cole

Kienzler, PM, Naef, F. 2008. Subsurface storm flow formation at different hillslopes and implications for the old water paradox. Hydrol. Process. 22(1), 104-116.

Kirchner, JW. 2003. A double paradox in catchment hydrology and geochemistry. Hydrol. Process. 17(4), 871-874.

Klute, A. 1986. Water retention: Laboratory methods, in: Ed. Klute, A (Eds.), Methods of soil analysis. Part 1. Physical and mineralogical methods. American Society of Agronomy, Madison, Wisconsin, 635-662.

Klute, A, Dirksen, C. 1986. Hydraulic conductivity and diffusivity: Laboratory methods, in: Ed. Klute, A (Eds.), Methods of soil analysis. Part 1. Physical and mineralogical methods. American Society of Agronomy, Madison, Wisconsin, 687-734.

Linden, DR, Dixon, RM. 1975. Water table position as affected by soil air pressure. Water Resour. Res. 11(1), 139-143.

Lischeid, G, Kolb, A, Alewell, C. 2002. Apparent translatory flow in groundwater recharge and runoff generation. J. Hydrol. 265(1-4), 195-211.

Lorentz, SA, Thornton-Dibb, S, Pretorius, C, Goba, P. 2004. Hydrological systems modelling research programme: Hydrological processes, Phase I:I Quantification of hillslope, riparian and wetland processes. WRC Report No. K5/1061 & K5/1086. Water Research Commission, Pretoria, South Africa.130 pp.

Marui, A, Yasuhara, M, Kuroda, K, Takayama, S. 1993. Subsurface water movement and transmission of rainwater pressure through a clay layer. IAHS Publ.463-463.

Mathur D.S. 2003. Elements of properties of matter. Shyam Publishers, New Delhi

McDonnell, JJ. 1990. A rationale for old water discharge through macropores in a steep, humid catchment. Water Resour. Res. 26(11), 2821–2832.

Nachabe, MH. 2002. Analytical expressions for transient specific yield and shallow water table drainage. Water Resour. Res. 38(10), 1193.

Novakowski, KS, Gillham, RW. 1988. Field investigations of the nature of water-table response to precipitation in shallow water-table environments. J. Hydrol. 97(1-2), 23-32.

Peck, AJ. 1960. The water table as affected by atmospheric pressure. J. Geophys. Res. 65(8), 2383-2388.

Pinder, GF, Jones, JF. 1969. Determination of the ground-water component of peak discharge from the chemistry of total runoff. Water Resour. Res. 5(2), 438-445.

Rasmussen, TC, Baldwin Jr, RH, Dowd, JF, Williams, AG. 2000. Tracer vs. pressure wave velocities through unsaturated saprolite. Soil Sci. Soc. Am. J. 64(1), 75-85.

Richards, LA. 1931. Capillary conduction of liquids through porous mediums. Physics318-333.

Riley, KF, Hobson, MP, Bence, SJ. 2006. Mathematical methods for physics and engineering. Cambridge Univ Pr

Scheidegger, AE. 1960. The physics of flow through porous media. University of Toronto, Toronto.

Sklash, MG, Farvolden, RN. 1979. The role of groundwater in storm runoff. J. Hydrol. 43(1-4), 45-65.

Sokolnikoff, IS, Redheffer, RM, Avents, J. 1958. Mathematics of physics and modern engineering. Journal of The Electrochemical Society 105196C.

Torres, R, Dietrich, WE, Montgomery, DR, Anderson, SP, Loague, K. 1998. Unsaturated zone processes and the hydrologic response of a steep, unchanneled catchment. Water Resour. Res. 34(8), 1865-1879.

Trim, DW. 1990. Applied partial differential equations. Kent Publishing Company, Boston.

Waswa, GW, Clulow, AD, Freese, C, Le Roux, PAL, Lorentz, SA. 2013a. Transient pressure waves in the vadose zone and the rapid water table response. Vadose Zone J. 12(1), doi:10.2136/vzj2012.0054.

Waswa, GW, Clulow, AD, Freese, C, Lorentz, SA, le Roux, PAL. 2013b. Transient pressure waves through vadose zone and rapid water table response. Vadose Zone J.

Weeks, EP. 1979. Barometric fluctuations in wells tapping deep unconfined aquifers. Water Resour. Res. 15(5), 1167-1176.

Weeks, EP. 2002. The Lisse effect revisited. Ground Water 40(6), 652-656.

Wenninger, J, Uhlenbrook, S, Tilch, N, Leibundgut, C. 2004. Experimental evidence of fast groundwater responses in a hillslope/floodplain area in the Black Forest Mountains, Germany. Hydrol. Process. 18(17), 3305-3322.

Wu, L. 2003. Soil water diffusion, in: Stewart, BA, TA Howell (Eds.), Encyclopedia of Water Science. Marcel Dekker, New York, 865-867.

Yunus, C.A. 1990. Heat transfer, A practical approach. Tata McGraw-Hill, New York.

3.9   Appendices
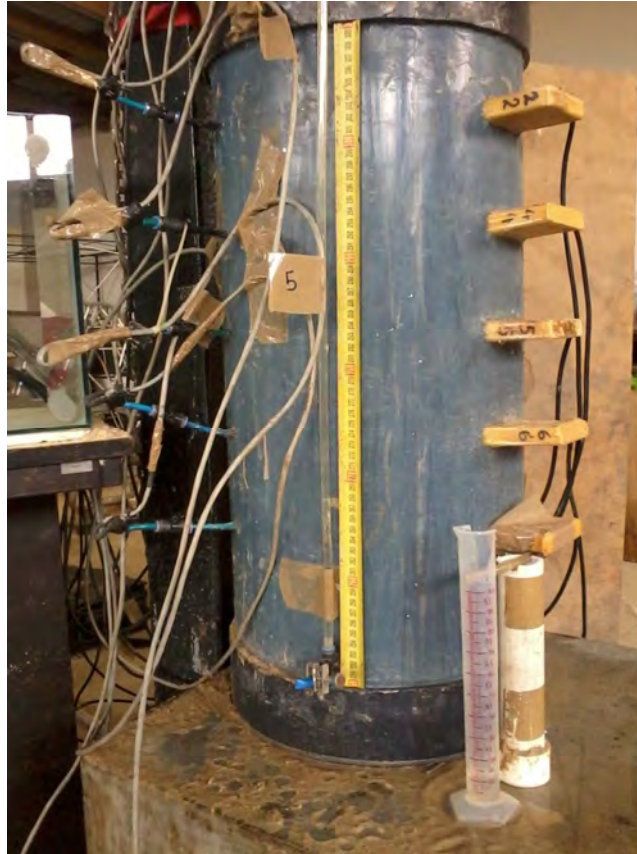

Figure A3.1 Laboratory column experiment

5 mm Ø PVC tube

2 mm Ø longitudinal hole

Hydrophobic membrane

0.1 bar differential

2 cm Ø Cylindrical solid

5 mm Ø transverse holes

To the data logger

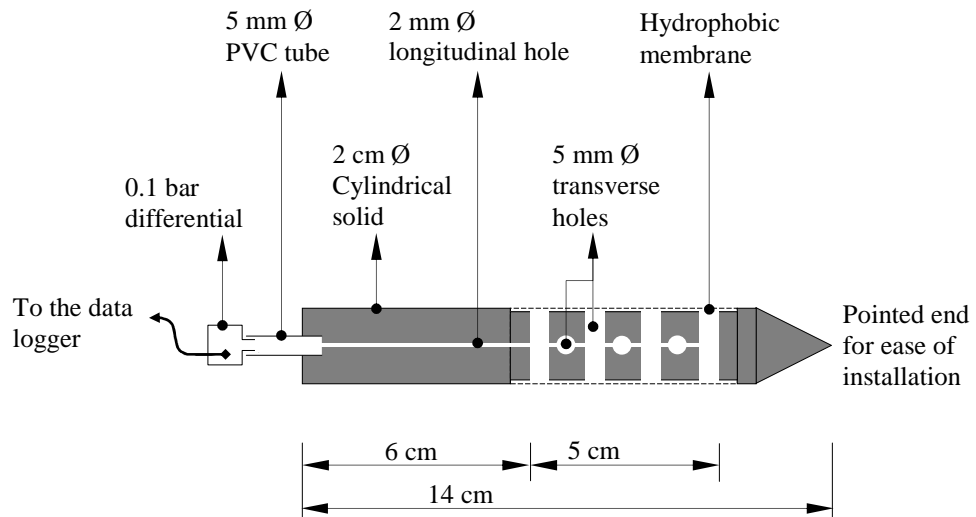Pointed end for ease of installation

6 cm

5 cm

14 cm

Figure A3.2 (a) A sketch and (b) pictures of the fabricated pore air pressure probe, used in monitoring compressed pore air pressure
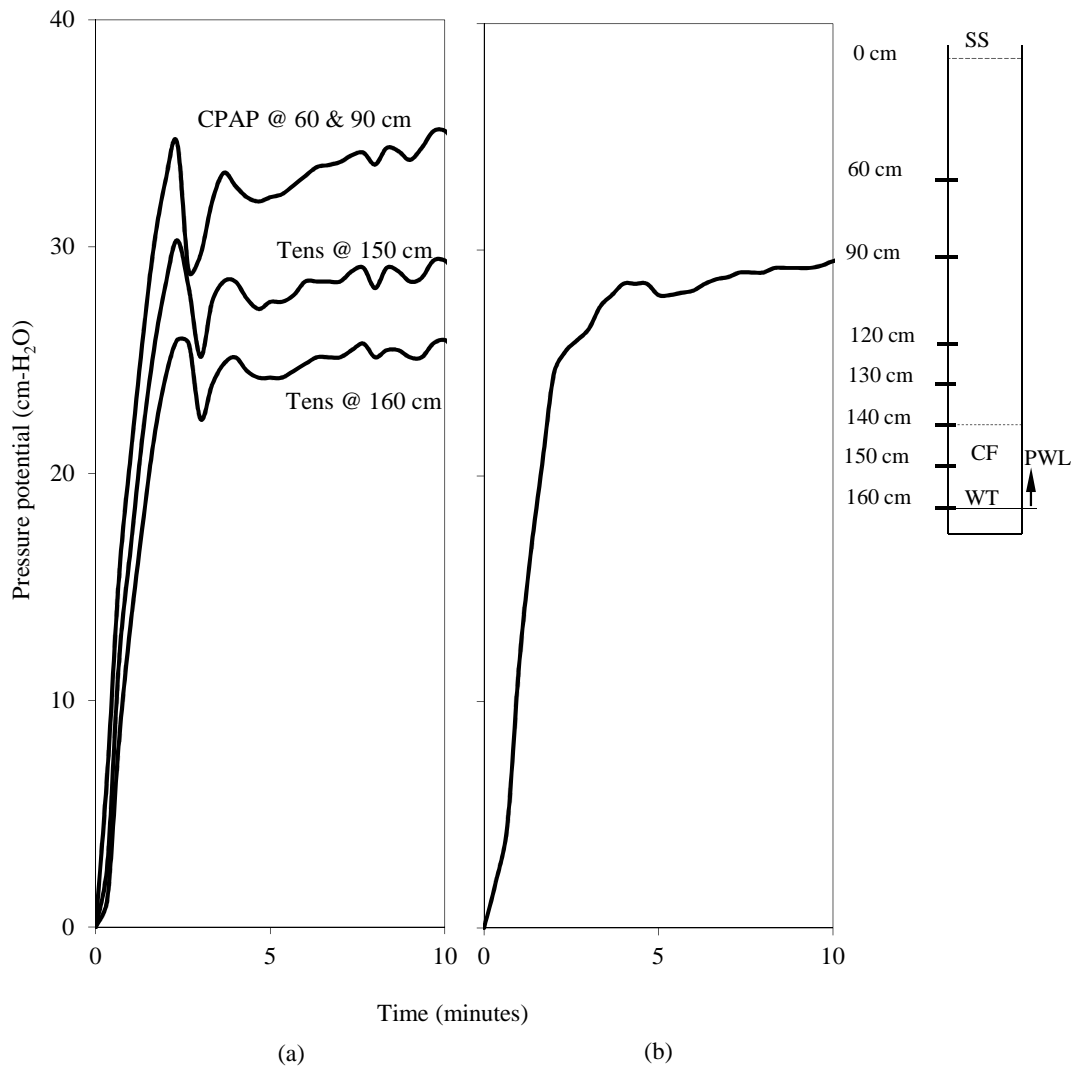
Figure A3.3 (a) Change in pressure potential within the capillary fringe (CF) in Coarse soil, when the soil surface (SS) was ponded with 15 cm of water in the laboratory experiment. Pressurized pore air pressure increased uniformly and to a maximum of about 35 cm-H_2O. Note that (b) the rise in the piezometric water level (PWL), was less than compressed pore air pressure
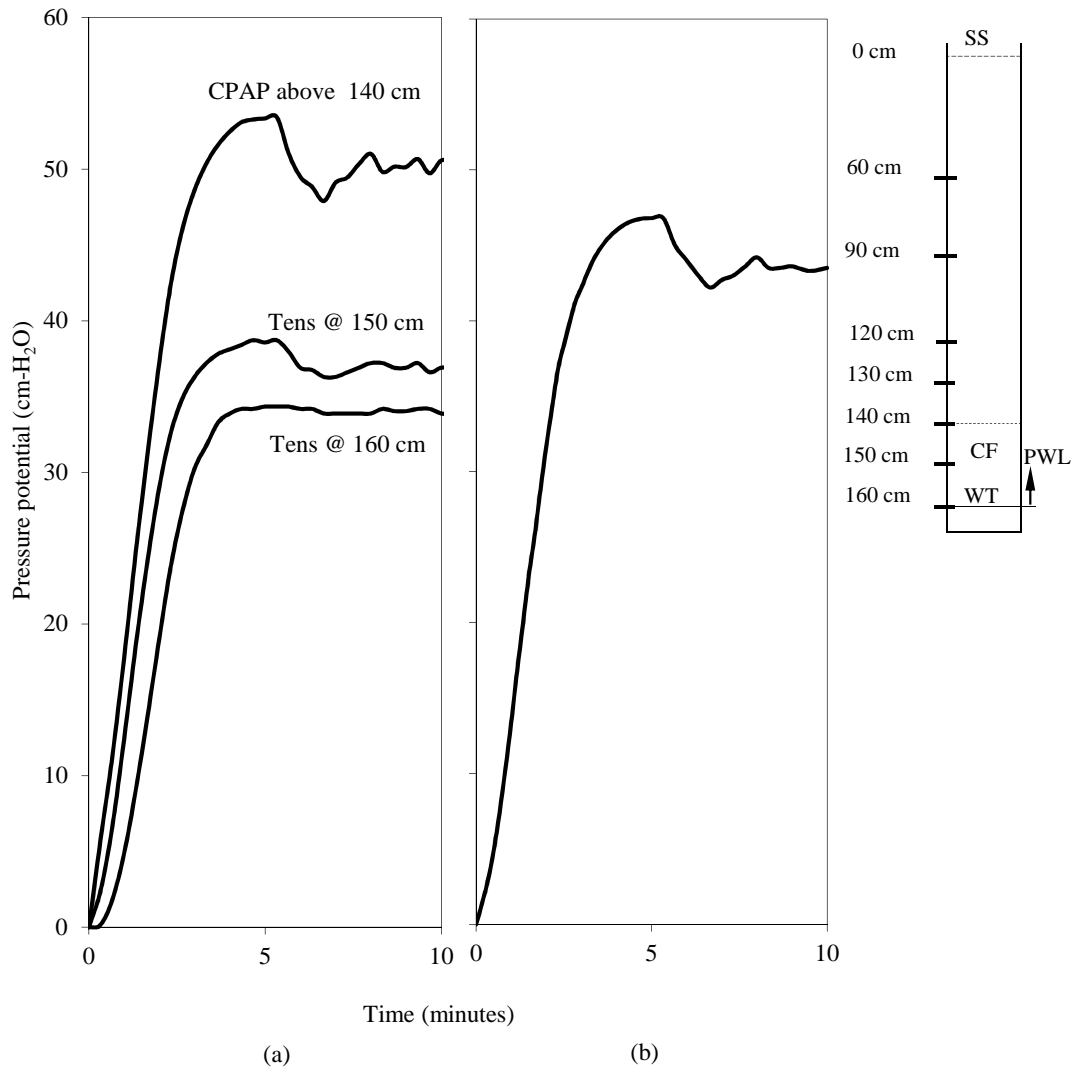
Figure A3.4 (a) Change in pressure potential within the capillary fringe (CF) in Coarse soil, when the soil surface (SS) was ponded with 30 cm of water in the laboratory experiment. Pressurized pore air pressure increased uniformly and to a maximum of about 50 cm-H_2O. Note that (b) the rise in the piezometric water level (PWL), was less than compressed pore air pressure.
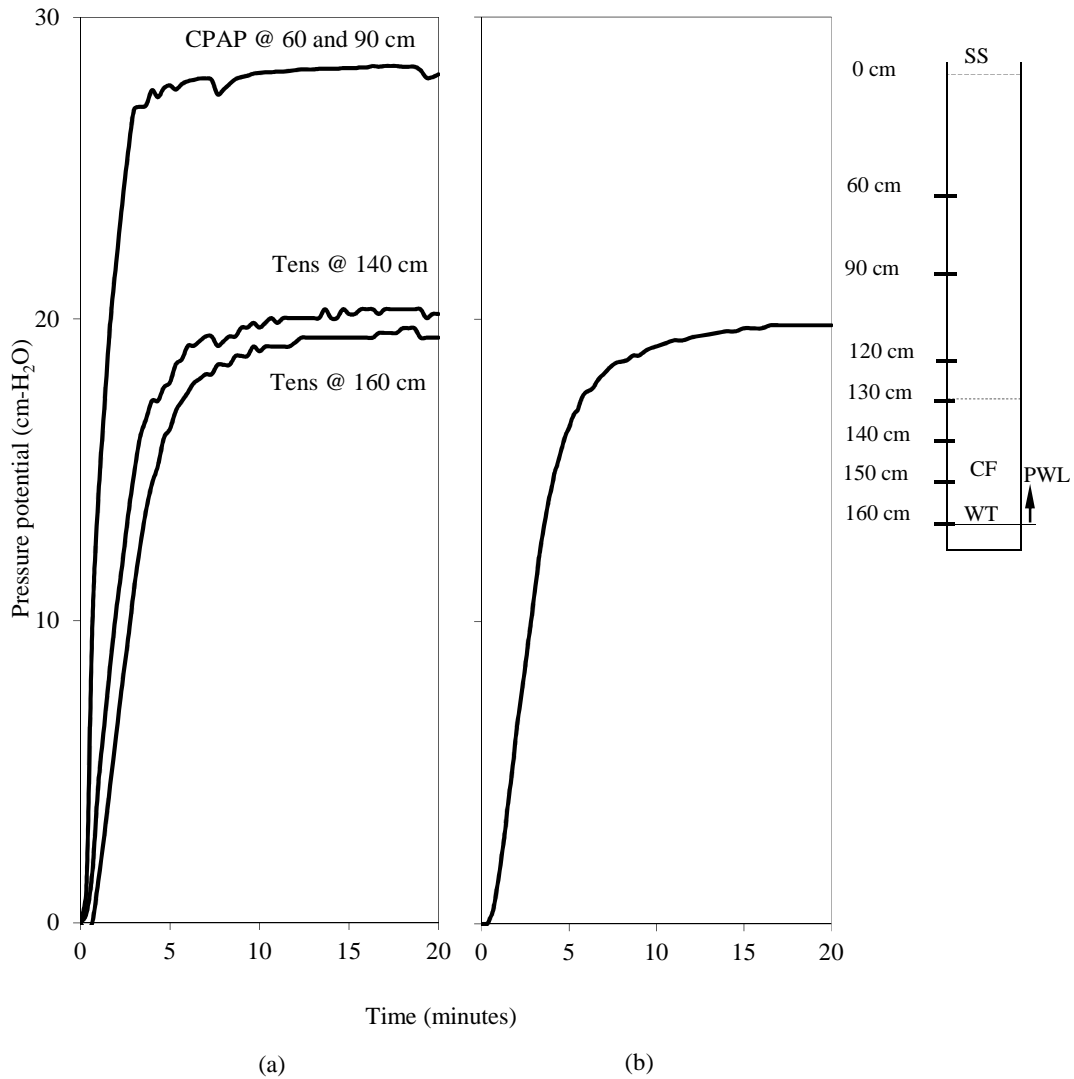
Figure A3.5 (a) Change in pressure potential within the capillary fringe (CF) in Medium soil, when the soil surface (SS) was ponded with 15 cm of water in the laboratory experiment. Pressurized pore air pressure increased uniformly and to a maximum of about 35 cm-H_2O. Note that (b) the rise in the piezometric water level (PWL), was less than compressed pore air pressure.
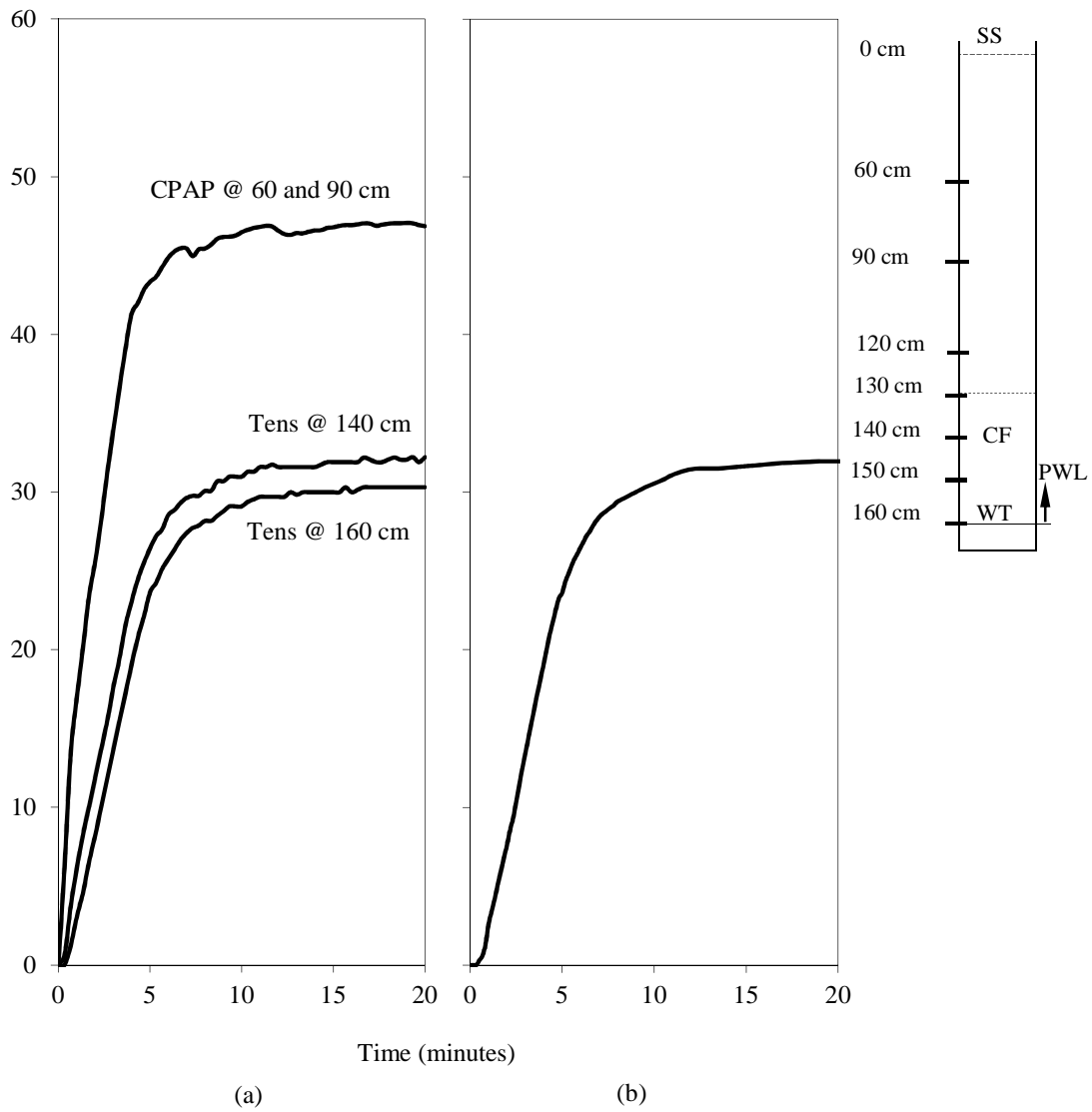
Figure A3.6 (a) Change in pressure potential within the capillary fringe (CF) in Medium soil, when the soil surface (SS) was ponded with 30 cm of water in the laboratory experiment. Pressurized pore air pressure increased uniformly and to a maximum of about 50 cm-H_2O. Note that (b) the rise in the piezometric water level (PWL), was less than compressed pore air pressure.

Figure A3.7 (a) Change in pressure potential within the capillary fringe (CF) in Fine soil, when the soil surface (SS) was ponded with 15 cm of water in the laboratory experiment. Pressurized pore air pressure increased uniformly and to a maximum of about 35 cm-H$_2$O. Note that (b) the rise in the piezometric water level (PWL), was less than compressed pore air pressure.
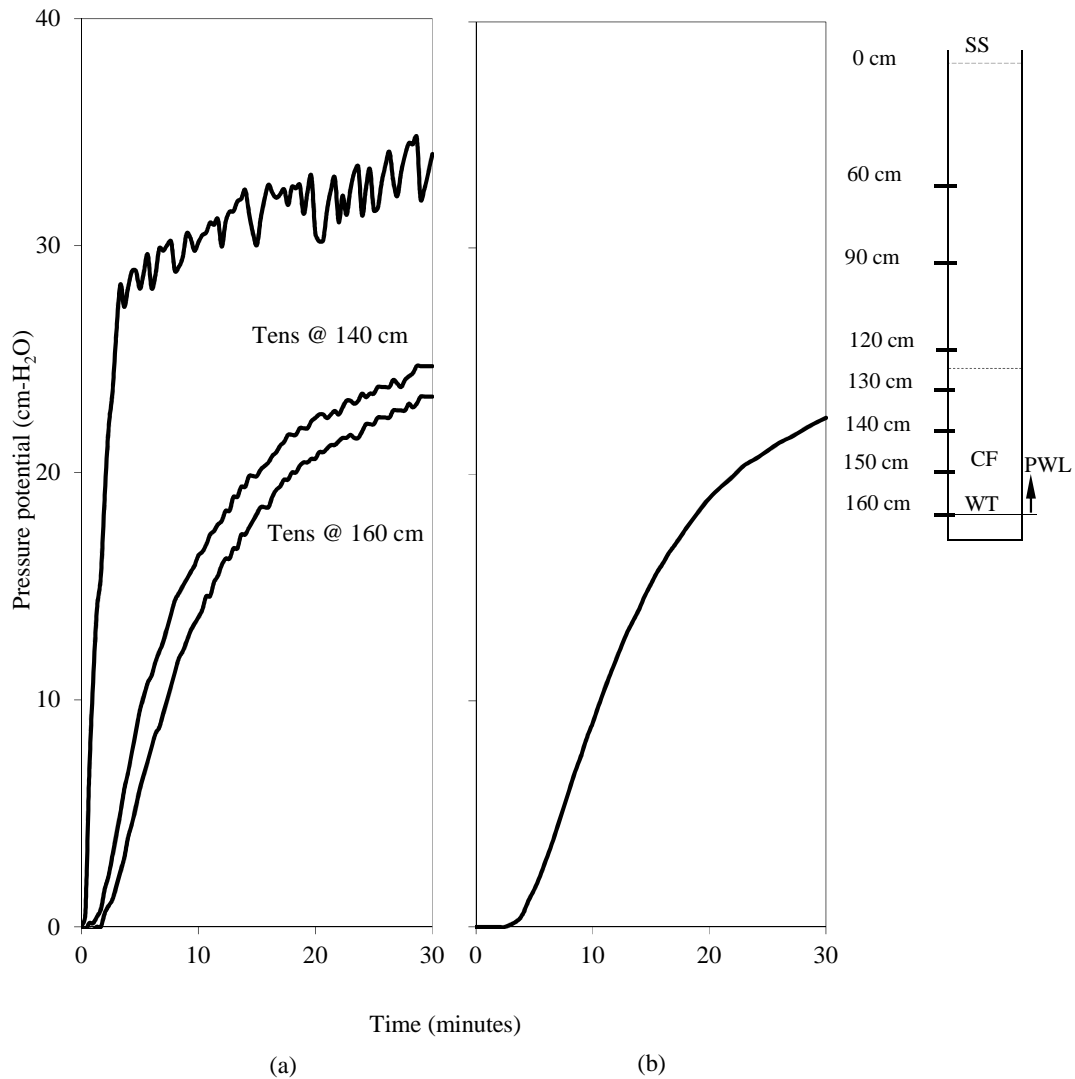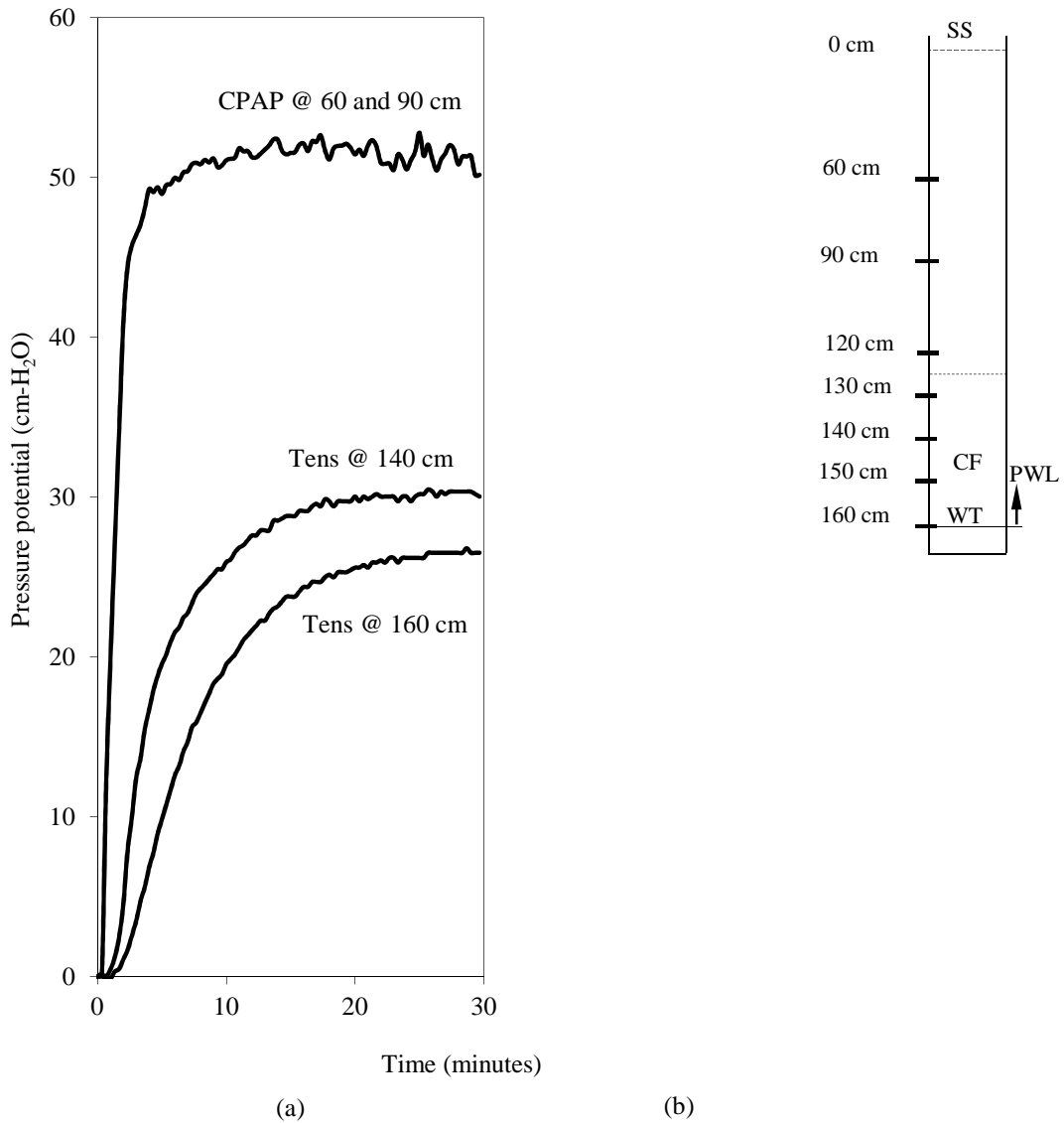
Figure A3.8 (a) Change in pressure potential within the capillary fringe (CF) in Fine soil, when the soil surface (SS) was ponded with 30 cm of water in the laboratory experiment. Pressurized pore air pressure increased uniformly and to a maximum of about 50 cm-H_2O. Note that (b) the rise in the piezometric water level (PWL), was less than compressed pore air pressure.
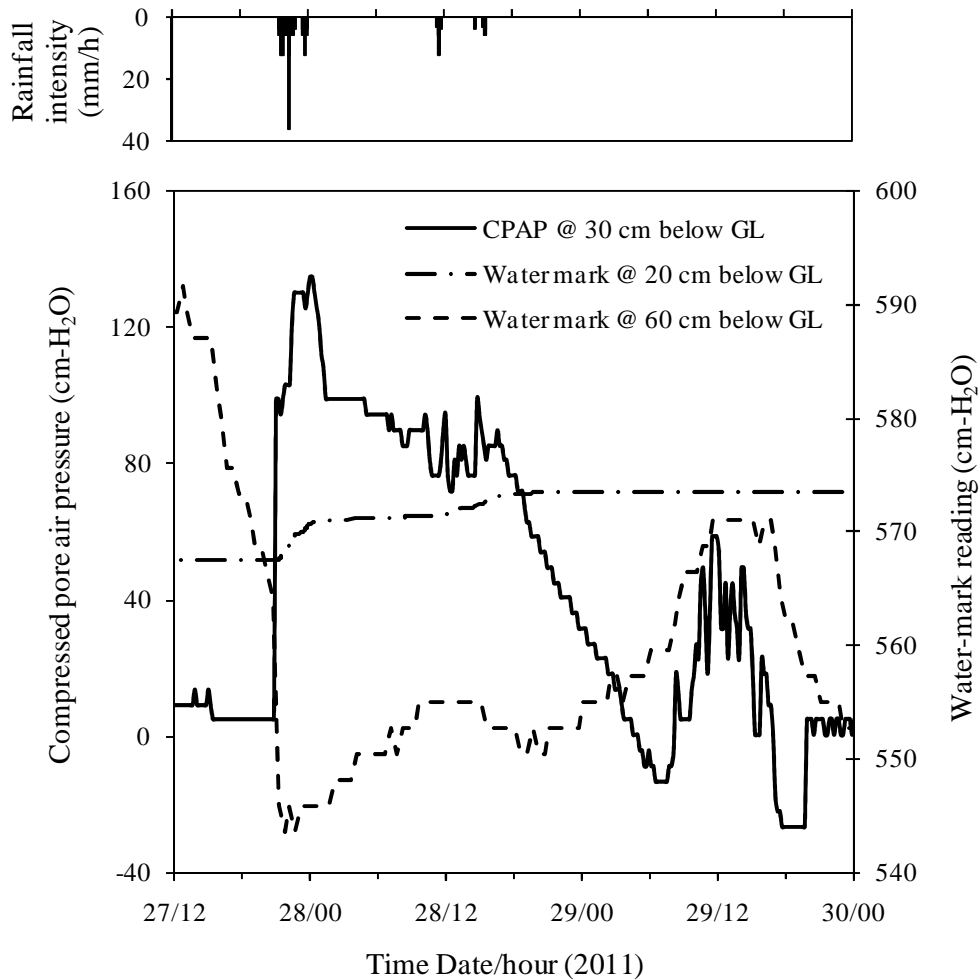
Figure A3.9 Some observations of compressed pore air pressure (by the fabricated compressed pore air pressure probe) and pore water pressure readings by the water marks from the field in the Weatherley Research Catchment, at the observation nest, L04. The observations were made during the summer season of 2011/2012. GL = ground level.

TRANSIENT PRESSURE WAVES IN HILLSLOPES

PhD thesis

Waswa GW

School of Engineering, University of KwaZulu-Natal, South Africa

CHAPTER 4

SUMMARY AND CONCLUSIONS

4.1   Summary

The appearance of pre-event water, or groundwater, in a significant amount in a stormflow hydrograph is a paradox (Kirchner, 2003) that requires an explanation. Transient pressure wave mechanisms, i.e, groundwater ridging and the Lisse Effect, are among many others that have been proposed to explain this paradox. While these transient pressure wave mechanisms can explain the paradox, the explanation of the physical processes involved in each of them have been misunderstood, insufficient and confusing, resulting in misinterpretation of results, in some studies.

For instance, (Gillham, 1984) argued that only an addition of a small amount of water on the ground surface, in an environment where the zone of tension saturation extended to the surface, would cause an instantaneous and disproportionate rise of a water table. Some researchers, e.g., Heliotis and DeWitt (1987) and Weeks (2002), have explained that the small amount of water is required to fill the capillary menisci, hence bringing the water table close to the ground surface. This explanation, as it is, appears not adequate. The Lisse effect has also been confusing, and the few authors who studied this phenomenon (e.g. Freeze and Cherry, 1979; Weeks, 2002) did not consider the role of the capillary fringe.

Using field data and laboratory column experiments, (Waswa *et al.*, 2013), demonstrated that the observed water table responses, manifested either as groundwater ridging for a shallow water table or the Lisse effect for a deep water table, are caused by the rapid introduction of additional energy into the zone of tension saturation. These authors showed that the water table response in groundwater ridging is directly related to the rainfall intensity, as these intensities are associated with different energy levels.

4.2   Principal Conclusions

This study explicitly expressed and recognized that pressure is the only primary variable between the water within the capillary fringe and the water below the water table. This is the main working principle in this study. It is upon this principle that the capillary fringe plays a significant role in groundwater ridging, as well as in the Lisse Effect. It may not be possible, therefore, that only a very small amount of water can cause the water table to rapidly rise to the ground surface in groundwater ridging mechanism.

In groundwater ridging, the magnitude of the rise of a water table is directly proportional to the rainfall intensity. The rainfall acting at the ground surface introduces into the capillary fringe, an additional amount of energy that is proportional to its (rainfall) intensity. In a similar physical process, the pressurized pore air in the unsaturated zone, introduces an additional energy into the capillary fringe, resulting in the rapid water table rise in the Lisse Effect.

The additional energy, injected into the capillary fringe, diffuses downwards through the capillary fringe to the water table, releasing the tension forces in the soil water. The arrival of the downward pressure wave front on the water table, results in the rise of the phreatic surface. A one-dimensional diffusion equation for propagation of energy through a capillary fringe was, formulated, evaluated and presented in this study. This equation can predict the water level rise in wells (change in pressure potential at the initial water table) in the Lisse Effect.

Due to energy losses in the capillary fringe, the water level in a well, in the Lisse Effect, does not rise to equal the compressed pore air. These energy losses depend on the physical properties of the soil material. In fine textured soils (e.g. clay soil), the losses are higher than in coarse textured soils (e.g. sand soil). In addition to higher energy losses, the travel time of energy, through a capillary fringe, in fine textured soils, is much higher than in coarse textured soils. This was explained as due to finer pores, more tortuous pathways and a thicker capillary fringe, in fine textured soils, compared to the coarse textured soils.

4.3 Future Perspectives and Recommendations for Further Research

From the derived equation, this study proposes new material parameters, which are important in the analysis and understanding of the diffusion of energy through soil water. The first is the energy diffusivity coefficient, d_e. This is analogous to the thermal and the hydraulic diffusivity, employed in understanding the flow of heat through solids and the flow of fluids through porous media, respectively. The second is the energy conductivity, k, encapsulated in energy diffusivity $d_e = k/c\rho_w$, where c is the specific energy capacity and ρ_w is the mass density of water. Parameter k is analogous to the thermal and the hydraulic conductivity, applied in the study of flow of heat through solids and flow of fluids through porous media, respectively. Methodologies for determining these new material parameters should be developed.

In this study, a probe for measurement of compressed pore air pressure was designed and fabricated. The probe, which was fabricated from a PVC cylindrical solid and a hydrophobic membrane, was successfully used in the laboratory experiment. This probe can be used to monitor the Lisse Effect in the field conditions. This probe was tried in the field and successfully monitored compressed pore air pressure, as indicated in Figure A3.9.

The equation developed in this study may also be applied to groundwater ridging phenomena, if the pressure perturbations (added energy), by the rainfall intensity, can be quantified. However, in the case of groundwater ridging, the imposed energy may be introduced into the analytical solution, via a Dirac delta – the unit impulse function. This is because in groundwater ridging, the energy is caused directly by rainfall intensity, which lasts only for a short period of time (a few minutes or hours), compared to the Lisse Effect compressed pore air pressure, which may last for a long period of time, e.g. 2-4 days even days (Heliotis and DeWitt, 1987) after the rainfall event..

The concept of diffusion of energy through saturated porous media, developed in this study, may also be applied in other fields of study. For example, it can be applied in the analysis of landslides.

More experiments are required to further understand the physics of diffusion of energy through pore fluid in a saturated porous media. For example, there is need to investigate the influence of soil material properties, e.g. pore sizes, tortuosity, as well as the fluid properties, e.g. density, on the diffusion of energy.

Further studies are required to understand the role of preferential flow and macropores in the rapid response of a water table.

The findings from this study may contribute to the advancement and understanding of the role of the capillary fringe in the transportation of pollutants in the subsurface.

4.4 References

Freeze, RA, Cherry, JA. 1979. Groundwater. Prentice-Hall, Englewood Cliffs, New Jersey.

Gillham, RW. 1984. The capillary fringe and its effect on water-table response. J. Hydrol. 67(1-4), 307-324.

Heliotis, FD, DeWitt, CB. 1987. Rapid water table response to rainfall in a Northern Peatland ecosystem. Water Res. Bull. 23(6), 1011-1016.

Kirchner, JW. 2003. A double paradox in catchment hydrology and geochemistry. Hydrol. Process. 17(4), 871-874.

Waswa, GW, Clulow, AD, Freese, C, Lorentz, SA, le Roux, PAL. 2013. Transient pressure waves through vadose zone and rapid water table response. Vadose Zone J.

Weeks, EP. 2002. The Lisse effect revisited. Ground Water 40(6), 652-656.

"The great God has shown … and the interpretation is trustworthy.

…

Surely, your God is the God of gods and the Lord of kings and a revealer of mysteries…"